NASA Contractor Report 4170

NASA-CR-4170 19880018650

Method To Predict External Store Carriage Characteristics at Transonic Speeds

Bruce S. Rosen

CONTRACT NAS1-18105
AUGUST 1988

NASA Contractor Report 4170

Method To Predict External Store Carriage Characteristics at Transonic Speeds

Bruce S. Rosen
Grumman Corporation
Grumman Aircraft Systems Division
Bethpage, New York

Prepared for
Langley Research Center
under Contract NAS1-18105

National Aeronautics
and Space Administration

Scientific and Technical
Information Division

1988

CONTENTS

ILLUSTRATIONS

ILLUSTRATIONS (cont'd.)

TABLES

SUMMARY

Development of a computational method for prediction of external store carriage characteristics at transonic speeds is described. The geometric flexibility required for treatment of isolated and underwing, pylon-mounted stores is achieved by computing finite difference solutions on a five-level embedded grid arrangement. A completely automated grid generation procedure facilitates applications. Store modelling capability consists of bodies of revolution with multiple fore and aft fins. A body-conforming grid improves the accuracy of the computed store body flow field. A nonlinear relaxation scheme developed specifically for modified transonic small disturbance flow equations enhances the method's numerical stability and accuracy. As a result, treatment of lower aspect ratio, more highly swept and tapered wing planforms is possible. A limited supersonic freestream capability is also provided. Pressure, load distribution, and force/moment correlations show good agreement with experimental data for several test cases. A detailed computer program description for the Transonic Store Carriage Loads Prediction (TSCLP) Code is included in Appendix D.

This Page Intentionally Left Blank

INTRODUCTION

Prediction of external store carriage characteristics at transonic speeds requires computations for rather complex geometries. Wing, fuselage, pylon, and store body and fin components each need to be modelled. While methods to obtain full potential, Euler, and Navier Stokes solutions for relatively simple geometries are maturing at a rapid pace, transonic small disturbance (TSD) formulations are still a practical alternative for treatment of these more complex configurations.

The NASA/Grumman Transonic Wing-Body Code (Refs. 1,2,3) represents the state-of-the-art for reliable TSD analysis of complex aircraft. An attempt to extend similar wing/fuselage methodology to treat wing/fuselage/pylon/store geometries (Refs. 4,5) attributed poor isolated body normal force correlations to the TSD formulation. Since approaches emphasizing the use of more exact flow equations (Refs. 6,7,8) are difficult to implement and require further development for practical three-dimensional applications, a more accurate TSD formulation was developed for treatment of store body shapes (Ref. 9). This was accomplished by solving TSD flow equations on grids which conform to the store body shape, subject to exact (inviscid) store body surface boundary conditions.

For this effort, refined TSD approaches (Refs. 1,2,3,9) have been combined for treatment of isolated and underwing, pylon-mounted stores. In the resulting Transonic Store Carriage Loads Prediction (TSCLP) code, geometric flexibility is achieved by computing solutions on a five-level embedded grid arrangement. In addition, a nonlinear finite difference relaxation scheme developed specifically for modified TSD flow equations enhances numerical stability and accuracy. As a result, treatment of lower aspect ratio, more highly swept and tapered wing planforms is possible. A limited supersonic freestream capability is also provided.

This Page Intentionally Left Blank

NOMENCLATURE

a,u,v	Coefficients in upwind difference formulae
A	Area
b/2	Semispan
c	Chord
c_{ave}	Wing average chord (reference area ' span)
c_d	Sectional drag coefficient
C_D	Drag coefficient
c_f	Sectional skin friction coefficient
$c_{f,\ ave}$	Average turbulent skin friction coefficient
C_F	Skin friction coefficient
c_ℓ	Sectional lift coefficient
C_ℓ	Rolling moment coefficient
C_L	Lift coefficient
c_m	Sectional moment coefficient
C_m	Pitching moment coefficient
CMX	Moment coefficient about x-axis
CMY	Moment coefficient about y-axis
CMZ	Moment coefficient about z-axis
C_n	Yawing moment coefficient
C_N	Normal force coefficient
C_p	Pressure coefficient, $(p-p_\infty)/ \frac{1}{2} \rho_\infty V_\infty^2$
c_x	Store body cross-section axial force coefficient
C_X	Axial force coefficient
c_y	Store body cross-section side force coefficient
C_Y	Side force coefficient
c_z	Store body cross-section normal force coefficient
C_Z	Normal force coefficient
f	Airfoil section shape function
$\tilde{f}$	Store body cross-section force coefficient
F	Force Coefficient
i,j,k	Grid indices

$\hat{i},\hat{j},\hat{k}$	Unit vectors
L	Reference length
M	Moment coefficient about reference center
M_∞	Freestream Mach number
$\bar{n}$	Surface normal
n_x,n_r,n_θ	Cylindrical components of surface normal
n_x,n_y,n_z	Cartesian components of surface normal
R	Store body radius
Re	Reynolds number
RMAX	Store body maximum radius
s	Arc length
S	Surface area
T,U,V	Coefficients of governing flow equation
$U_\infty,V_\infty,W_\infty$	Cylindrical components of freestream velocity
V	Local velocity
V_∞	Freestream velocity
$\bar{x}$	Vector coordinate
x,r,θ	Cylindrical coordinates
x,y,z	Cartesian coordinates
$\bar{z}$	x,r location in physical domain of conformal mapping
α	Aircraft or isolated store angle-of-attack relative to freestream
α_s	Store pitch angle relative to aircraft (positive, nose up)
β_p	Pylon yaw angle relative to aircraft (positive, leading edge outboard)
β_s	Store yaw angle relative to aircraft (positive, nose outboard)
γ	Specific heat ratio
Γ	Circulation
δ_{fin}	Store fin deflection angle (positive, leading edge counter-clockwise looking upstream)
Δ	Incremental quantity, or mesh cell size
$\bar{\zeta}$	ξ,η location in transformed domain of conformal mapping
η	Wing or fin non-dimensional spanwise location (2y/b or 2r/b)
Λ	Local sweep angle of constant percent chord line
μ	Viscosity
ξ,η,ζ	Computational coordinates in Cartesian grids
ξ,η,θ	Computational coordinates in cylindrical grids

ρ	Density
ϕ	Perturbation potential, or store pressure-tap roll orientation angle
ϕ_{nn}, ϕ_{ss}	Central and upwind second derivatives of perturbation potential
ω_s	Store roll rate, p/V_∞ (radians per unit length)
∞	Infinity

Subscripts

b,body	Store body
c	Viscous crossflow quantity
f,fin	Store fin
LE,TE	Leading edge or trailing edge
p,pylon	Pylon
REF	Configuration or isolated store reference parameter
REFS	Store reference parameter
s,store	Store
u,l	Upper or lower
w,wing	Wing
wet	Wetted area
x,r,θ	Partial derivatives in cylindrical coordinates
x,y,z	Partial derivatives in Cartesian coordinates

Superscripts

D	Dummy value
+	New or updated value

This Page Intentionally Left Blank

COMPUTATIONAL METHOD

Inputs to the TSCLP code consist of configuration geometry, freestream flow conditions, and number of solution iteration cycles. No additional solution or grid generation parameters are required. The grid generation procedure has been completely automated to facilitate applications. Treatment of wing/fuselage/pylon geometry is similar to that found in the basic NASA/Grumman Transonic Wing-Body Code (Refs. 1, 2), with enhancements as noted. Modelling capability for isolated and underwing, pylon-mounted stores is described below.

An example of the complexity of store geometry that can be modelled is the GBU-15-CWW, shown in Fig. 1. In general, the store body must be axisymmetric and may be either sharp or blunt nosed. Two sets of fins may be input, each set consisting of from one to four identical fins at different angular locations. When two sets of fins are input, they must be of the fore and aft type, and they must have the same number of fins at the same angular locations. Fore and aft fins can have different planforms and (symmetric) airfoil sections. Individual, all-moveable fin deflection and quasi-steady, isolated store roll rate capabilities have also been incorporated.

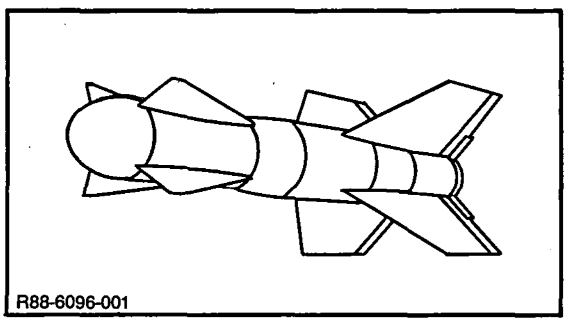

Figure 1 GBU-15-CWW Store

Transonic Small Disturbance Formulation

Wing/fuselage/pylon (Cartesian grid) calculations employ the following "modified" TSD flow equation (Refs. 1, 2):

$$T\phi_{xx} + U\phi_{xy} + V\phi_{yy} + \phi_{zz} = 0 \tag{1}$$

where

$$T = 1 - M_\infty^2 - (\gamma + 1)\, M_\infty^2\, \phi_x - \frac{\gamma + 1}{2}\, M_\infty^2\, \phi_x^2$$

$$U = -2M_\infty^2\, \phi_y$$

$$V = 1 - (\gamma - 1)\, M_\infty^2\, \phi_x$$

Store body and fin (cylindrical grid) calculations employ a similar equation (Refs. 3, 9):

$$T\, \phi_{xx} + U\phi_{xr} + V\phi_{rr} + \frac{1}{r}\, \phi_r + \frac{1}{r^2}\, \phi_{\theta\theta} = 0 \qquad (2)$$

where

$$T = 1 - M_\infty^2 - (\gamma + 1)M_\infty^2\, \phi_x - \frac{\gamma + 1}{2}\, M_\infty^2\, \phi_x^2$$

$$U = -2M_\infty^2\, (\alpha \sin\Theta + \phi_r)$$

$$V = 1 - (\gamma - 1)\, M_\infty^2\, \phi_x$$

These TSD flow equations are "modified" by the retention of terms neglected by "classical" TSD flow equations (Ref. 10). The retention of the $\phi_x^2\, \phi_{xx}$ term provides a better approximation to the transition between subsonic and supersonic flow. The $\phi_y\phi_{xy}$, $\phi_x\phi_{yy}$ and $\phi_r\phi_{xr}$, $\phi_x\phi_{rr}$ terms are retained to more accurately resolve shock waves with appreciable sweep in the x-y (wing) and x-r (fin) planes, respectively.

Lifting surfaces are treated using a small disturbance, planar approximation. For example, wing boundary conditions are imposed on the wing reference plane ($z=z_{wing}$) and, for an airfoil upper and/or lower surface section shape f(x), are given by:

$$\pm\, \phi_z = -\, n_x \qquad (3)$$

with the assumptions that:

$$n_x = \mp \left[\tan^{-1} (f_x) - \alpha\right]$$

$$n_y = 0$$

$$n_z = \pm 1$$

In the wing fine grid, where wing leading and trailing edges are always located at grid mesh cell midpoints, it is possible to use a more accurate approximation for n_x:

$$n_x = \mp (f_x - \alpha)$$

Pressure coefficients on the wing surface are defined as:

$$C_p = -2\,\phi_x - \phi_y^2 - (1 - M_\infty^2)\,\phi_x^2 \tag{4}$$

Pylon surfaces receive similar treatment. Boundary conditions are imposed on the pylon reference plane ($y=y_{PYLON}$), and are given by:

$$\pm\phi_y = -\,(\cos\alpha\; n_x + \sin\alpha\; n_z) \tag{5}$$

where

$$n_x = \mp \left[\tan^{-1}(f_x) - \beta_p\right]$$

$$n_y = \pm 1$$

$$n_z = \pm \tan(\Lambda)\,\tan^{-1}(f_x)$$

Here the pylon surface normals are assumed to be perpendicular to swept, constant percent chord lines. Pressure coefficients on the pylon surface are defined as:

$$C_p = -2\phi_x - \phi_z^2 - (1 - M_\infty^2)\,\phi_x^2 \tag{6}$$

Body-type components require a different approach. The fuselage is treated using an approximate, constant cross-section boundary condition support surface (Ref. 1). For the store body, a more exact boundary condition is used:

$$(U_\infty + \phi_x)\, n_x + (V_\infty + \phi_r)\, n_r = 0 \tag{7}$$

where

$$n_x = -\frac{dR}{dx} \Big/ \sqrt{1 + \left(\frac{dR}{dx}\right)^2}$$

$$n_r = 1 \Big/ \sqrt{1 + \left(\frac{dR}{dx}\right)^2}$$

$$n_\Theta = 0$$

and

$$U_\infty = \cos\,(\alpha + \alpha_s)\, \cos\,(\beta_s)$$

$$V_\infty = \sin\,(\beta_s)\, \cos\,(\Theta) + \sin\,(\alpha + \alpha_s)\, \cos\,(\beta_s)\, \sin\,(\Theta)$$

$$W_\infty = \sin\,(\alpha + \alpha_s)\, \cos\,(\beta_s)\, \cos\,(\Theta) - \sin\,(\beta_s)\, \sin\,(\Theta)$$

This boundary condition is consistent with the body-conforming grids used for modelling the store body shape. The isentropic form of the pressure coefficient is also used on the store body surface:

$$C_p = \frac{2}{\gamma M_\infty^2} \left\{ \left[1 + \frac{\gamma - 1}{2} M_\infty^2 \,(1 - V^2)\right]^{\gamma/(\gamma-1)} - 1 \right\} \tag{8}$$

where

$$V^2 = (U_\infty + \phi_x)^2 + (V_\infty + \phi_r)^2 + (W_\infty + \frac{1}{r}\phi_\Theta)^2$$

Store fin surfaces are treated using a small disturbance, planar approximation similar to that for wings and pylons. Fin boundary conditions are imposed on the fin reference plane ($\Theta = \Theta_{FIN}$), and are given by:

$$\pm \frac{1}{r}\phi_\Theta = -\,(U_\infty n_x + V_\infty\, n_r) \mp (W_\infty - r\omega_s) \tag{9}$$

where

$$n_x = \mp [\tan^{-1}(f_x) - \delta_{FIN}]$$

$$n_r = \tan(\Lambda)\ \tan^{-1}(f_x)$$

$$n_\Theta = \pm 1$$

and pressure coefficients on store fin surfaces are defined as:

$$C_p = -2\phi_x - \phi_r^2 - (1 - M_\infty^2)\ \phi_x^2 \qquad (10)$$

Grid System Arrangement

A five-level, Cartesian/cylindrical, embedded grid arrangement is employed to facilitate treatment of wing/fuselage/pylon/store configurations. Geometry input verification plots and grid system arrangements are shown for the isolated GBU-15-CWW store in Figs. 2 and 3, for a Douglas wing/pylon/store test configuration in Figs. 4 and 5, and for a Nielsen wing/fuselage/pylon/store test configuration in Figs. 6 and 7. These figures supplement the general discussion of grid system arrangement which follows. A detailed description of the automated grid generation procedure can be found in Appendix A.

No provision is made for representing wing or fuselage surfaces in cylindrical grid systems, or for representing store body and fin surfaces in Cartesian grid systems. The pylon surface is modelled in both types of grids. Current grid setup will treat wing/store gaps as small as one store diameter, excluding fins, or one-half store radius, including fins, whichever is larger. Smaller gaps may compromise the grid generation procedure or result in erroneous solutions.

First, a Cartesian global coarse grid is arranged about the entire configuration. This grid is used to impose far field boundary conditions and to compute a coarse wing/fuselage/pylon (i.e., store off) flow field, which in turn provides a starting solution for embedded grid systems. A global coarse grid inner boundary surrounding the store is then defined. Inside this boundary no further global coarse grid computations are performed.

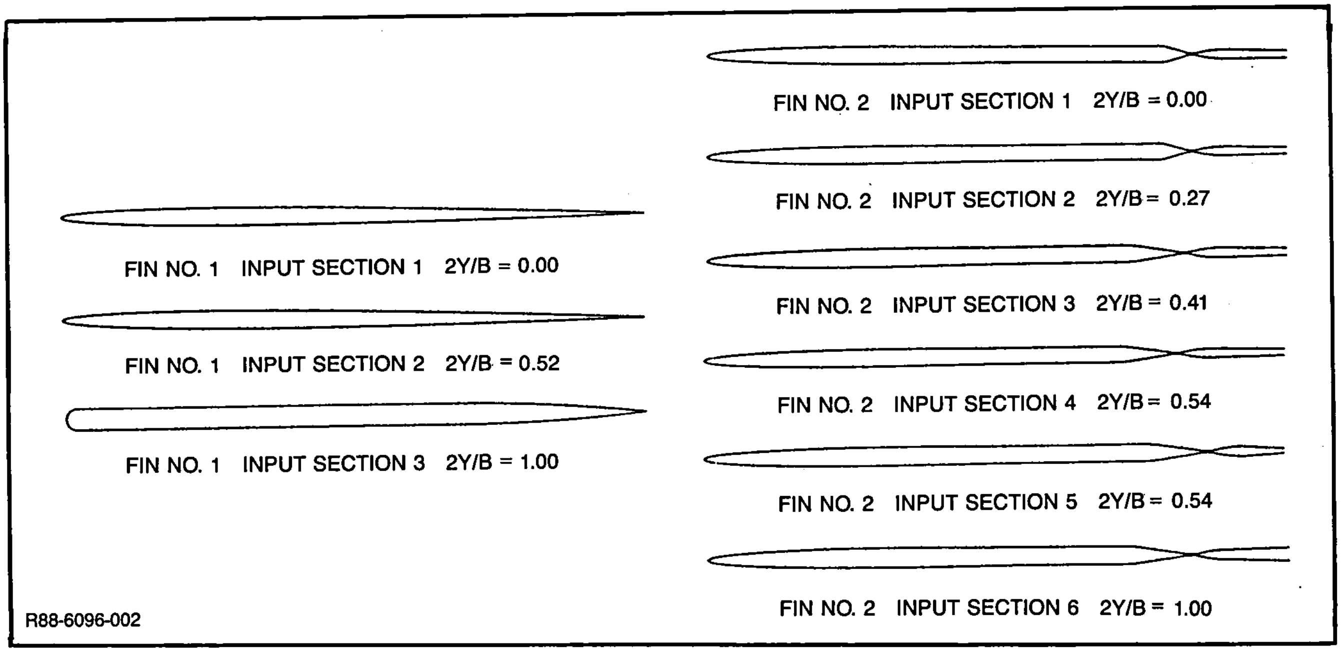

Figure 2 Input Geometry Verification Plots for GBU-15-CWW Store

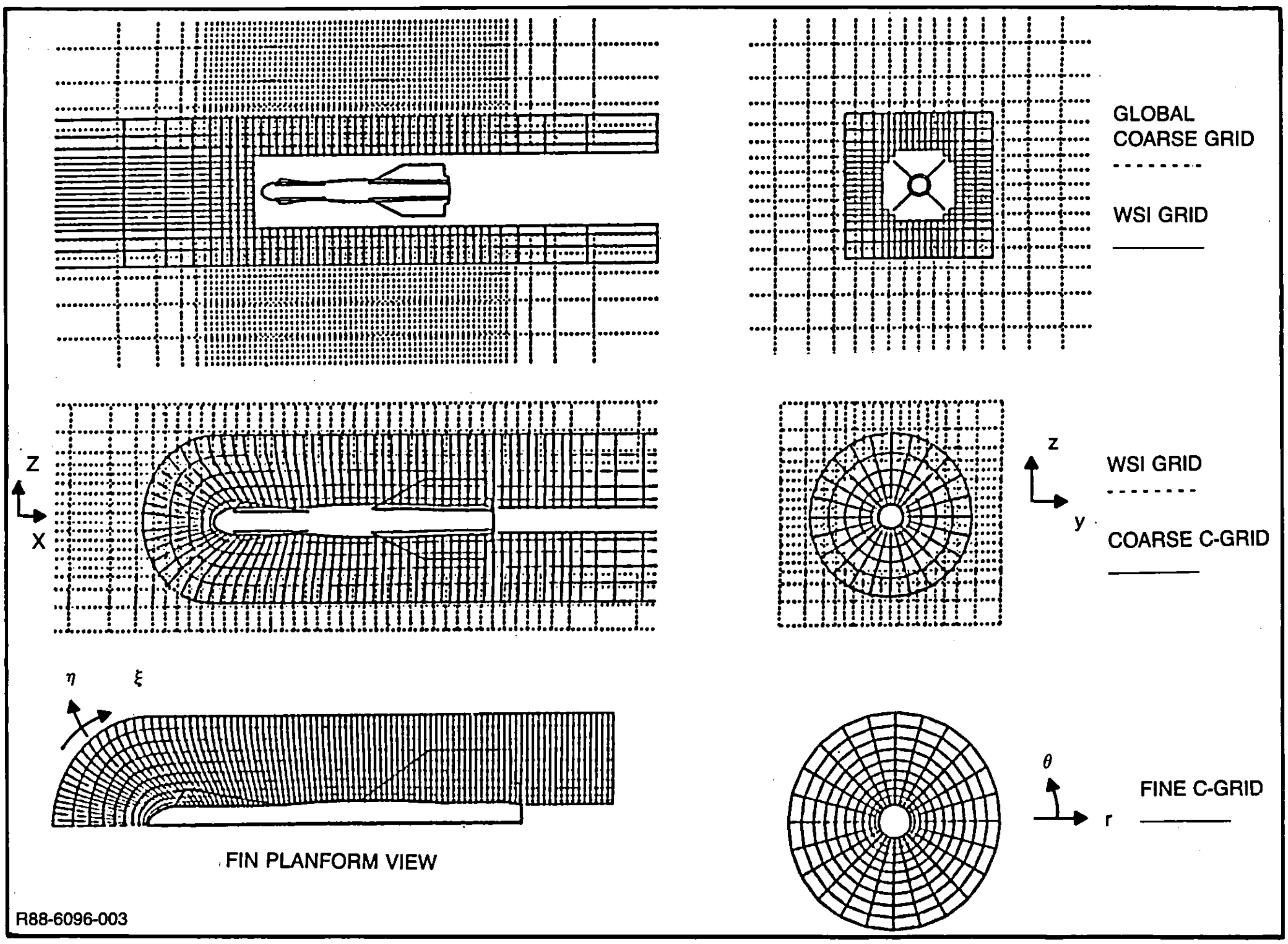

Figure 3 Grid System Arrangement for GBU-15-CWW Store

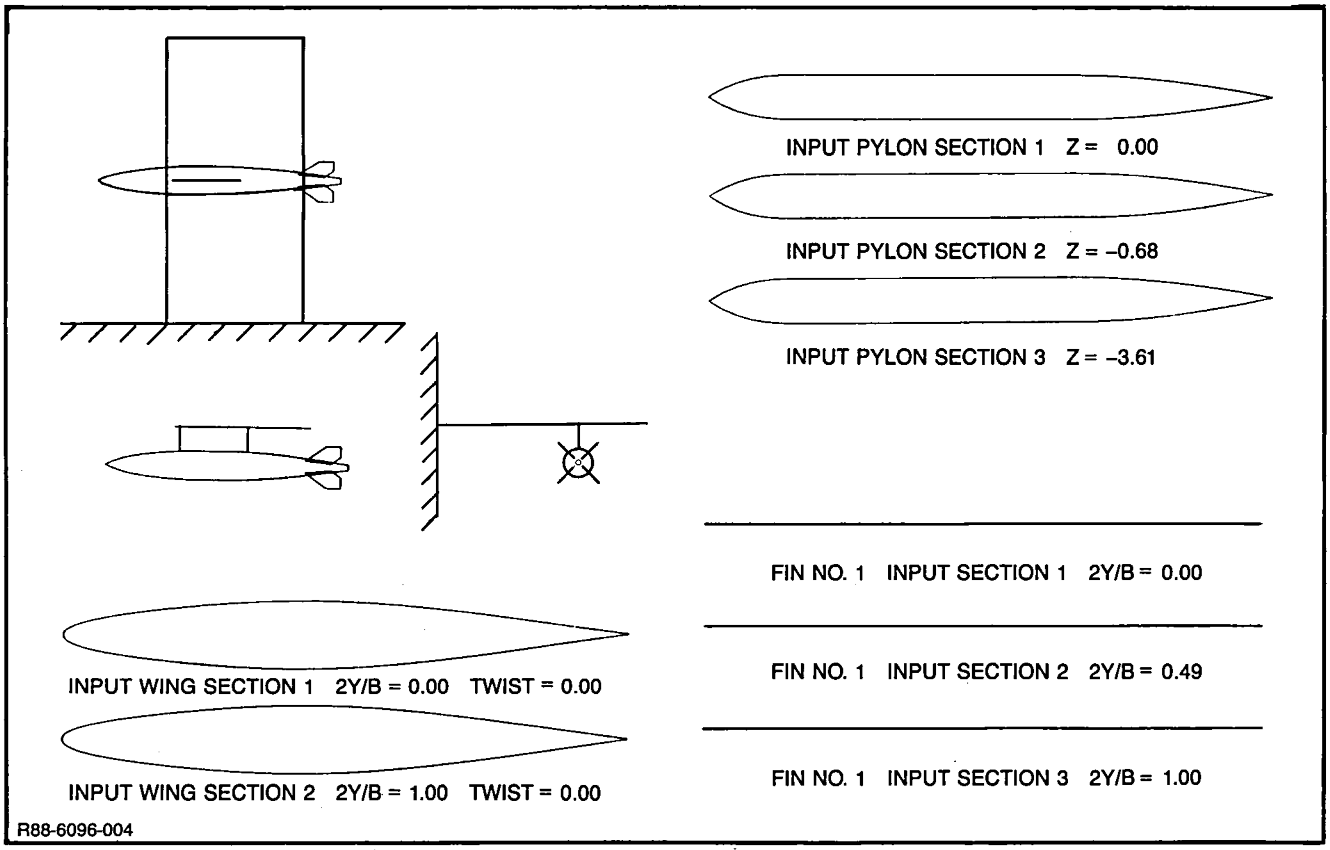

Figure 4 Input Geometry Verification Plots for Douglas Wing/Pylon/Store Configuration

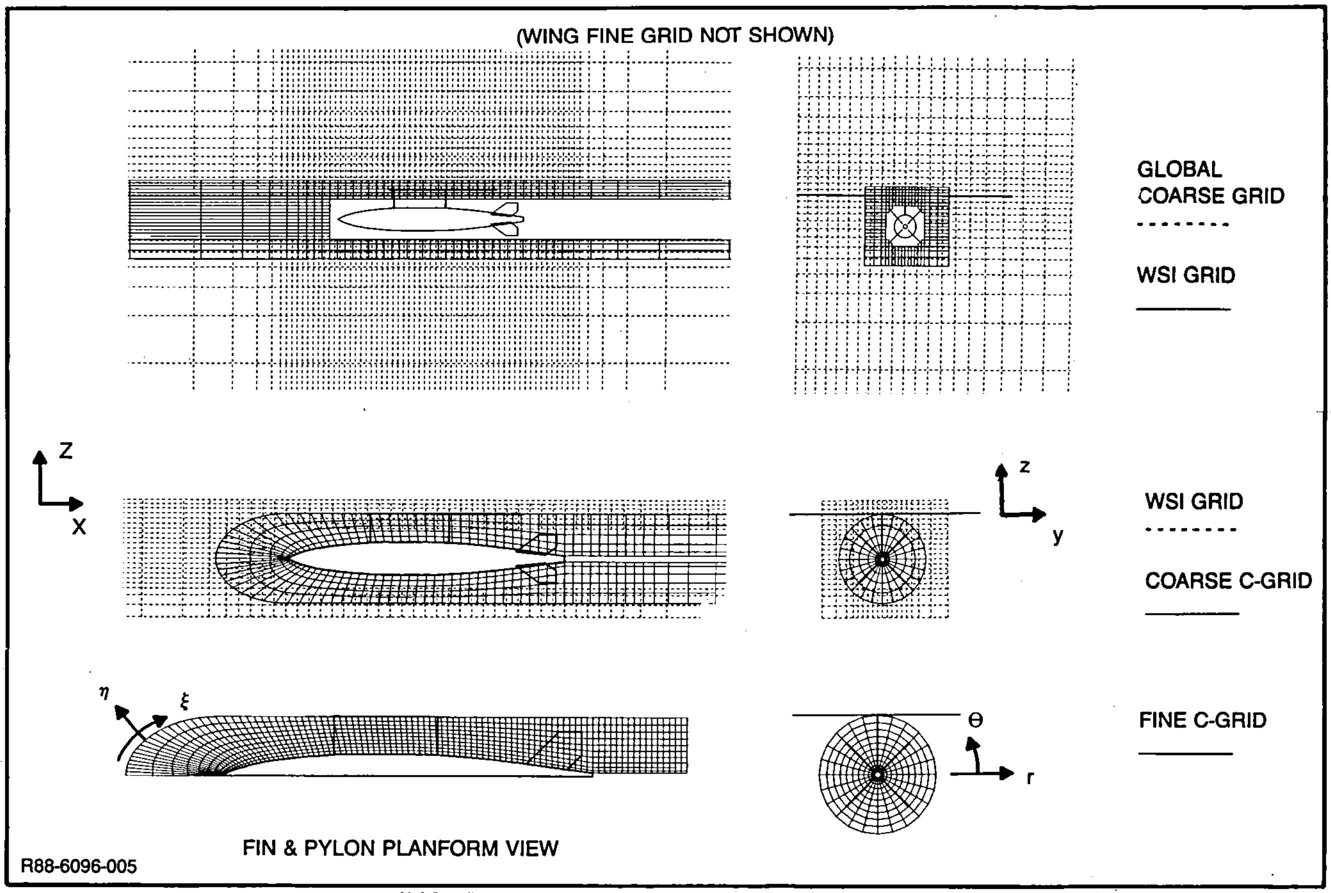

Figure 5 Grid System Arrangement for Douglas Wing/Pylon/Store Configuration

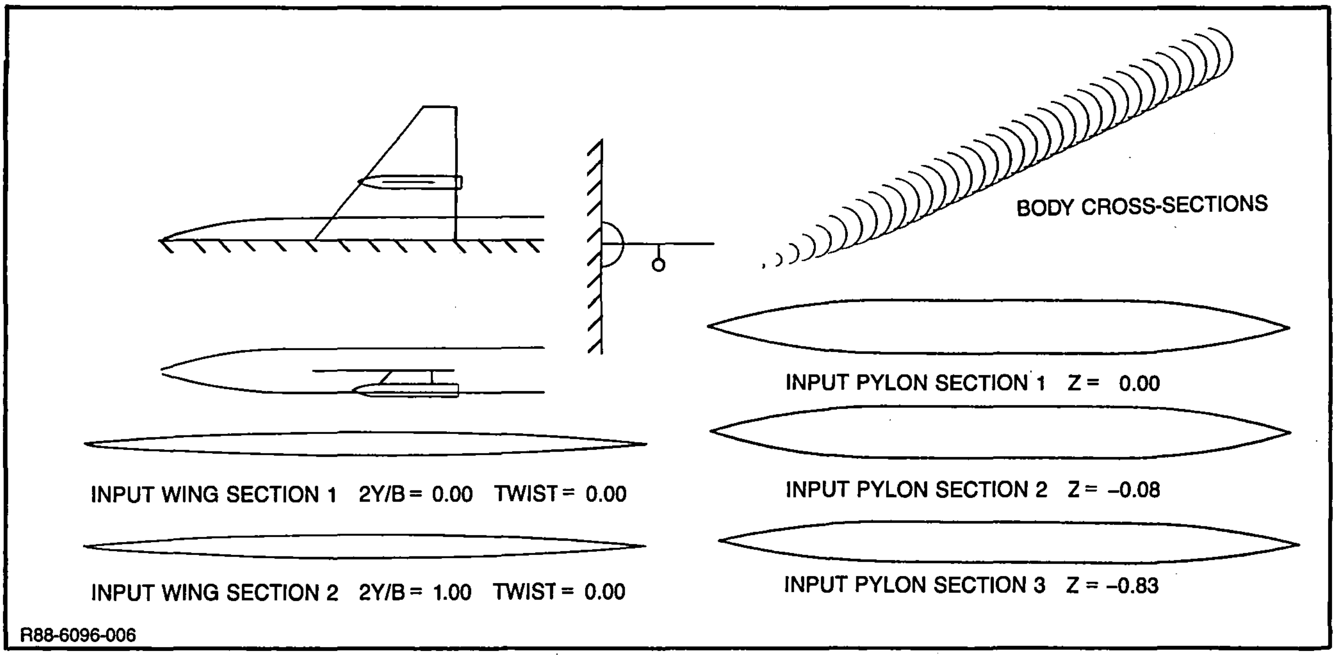

Figure 6 Input Geometry Verification Plots for Nielsen Wing/Fuselage/Pylon/Store Configuration

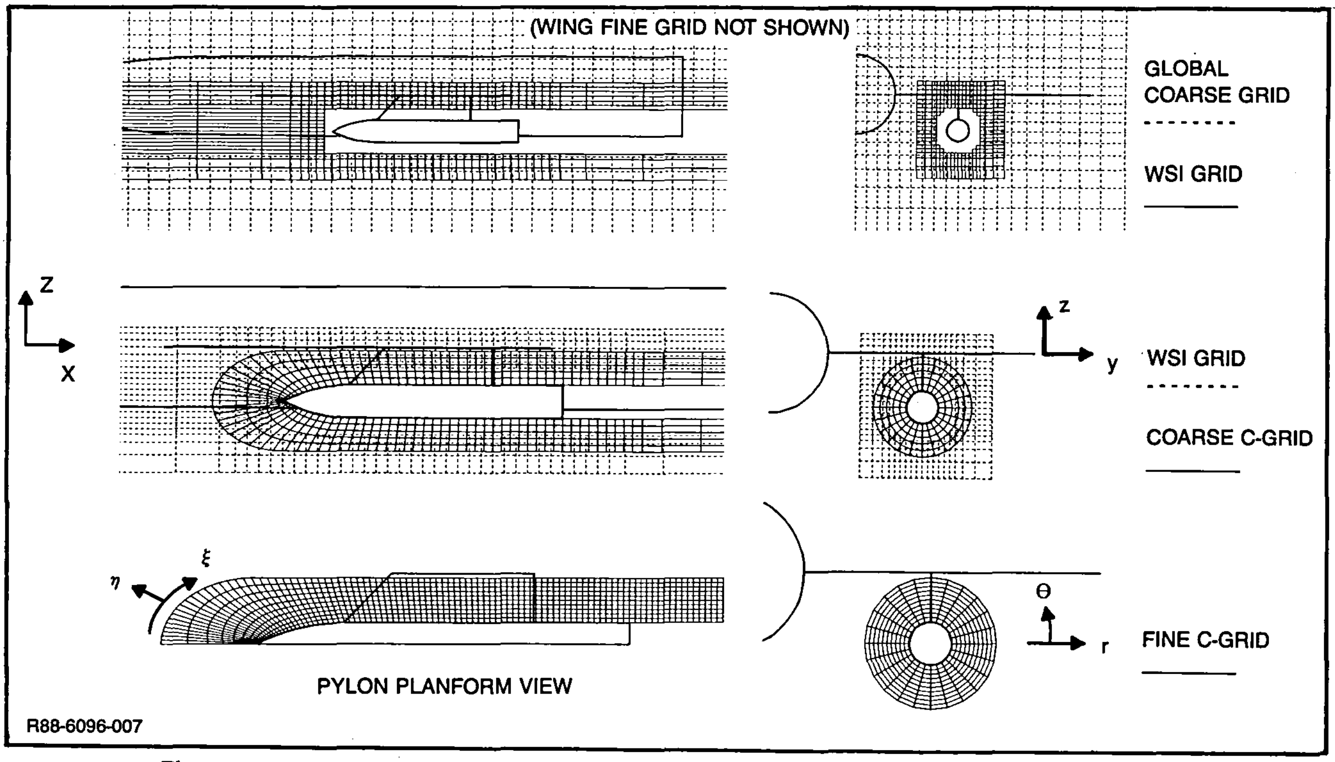

Figure 7 Grid System Arrangement for Nielsen Wing/Fuselage/Pylon/Store Configuration

Next, a Cartesian Wing/Store Interaction (WSI) grid is embedded about the store, within the global coarse grid. This is a medium density grid which functions primarily as a means of communication between Cartesian and cylindrical grid systems. An overlap region is created between the global coarse grid inner boundary and the WSI grid outer boundary, so that each can be updated using flow field information from the other grid. A WSI grid inner boundary surrounds the store (more closely than the global coarse grid inner boundary). Inside this boundary no WSI grid computations are performed.

A coarse cylindrical C-grid is then embedded about the store body, within the WSI grid. The use of a body-conforming grid improves the accuracy of the computed store body flow field. A conformal mapping provides the basic C-grid transformation (Ref. 11):

$$\bar{z} = \ln (1 - \cosh \bar{\zeta}). \tag{11}$$

Stretching and shearing transformations are also employed. An overlap region is created between the WSI grid inner boundary and the coarse C-grid outer boundary, so that each may be updated using information from the other grid. The C-grid is further modified so that constant coordinate grid lines approximate the fin tip vortex streamline locations. This facilitates treatment of fins and their wakes.

As in the basic Transonic Wing-Body Code, an embedded wing fine grid system is used to improve solution accuracy near the wing. In a similar fashion, a fine cylindrical C-grid is embedded within the coarse C-grid, to improve the accuracy of the computed flow field near the store.

For subsonic freestreams ($M_\infty < 1.0$), transformations locate outermost grid boundaries at infinity, where appropriate far field boundary conditions are applied. For supersonic freestreams ($M_\infty \geq 1.0$), outermost grid boundaries are located a finite distance from the configuration, where supersonic inflow, outflow, and radiation-type boundary conditions are employed.

Solution Algorithm

The following discussion gives a general overview of the solution algorithm. A detailed description of the finite difference approximations employed can be found in Appendix B.

At each grid point, finite difference approximations are substituted for terms appearing in the governing flow equations, Eqs. 1 and 2. An upwind, rotated difference scheme (Ref. 12) provides the proper domain of dependence at supersonic points. A variation of this scheme, developed specifically for modified TSD flow equations (Ref. 3), determines the rotation from the coefficients T,U,V rather than from local flow angularities. This greatly enhances the method's numerical stability and accuracy.

As a result, treatment of lower aspect ratio, more highly swept and tapered wings is possible. In conjunction with appropriate inflow, outflow, and radiation-type boundary conditions (Ref. 13), a supersonic freestream capability is also provided. This works well for wing/fuselage combinations, but only limited success was achieved for supersonic treatment of stores.

Communication across embedded grid boundaries is accomplished via Neumann-type boundary conditions for central first derivatives and, where required, upwind second derivatives of the potential in a direction normal to the computational grid boundary. An overlap region is always created between embedded grid boundaries, so that each can be updated using flow field information from the other grid. The desired flow field quantity is obtained from the other grid by linear interpolation between mesh cell corner points. Neumann-type boundary conditions were found to improve code covergence and minimize shock reflections at embedded grid boundaries, relative to Dirichlet-type boundary conditions.

Treatment of wing, fuselage, and pylon surfaces is similar to that found in the basic Transonic Wing-Body Code (Refs. 1,2), with the following exceptions. To retain second order accuracy, pylon surface boundary conditions are imposed in the wing fine grid using a Z-scheme (Ref. 14). To maintain numerical stability at the wing/pylon junction, second order accurate wing and pylon junction boundary conditions are replaced in all grids by a combination of first and second order accurate formulae.

The accuracy of the computed store body flow field is improved by the use of body-conforming grids. First order accurate boundary conditions are used to set potentials on the store body surface. Fin surfaces are treated using a small disturbance, planar approximation similar to that used for the wing and pylon. At a store body/fin or store body/pylon junction, the second order accurate fin or pylon surface boundary condition is replaced by a first order accurate formula. This formula is combined with the store body surface boundary condition, so that a single value of the potential can be set in the junction.

The embedded grid solution process is divided into three phases. Computations during each phase proceed as follows.

A "coarse grid" solution is first obtained for wing/fuselage/pylon (i.e., store off) geometry in the global coarse grid. This initial phase allows for rapid propagation of disturbances and also provides starting flow fields for the other grid systems. Each iteration cycle consists of a global coarse grid relaxation sweep and, for supersonic freestreams, an outer boundary update. For isolated stores, global coarse grid potentials are merely set to zero.

Next, an "intermediate grid" solution is obtained for the complete wing/fuselage/pylon/store geometry. This phase allows for rapid calculation of the store body and fin flow field as well as any airframe/store interference effects. It also provides starting flow fields for the wing and store fine grid systems. First, WSI grid and coarse C-grid potentials are initialized based on the "coarse grid" solution. Each "intermediate grid" iteration cycle then consists of inner and outer grid boundary updates and grid relaxation sweeps for the global coarse grid, WSI grid, and coarse C-grid. After each WSI grid relaxation sweep any global coarse grid wing surface points coincident with the global coarse grid inner boundary are set based on WSI grid values. Potentials at these points are then held fixed during each global coarse grid relaxation sweep.

The third phase consists of the "fine grid" solution process. First, the wing fine grid and fine C-grid are initialized based on the "intermediate grid" solution. Each "fine grid" iteration cycle then includes inner and outer grid boundary updates and grid relaxation sweeps for all grid systems. After each wing fine grid relaxation sweep all global coarse grid and WSI grid wing surface points are set based on wing fine grid values. Potentials at these points are then held fixed during each global coarse grid and WSI grid relaxation sweep. After each fine C-grid relaxation sweep all coarse C-grid store body, store fin, and pylon surface points are set based on fine C-grid values. Potentials at these points are then held fixed during each coarse C-grid relaxation sweep.

Force and Moment Coefficients, Including Viscous Effects

After a solution has been obtained, surface pressures are integrated to yield load distributions and force and moment coefficients. For cases where the wing finite difference boundary layer calculation is not activated, estimated wing upper and lower surface section skin friction coefficients are obtained in the same manner as for the fuselage, using the Prandtl-Schlichting formula (Ref. 15) corrected for compressibility effects:

$$c_{f,ave} = (1 + 0.028\ M_\infty)\ 0.455/[\log\ (Re)]^{2.58} \qquad (12)$$

where the Reynolds number is based on local wing chord.

In general, the pylon surface will not be represented in its entirety in any one grid system. It therefore becomes necessary to piece together pylon coefficient contributions from several grid systems. First, contributions from that portion of the pylon located in the fine C-grid are computed. Next, contributions from that portion of the pylon surface located in the wing fine grid (but not in the fine C-grid) are considered. Similarly, contributions from portions of the pylon surface in the global coarse grid and WSI grid are considered, as required, until the entire pylon surface has been accounted for. Pylon section skin friction coefficients are also estimated using Eq. 12 and a Reynolds number based on local pylon chord.

Store body loads are calculated based on computed inviscid pressure coefficients. A skin friction coefficient for the store body, based on wetted area, is estimated using Eq. 12 and a Reynolds number based on store body length. Fin section skin friction coefficients are estimated using Eq. 12 and a Reynolds number based on local fin chord. Store body viscous crossflow effects (Refs. 16, 17) are also estimated, based on crossflow Reynolds number, flow angularity with respect to the freestream, and store body fineness ratio. This viscous crossflow estimate is strictly valid for isolated store bodies only, since it does not account for fin and/or airframe interference effects.

A detailed description of the computation of force and moment coefficients can be found in Appendix C.

EVALUATION OF RESULTS

Results computed by the TSCLP code for a variety of test cases are evaluated by comparisons with more exact methods and with experimental data. Test cases considered include isolated stores and simple wing/fuselage combinations, as well as complete wing/fuselage/pylon/store configurations. Component interference effects are also examined.

Isolated Stores

Test cases for isolated stores include several body-alone geometries and one which features multiple fore and aft fins. All calculations were made using 200 "medium grid" iterations and 200 "fine grid" iterations.

The first two test cases are the National Transonic Facility (NTF) 5° Calibration Cone at M_∞=0.6 and α=0°, and the Pathfinder I Nosecone at M_∞=0.84 and α=0°. Body shapes appear in Fig. 8. Note the rather sharp nose of the former, and the relatively blunt nose of the latter. The figure compares calculated body pressure distributions with results (Ref. 9) obtained using a two-dimensional (axisymmetric) full potential method. Results compare well for both test cases.

The next test case is the isolated Nielsen generic store at M_∞=0.925 and α=5°. This store is shown in the carriage position in Fig. 6. Calculated body pressure and normal force load distributions for the isolated store are compared to experimental data (Ref. 18) in Fig. 9. Good correlation with data is observed. Note the small, almost imperceptible change in the load distribution due to estimated viscous crossflow effects.

Total integrated normal force and pitching moment coefficients are presented in Table I. Computed inviscid coefficients agree well with slender body theory. Upon integration, estimated viscous crossflow effects are significant and markedly improve the correlation with experiment.

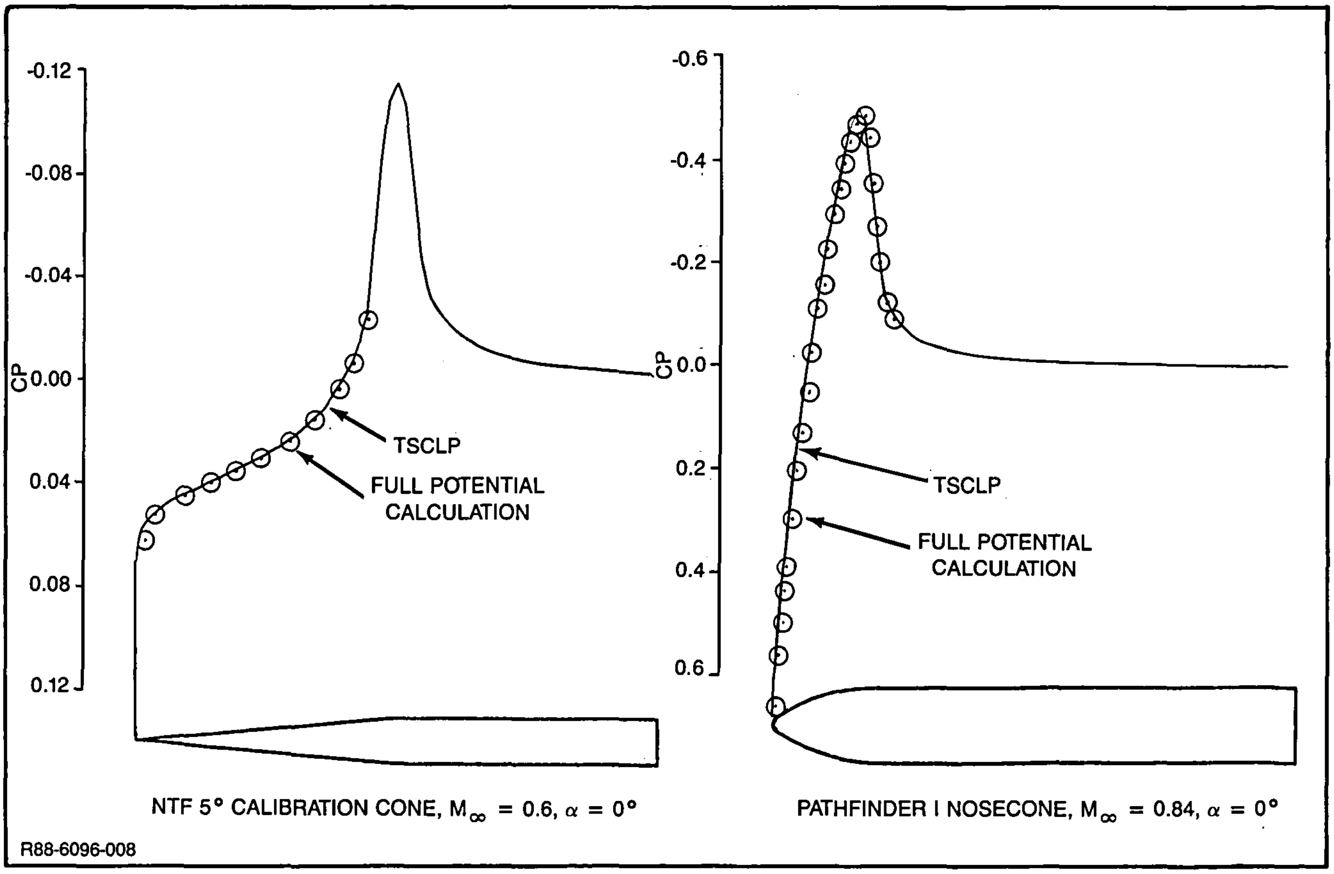

Figure 8 Comparison of Isolated Body Pressure Predictions with Axisymmetric Full Potential Calculations

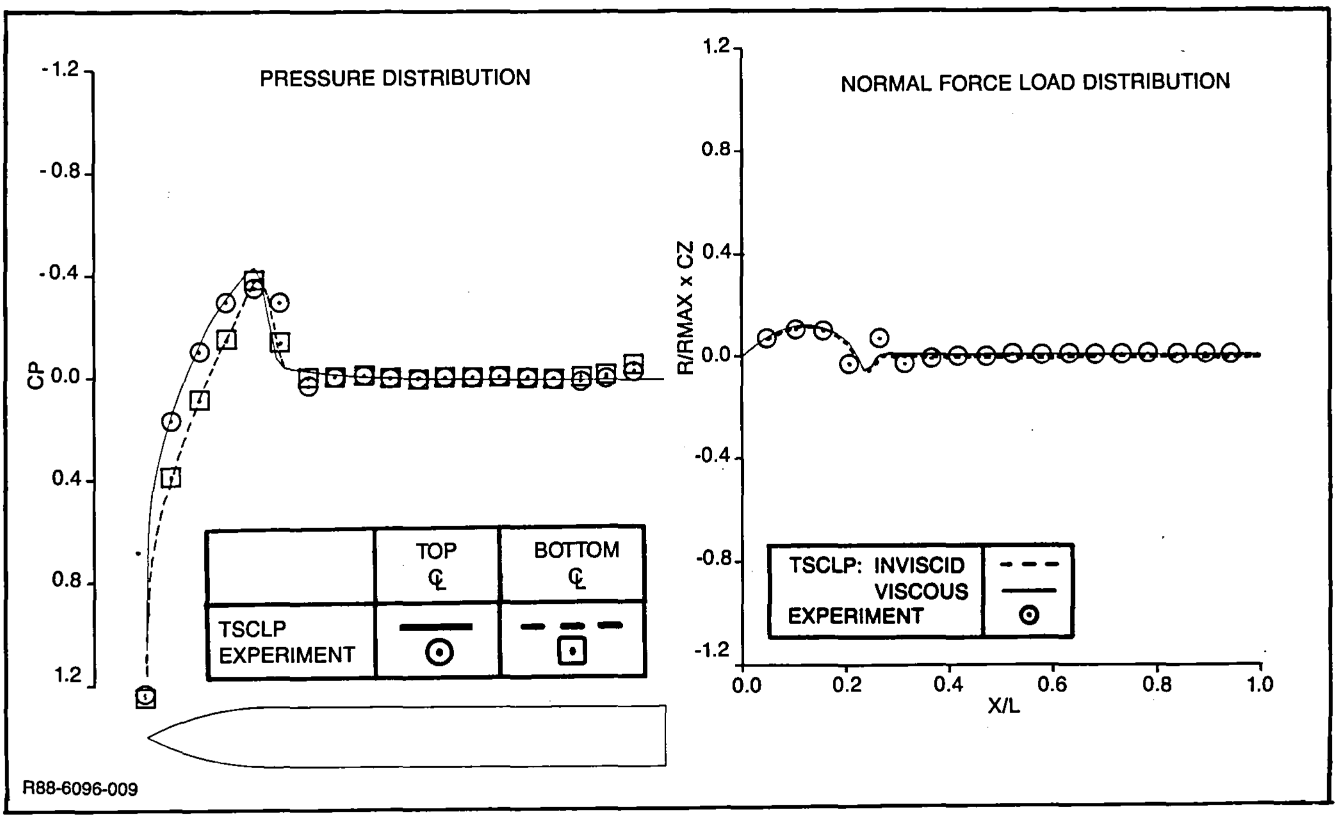

Figure 9 Isolated Nielsen Store: Pressure and Load Distribution Correlations, M_∞ = 0.925, α = 5°

Table I Isolated Nielsen Store: Force and Moment Correlation at M_∞ = 0.925 and α = 5°

	Slender Body Theory	TSCLP (Inviscid)	TSCLP w/Viscous Crossflow	Experiment
C_N	0.175	0.176	0.239	0.221
C_m	0.582	0.578	0.558	0.462

6096-026

Attempts to analyze stores at supersonic speeds met with limited success. Lack of convergence for most cases is attributed to the C-grid relaxation scheme. In the forward portion of this grid, sweeping from the body surface to the grid outer boundary is commensurate to marching in an upstream direction. To compound the situation, grid stretching in this region is rather severe. Further development is required for reliable treatment of stores at supersonic speeds.

A converged solution was, however, obtained for a NACA research body at M_∞=1.0 and α=8°. The body shape appears in Fig. 10, which compares calculations at M_∞=0.99 and M_∞=1.00 to experimental data (Ref. 19) at M_∞=1.0. Corresponding body normal force correlations appear in Table II. Predictions agree fairly well with data. Despite the difficulties mentioned earlier, these calculations demonstrate that the supersonic inflow, outflow, and radiation-type boundary conditions implemented are indeed viable.

Table II NACA RM L53H04 100-inch Body: Normal Force Correlation at M_∞ = 1.0 and α = 8°

	Slender Body Theory	TSCLP (Inviscid) M_∞ = 0.99/1.00	TSCLP w/Viscous Crossflow M_∞ = 0.99/1.00	Experiment
C_N	0.074	0.073/0.075	0.160/0.162	0.190

6096-027

The final isolated store test case is the GBU-15-CWW store featuring multiple fore and aft fins. Calculations were made at M_∞=0.95 and α=6° for several fin arrangements. Calculated pressure distributions are compared to experimental data (Ref. 20) in the following figures:

Fig. 11: Body pressures, wings and canards off
Fig. 12: Body pressures, wings and canards on
Fig. 13: Wing pressures, canards off
Fig. 14: Wing pressures, canards on
Fig. 15: Canard pressures.

Overall, correlation with data is very good. A forebody double shock system which is predicted for the fins off arrangement is not present in the data. This discrepancy affects the canard pressure comparisons as well, although the latter are fairly good considering the sparse number of grid points used to represent the canard surfaces (see Fig. 3). The effect of the fins on the body is accurately predicted, as is the downwash effect of the canards on the wings.

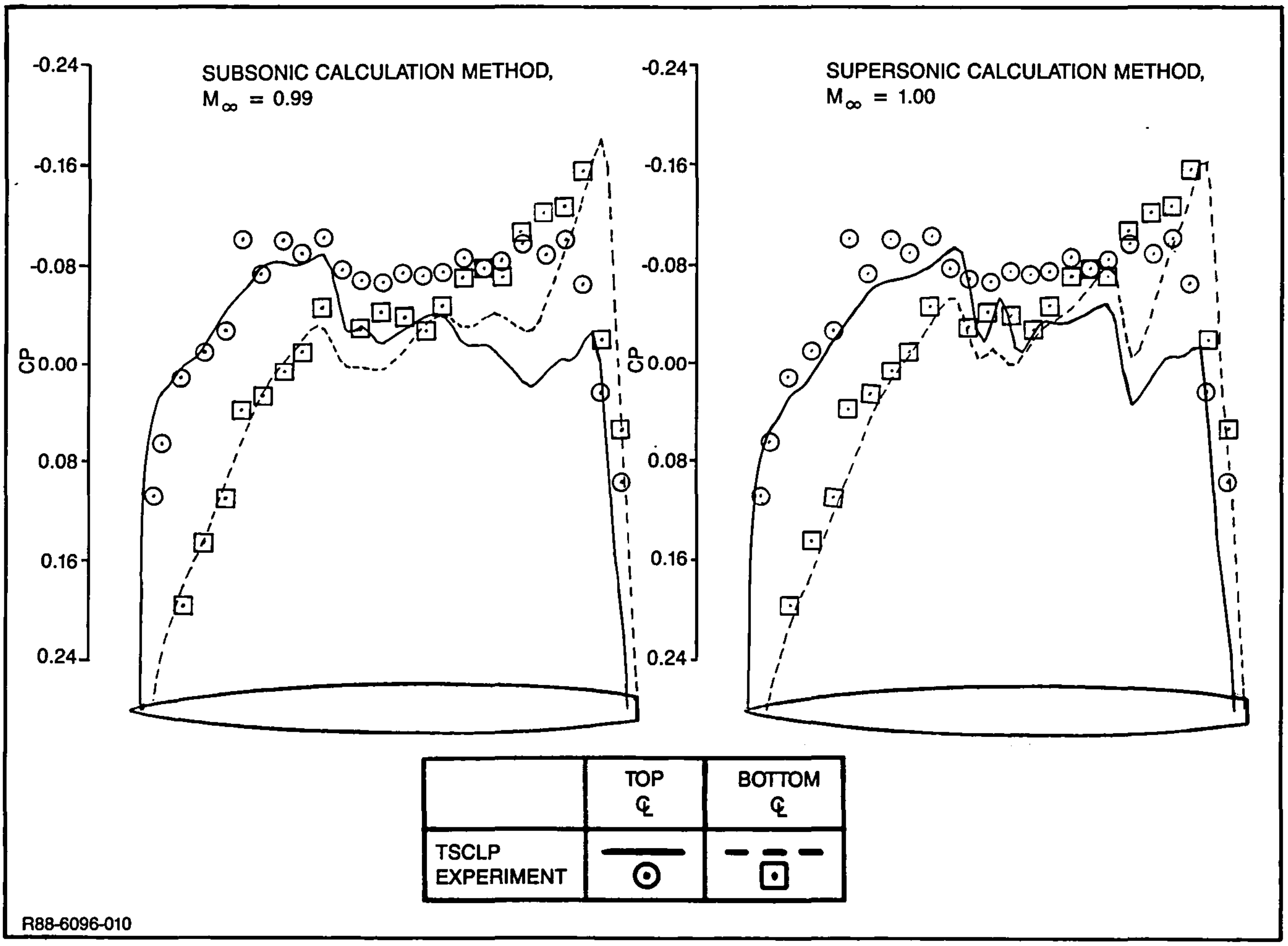

Figure 10 NACA RM L53H04 100-inch Body: Pressure Distribution Correlations, M_∞ = 1.0, α = 8°

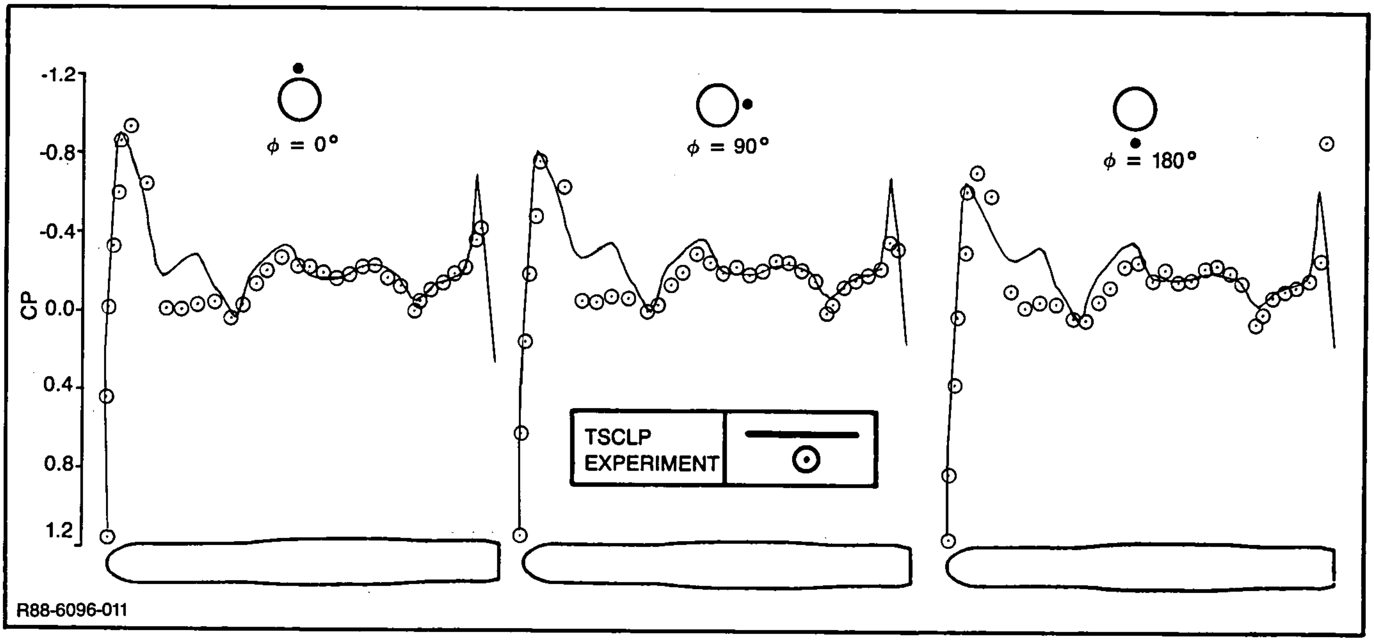

Figure 11 GBU-15-CWW Store: Body Pressure Distribution Correlations, Wings and Canards Off, M_∞ = 0.95, α = 6°

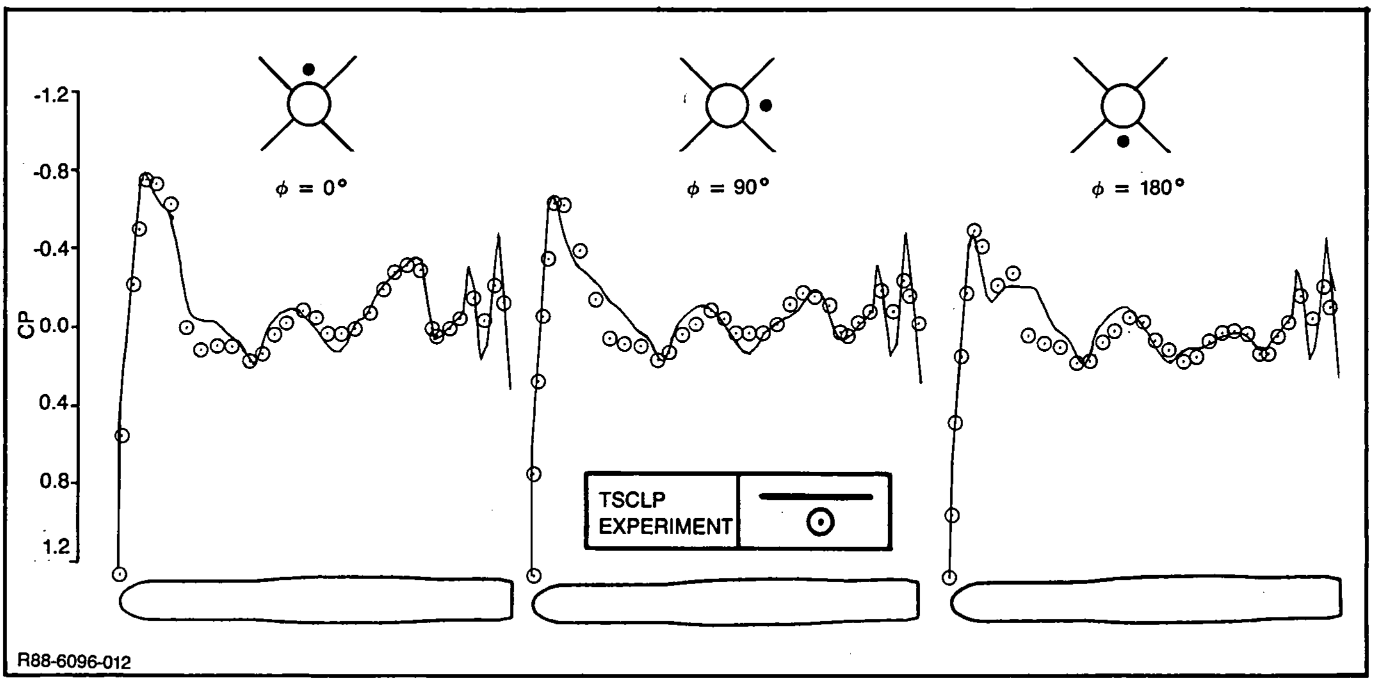

Figure 12 GBU-15-CWW Store: Body Pressure Distribution Correlations, Wings and Canards On, M_∞ = 0.95, α = 6°

Total integrated normal force and pitching moment coefficients for the GBU-15-CWW store are compared with data in Fig. 16. Results are shown as a buildup of body, wing, and canard components, and include body viscous crossflow effects. The underprediction of wing-on normal force is attributed to sparse wing grid point

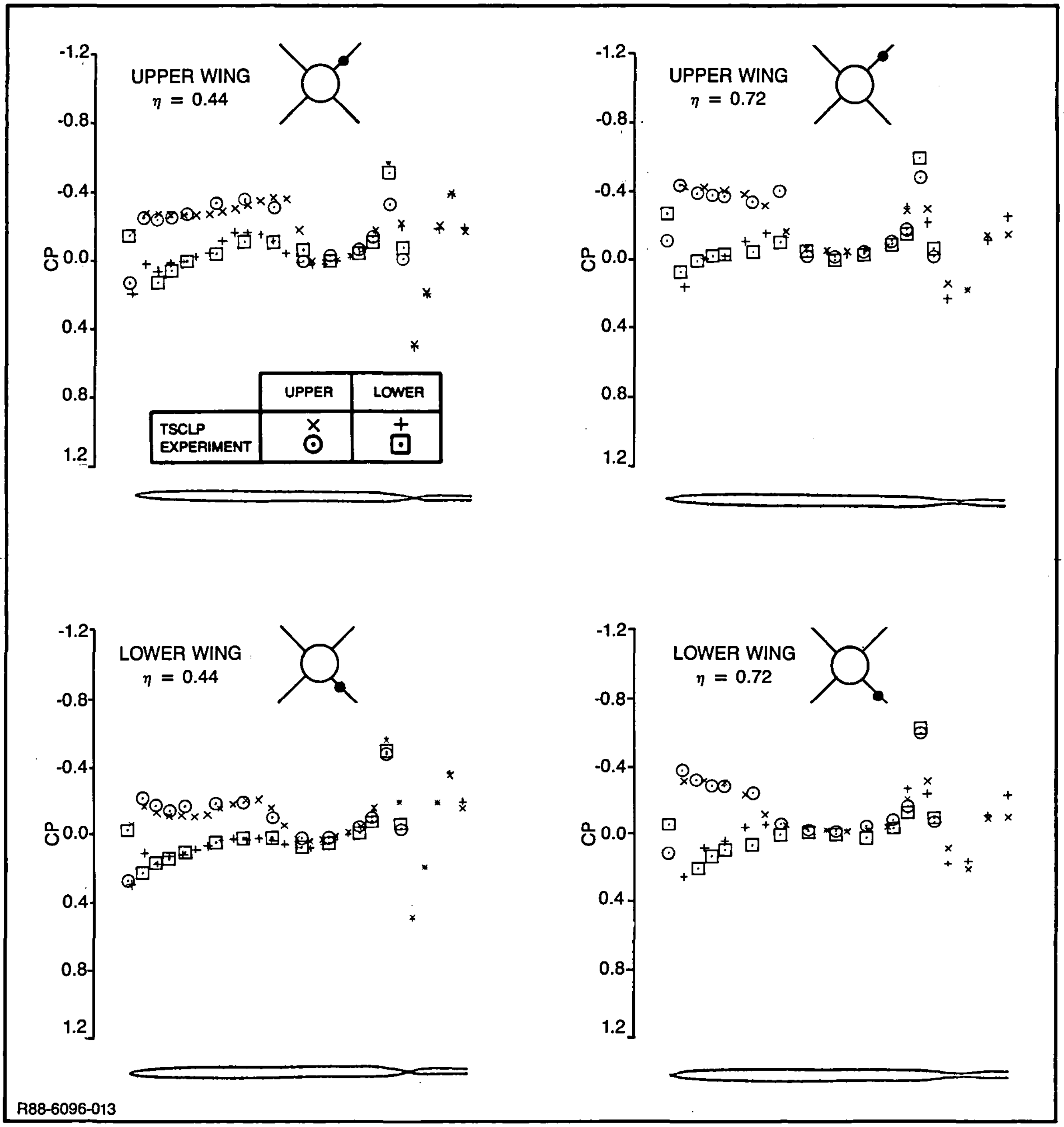

Figure 13 GBU-15-CWW Store: Wing Pressure Distribution Correlations, Canards Off, M_{∞} = 0.95, α = 6°

distribution and to a not yet fully converged solution (complete convergence requires several times the number of iteration cycles typically used for the present, engineering calculations), as well as to flow phenomena not modelled by the governing flow equations. Canard normal force and pitching moment increments are again indicative of their downwash effect on the wings, and are properly predicted.

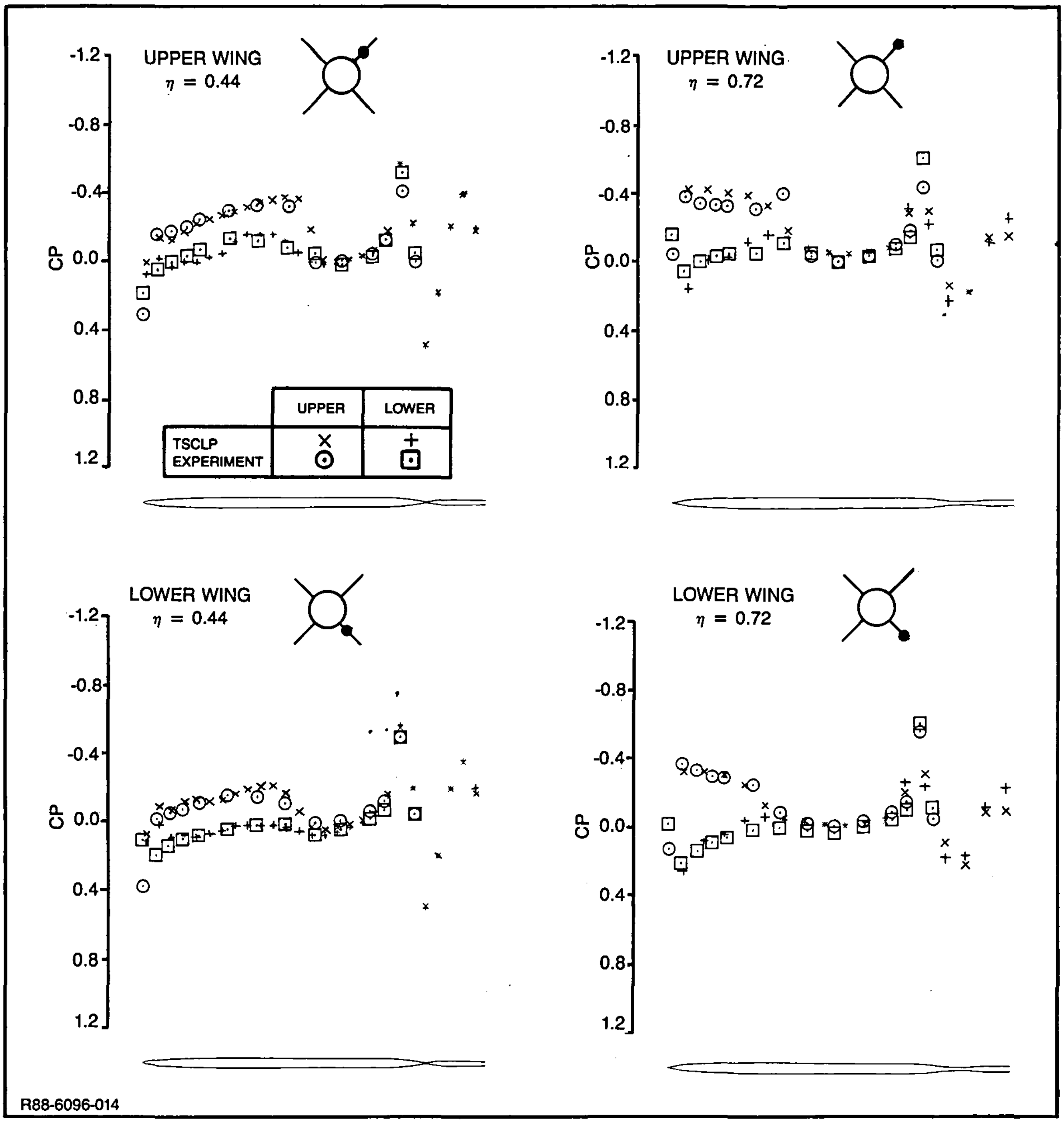

Figure 14 GBU-15-CWW Store: Wing Pressure Distribution Correlations, Canards On, M_∞ = 0.95, α = 6°

Store Carriage Configurations

Results for two store carriage configurations are evaluated by comparisons with experimental data. All calculations were made using 200 "coarse grid" iterations, 200 "medium grid" iterations, and 200 "fine grid" iterations. Since no boundary layer computations are provided for pylon and store surfaces, those for the wing were not employed. Store characteristics do, however, include the simple estimate of body viscous crossflow effects.

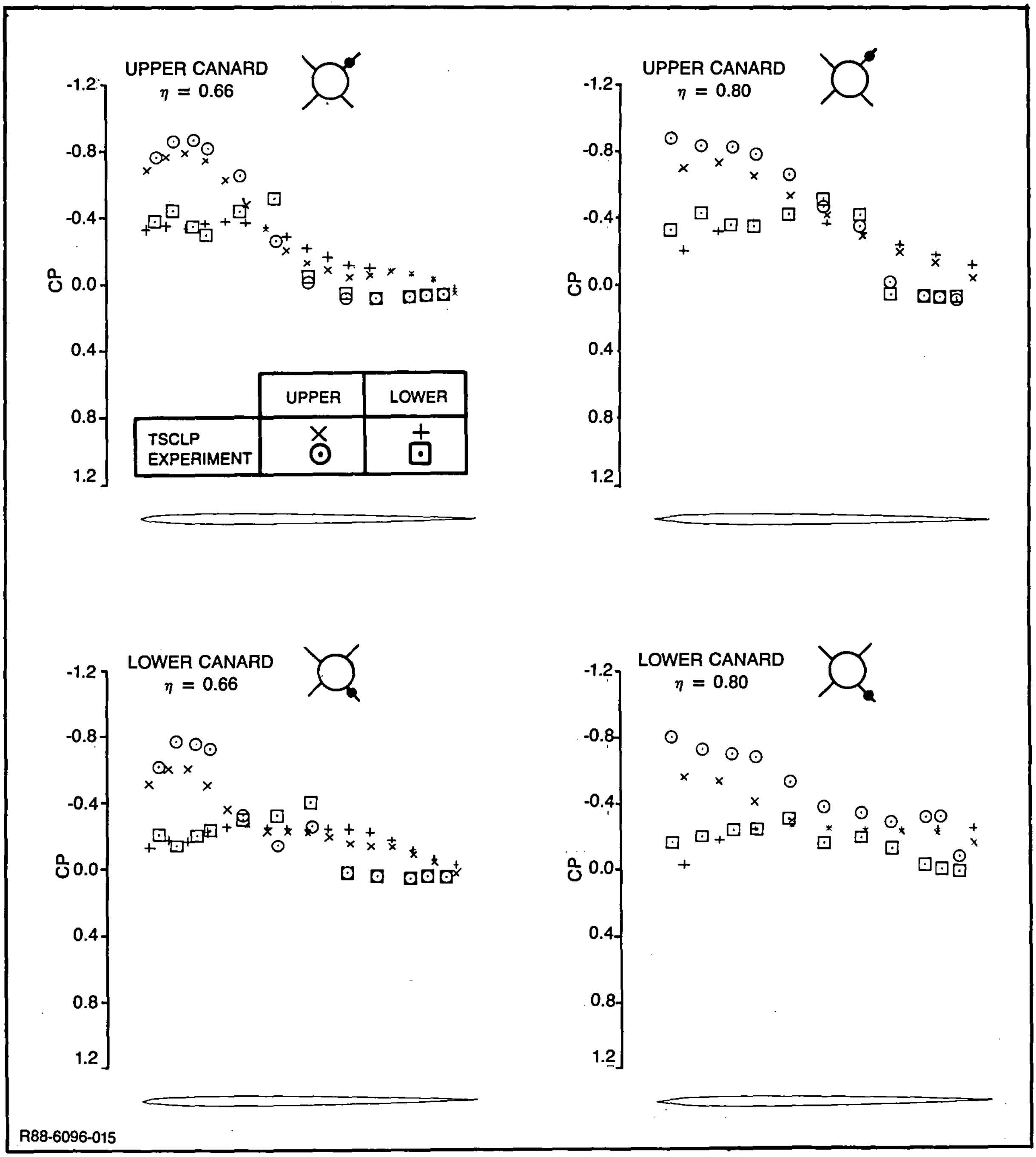

Figure 15 GBU-15-CWW Store: Canard Pressure Distribution Correlations, M_∞ = 0.95, α = 6°

The first store carriage test case is the Douglas wing/pylon/store configuration shown in Fig. 4. Although no store surface pressure or loads data is available, wing surface pressure data obtained at a span station in the vicinity of the pylon (Ref. 21) permits an evaluation of computed results. Correlations for the isolated wing and for the complete wing/pylon/store combination at M_∞=0.75 and α=4° appear in Fig. 17.

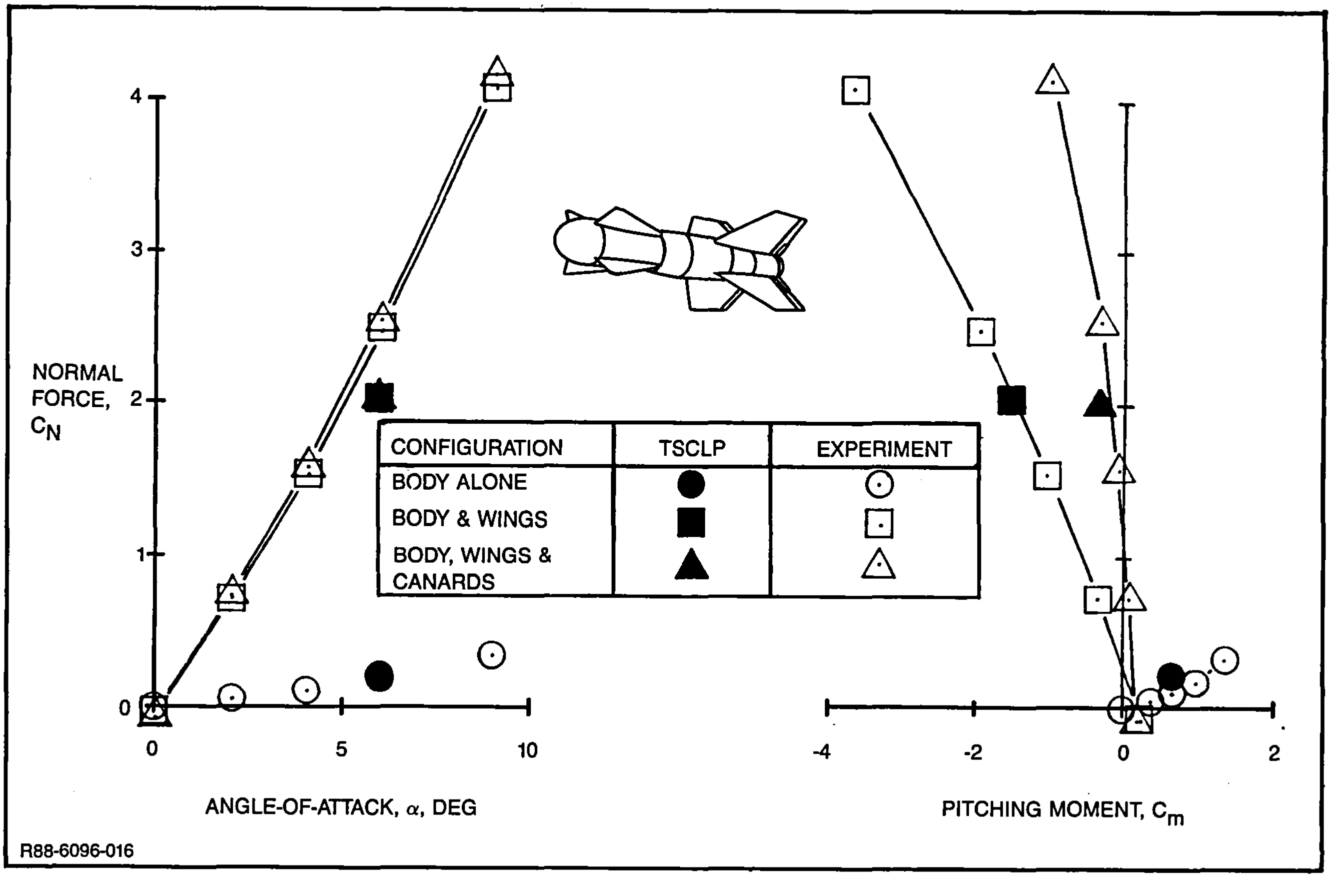

Figure 16 GBU-15-CWW Store: Force and Moment Correlation, M_∞ = 0.95

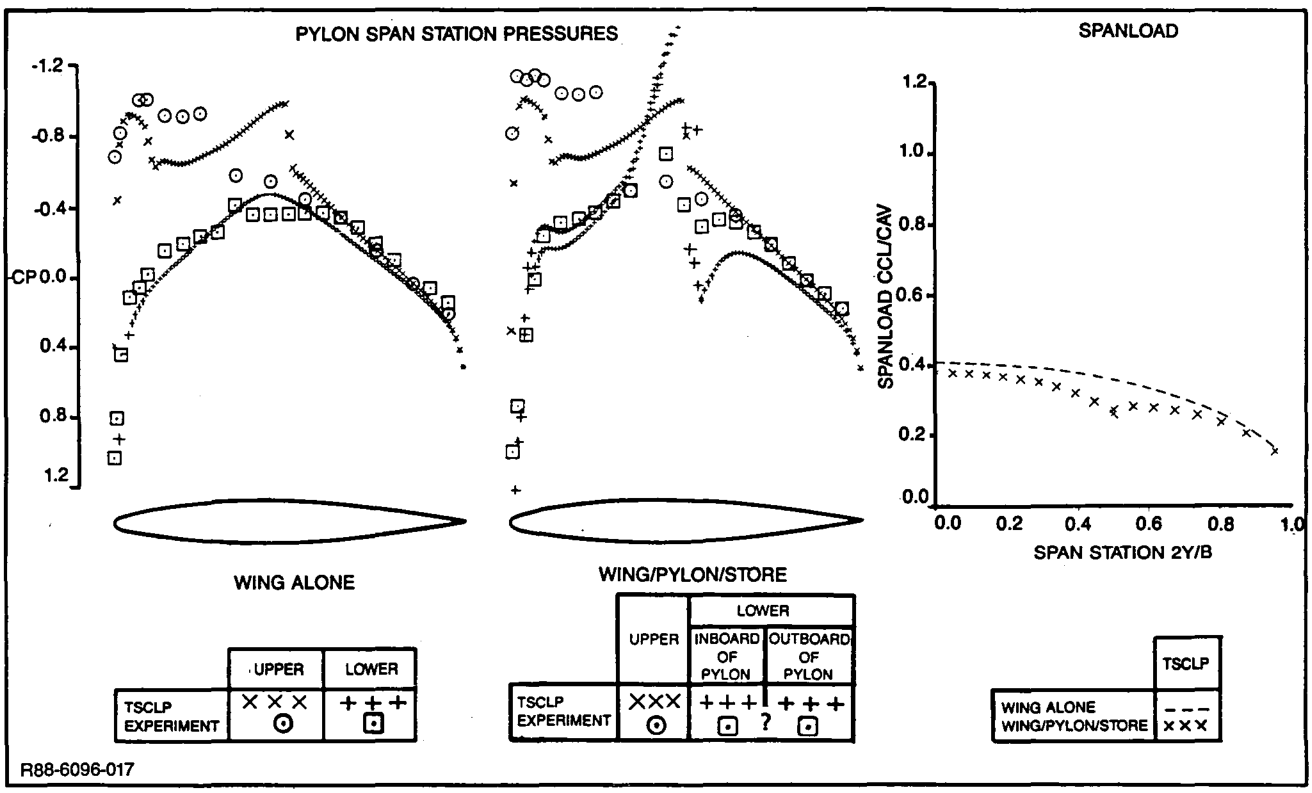

Figure 17 Douglas Wing/Pylon/Store Configuration: Wing Pressure Distribution Correlations and Spanload Comparison, M_∞ = 0.75, α = 4°

Even for the isolated wing, correlation of pressures on the upper surface is poor. Airfoil section analyses using the more sophisticated 2-D GRUMFOIL method (Ref. 22) gave similar predictions, suggesting that test anomalies, rather than flow simulation inaccuracies, are to blame. Nevertheless, the predicted and measured effect of the pylon and store on wing upper surface pressures is a more pronounced leading edge expansion.

Correlation with data in Fig. 17 is better on the wing lower surface. The pylon leading edge compression and subsequent expansion propagate onto the wing lower surface, as do the pylon trailing edge expansion and recompression. These effects occur in the presence of an overall acceleration through the converging/diverging region created by the wing and store. The very large expansion and strong shock predicted at the pylon trailing edge closure occur in the data to a lesser degree, possibly due to viscous effects and/or flow separation which have not been modelled.

Computed wing spanload distributions are also shown in Fig. 17. The combined effect of pylon and store is a marked decrease in wing loading which is greatest at the wing/pylon junction itself. The side force carried on the pylon appears as a discontinuity in the wing spanload.

The second store carriage test case considered is the Nielsen wing/fuselage/pylon/store configuration shown in Fig. 6. Results were computed at M_∞=0.925 and α=5° for isolated wing/fuselage and store components as well as for the wing/fuselage/pylon and wing/fuselage/pylon/store combinations. Experimental data (Ref. 18) is available for fuselage and store components only.

Fuselage bottom centerline pressure distribution correlations appear in Fig. 18. For the wing/fuselage configuration, the wing lower surface pressure field propagates onto the fuselage bottom centerline as expected. With the pylon present this effect is enhanced slightly, and even more so with both pylon and store present. Predictions correlate well with data.

Store surface pressure correlations are presented in Fig. 19. Overall, agreement is good. While predicted expansions and compressions are slightly larger than those present in the data (as noted previously for the Douglas test configuration), the strong store/airframe interactions are properly predicted.

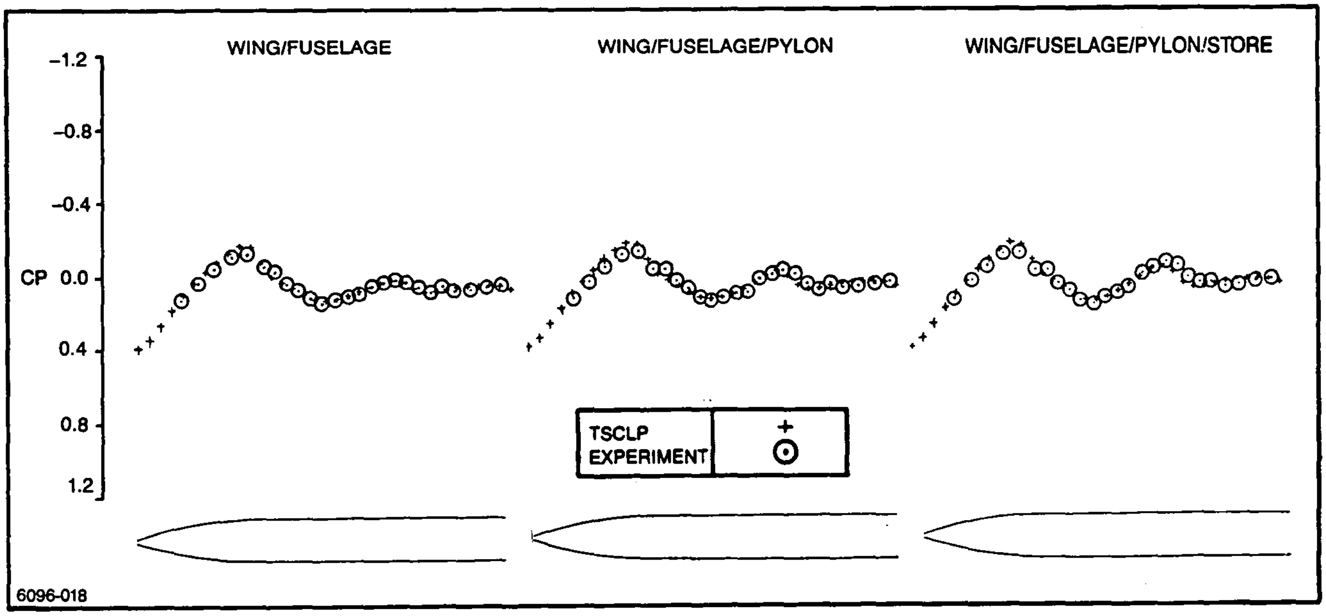

Figure 18 Nielsen Wing/Fuselage/Pylon/Store Configuration: Fuselage Bottom Centerline Pressure Distribution Correlations, M_∞ = 0.925, α = 5°

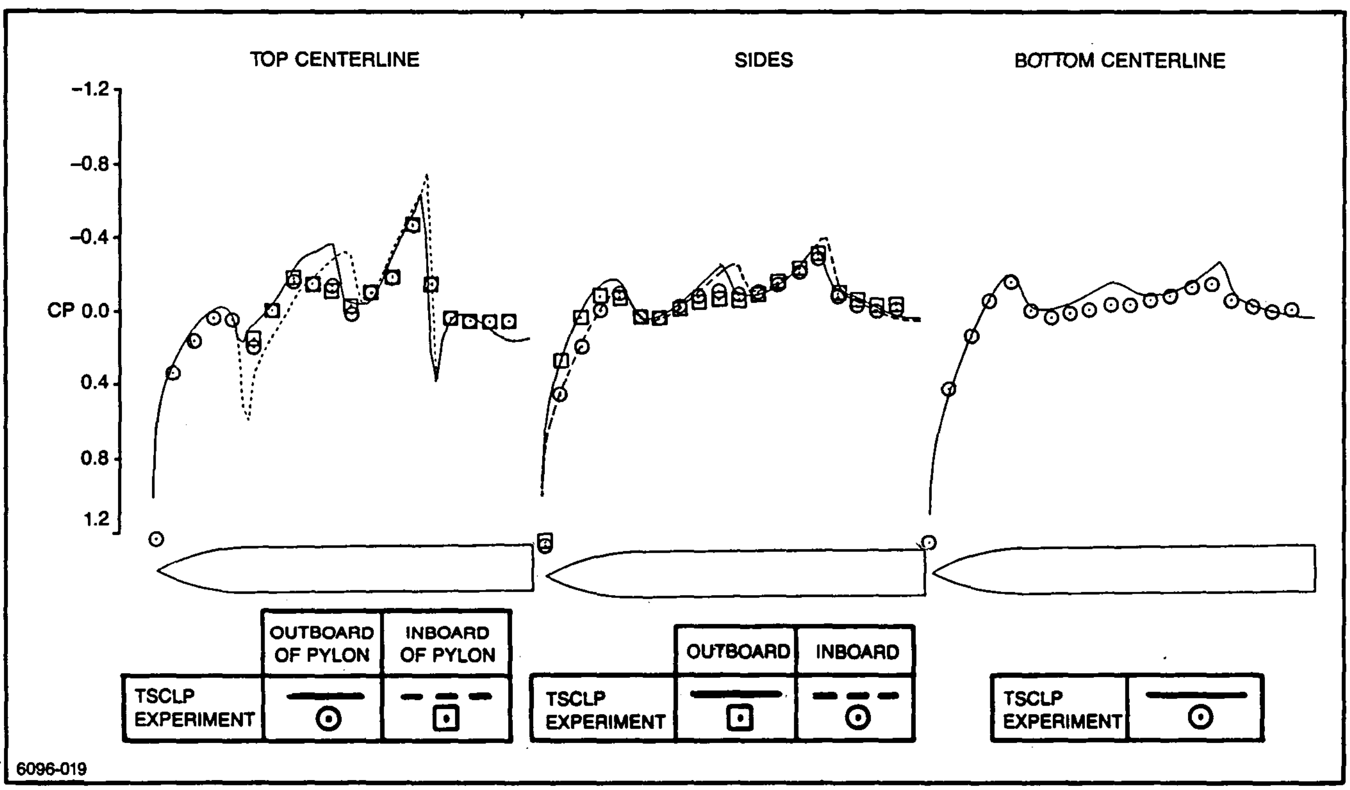

Figure 19 Nielsen Wing/Fuselage/Pylon/Store Configuration: Store Pressure Distribution Correlations, M_∞ = 0.925, α = 5°

Pylon-mounted store axial load distribution correlations are shown in Fig. 20. Good correlation is shown for both normal force and side force load distributions, except for anomalies in predicted side force in the vicinity of the pylon and wing trailing edges. These anomalies are attributed to small misalignments of predicted inboard/outboard pylon and wing trailing edge shock locations (see Fig. 19). Unfortunately, relatively large loads result from rather small differences in surface pressures. Modelling of viscous effects and/or flow separation might correct this computational deficiency.

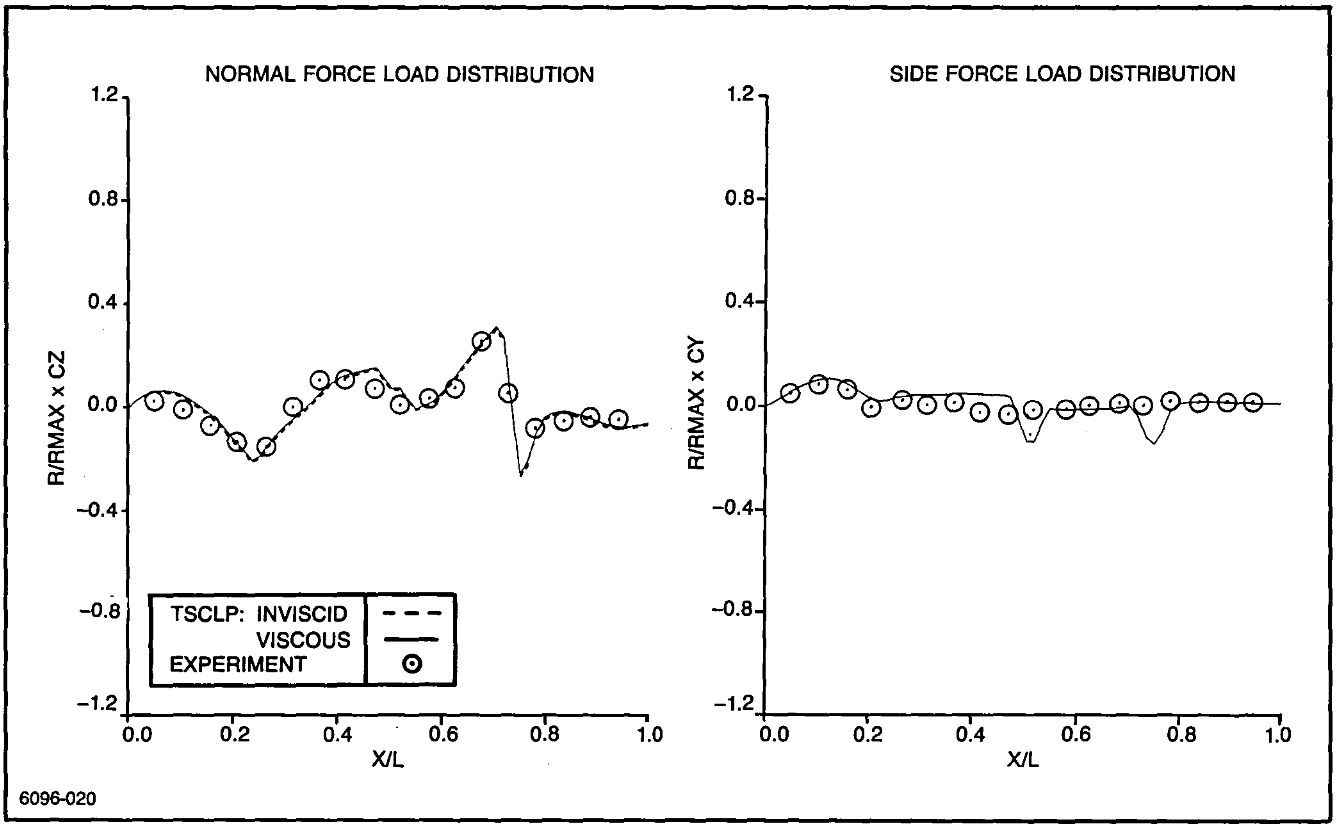

Figure 20 Nielsen Wing/Fuselage/Pylon/Store Configuration: Store Load Distribution Correlations, M_∞ = 0.925, α = 5°

Incremental forces and moments for the pylon-mounted store, relative to the isolated store, appear in Table III. While qualitatively correct, the predicted incremental effects of the airframe on the store lack the desired accuracy. Again, modelling of viscous effects and/or flow separation might improve predictions.

Table III Nielsen Wing/Fuselage/Pylon/Store Configuration: Correlation of Store Incremental Forces and Moments (Relative to Isolated Store) at M_∞ = 0.925 and α = 5°

	TSCLP	Experiment
ΔC_N	-0.126	-0.063
ΔC_m	-0.510	-0.712
ΔC_Y	0.158	0.190
ΔC_n	-0.694	-0.294

6096-028

The Nielsen wing/fuselage/pylon/store configuration was tested at supersonic, as well as subsonic, Mach numbers. Although limited success was achieved for supersonic treatment of stores, calculations for this configuration did converge, possibly because the underwing store is in a region of reduced, lower Mach number flow. Results computed at M_∞=1.1 and α=5° are shown in Figs. 21-23.

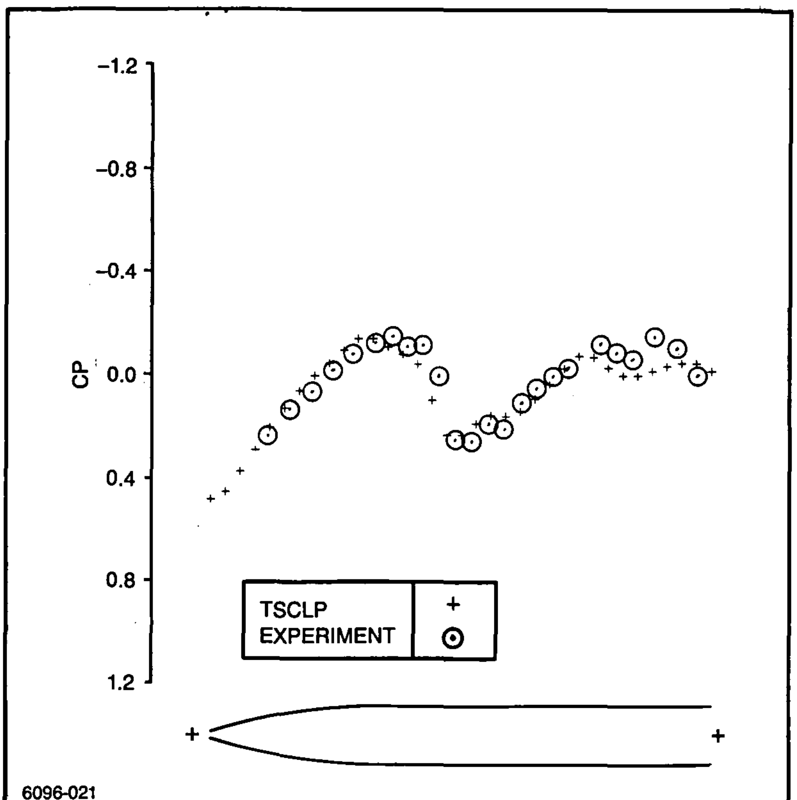

Figure 21 Nielsen Wing/Fuselage/Pylon/Store Configuration: Fuselage Bottom Centerline Pressure Distribution Correlation, M_∞ = 1.1, α = 5°

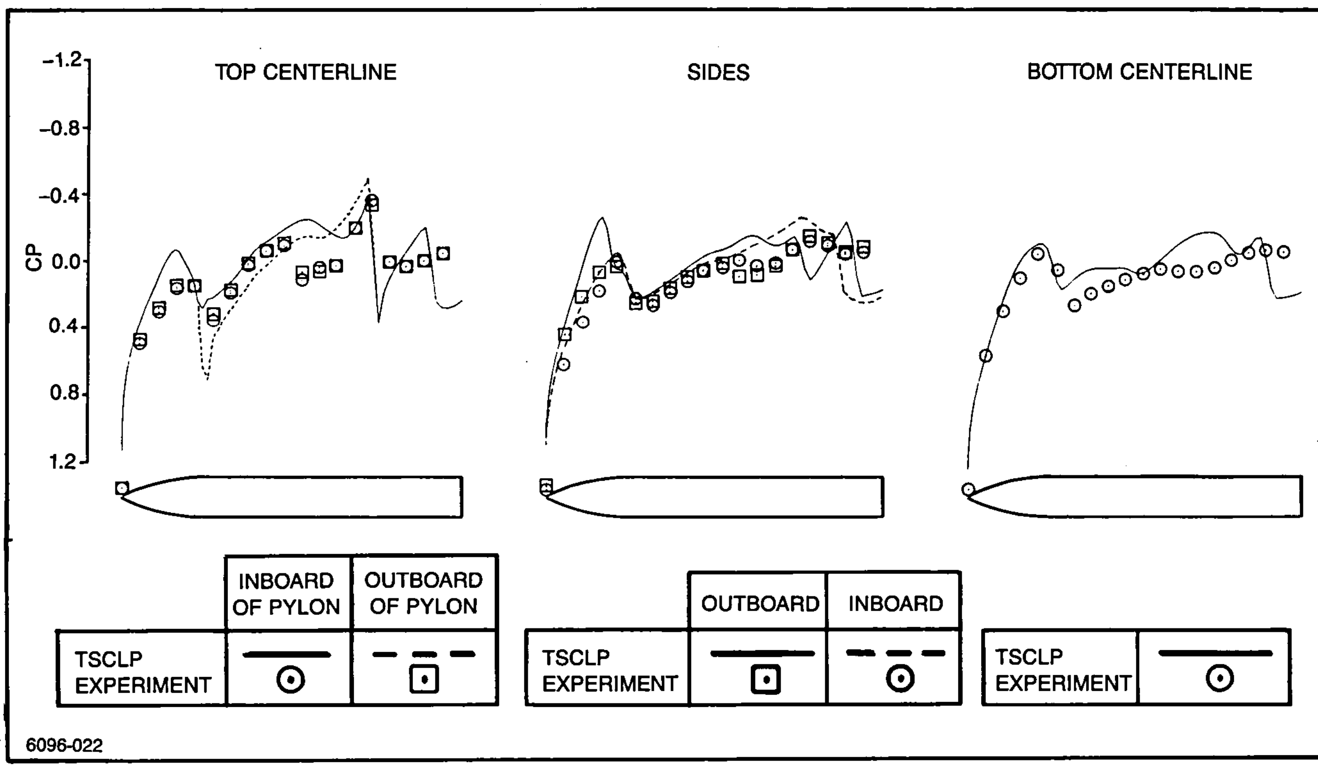

Figure 22 Nielsen Wing/Fuselage/Pylon/Store Configuration: Store Pressure Distribution Correlations, $M_\infty = 1.1$, $\alpha = 5°$

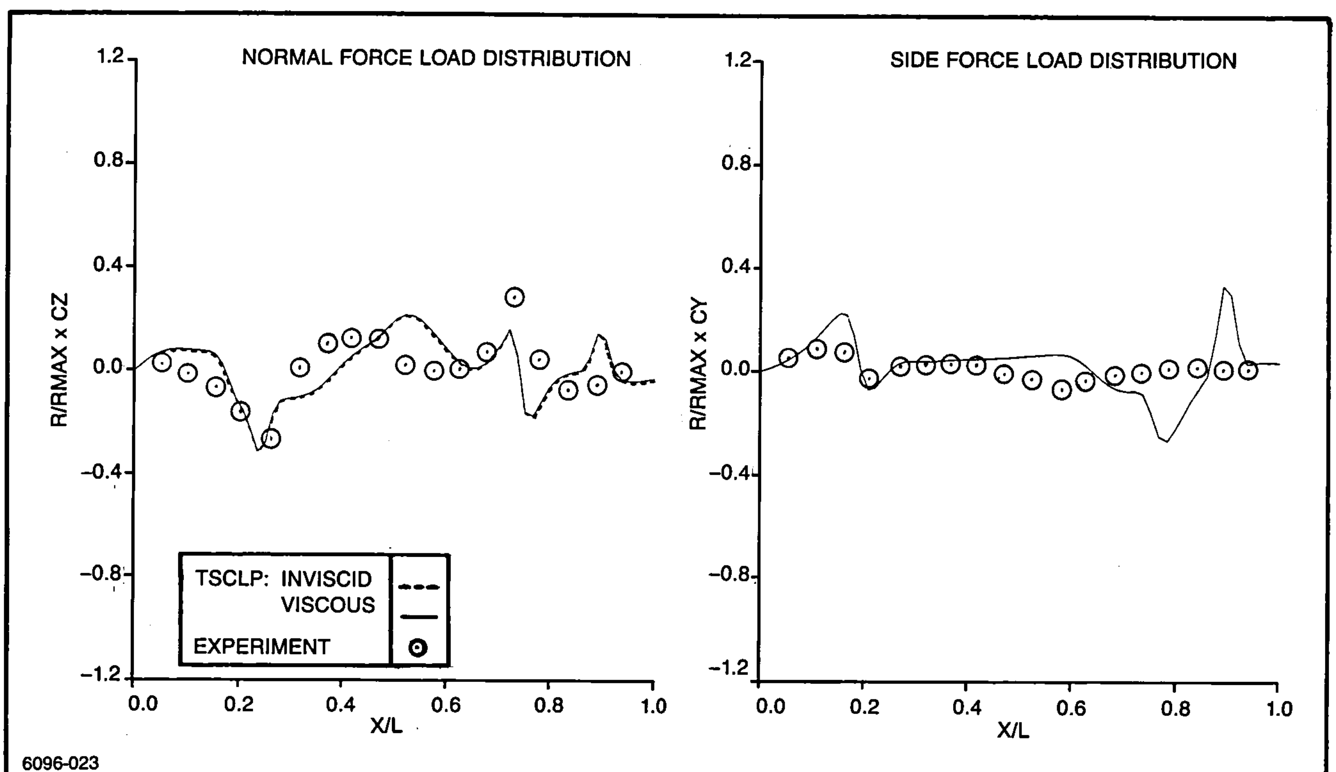

Figure 23 Nielsen Wing/Fuselage/Pylon/Store Configuration: Store Load Distribution Correlations, $M_\infty = 1.1$, $\alpha = 5°$

The fuselage bottom centerline pressure distribution correlation is shown in Fig. 21. Predictions agree well with data. Store surface pressure comparisons appear in Fig. 22. Strong shocks which are predicted near the back end of the store do not occur in the data. These discrepancies compromise the store axial load distribution correlations, which appear in Fig. 23. Overall, correlation with data is fair, not nearly as good as for the subsonic (M_∞=0.925) condition.

Discrepancies in Figs. 21 through 23 are attributed to viscous effects and/or flow separation which have not been modelled, and also to the numerical deficiencies discussed earlier relative to supersonic treatment of isolated stores. In addition, it is possible that grid setup and embedded grid boundary treatment require further development to reliably predict store carriage characteristics at supersonic speeds.

Low Aspect Ratio, Highly Swept and Tapered Wings at Supersonic Speeds

Supersonic calculations were made for two low aspect ratio, highly swept and tapered wing geometries. Results illustrate the enhanced numerical stability of the upwind rotated finite difference scheme. Calculations were performed using 200 "coarse grid" iterations and 200 "fine grid" iterations. Wing boundary layer computations were not employed.

The first swept wing test case is the F-14 aircraft at M_∞=1.3 and α=5°. The wing leading edge sweep is 68°. Computed pressure distributions are compared to experimental data (Ref. 23) in Fig. 24. Although some of the data appears erratic, several trends can be identified. Correlation with data is better at inboard stations than at outboard stations. Outboard, upper surface leading edge expansions are overpredicted. Also, a region of supercritical crossflow is observed in the data (terminated by the shock swept from the inboard leading edge location to the tip midchord location) but not at all in the calculation. Discrepancies are attributed to flow separation which is not modelled and to numerical deficiencies which are discussed below.

The second swept wing test case is the SC3 Demonstration Wing. Leading edge sweep is 65° inboard and 57° outboard. This wing was designed for supersonic maneuver using a full potential method. It features attached flow and controlled supercritical crossflow at the design conditions M_∞=1.62 and α=12°. Computed spanwise pressure distributions are compared to experimental data (Ref. 24) in Fig. 25. Again, the supercritical crossflow is not adequately resolved in the compu-

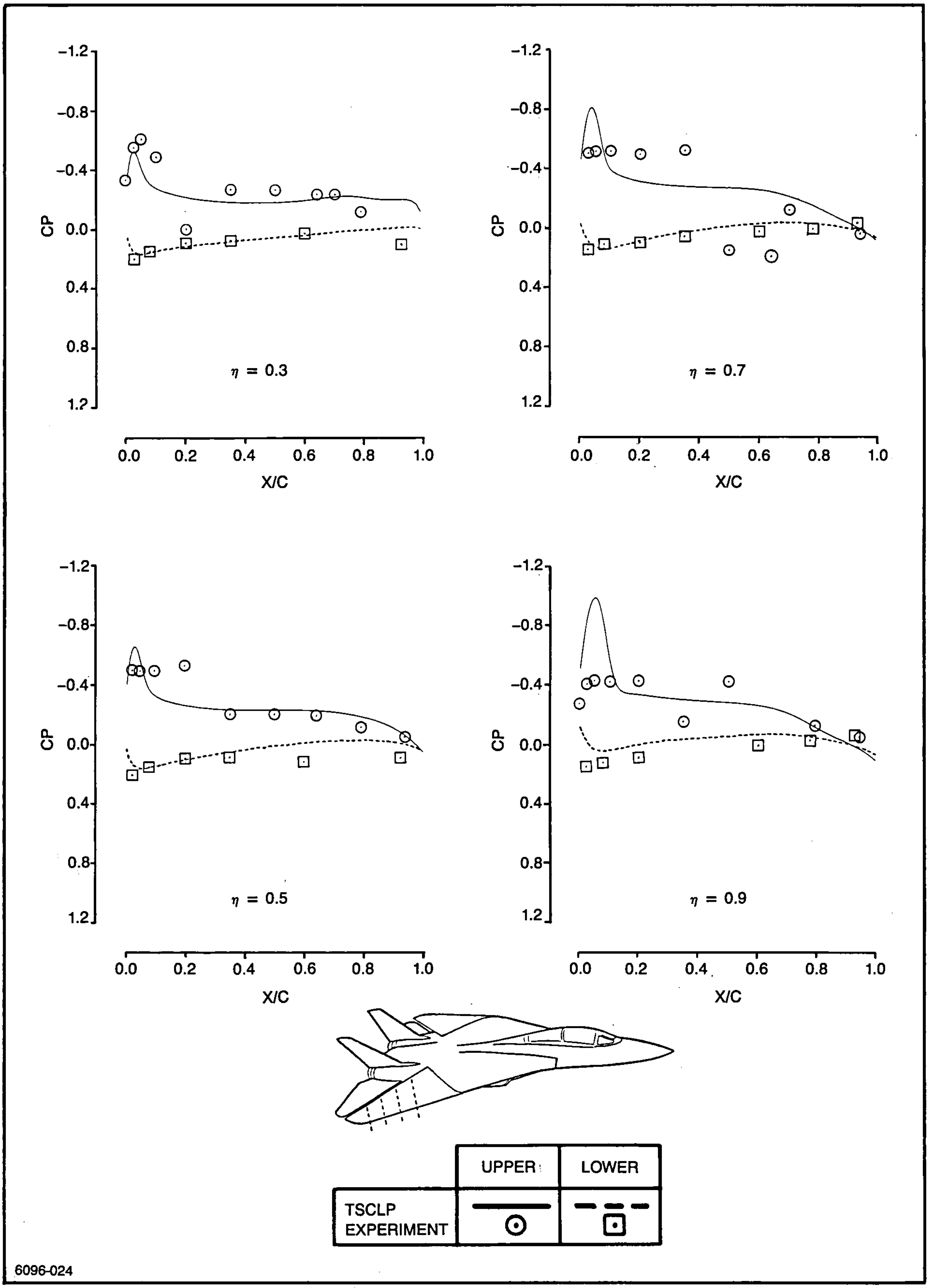

Figure 24 F-14 Wing Pressure Distribution Correlations, M_∞ = 1.3, α = 5°

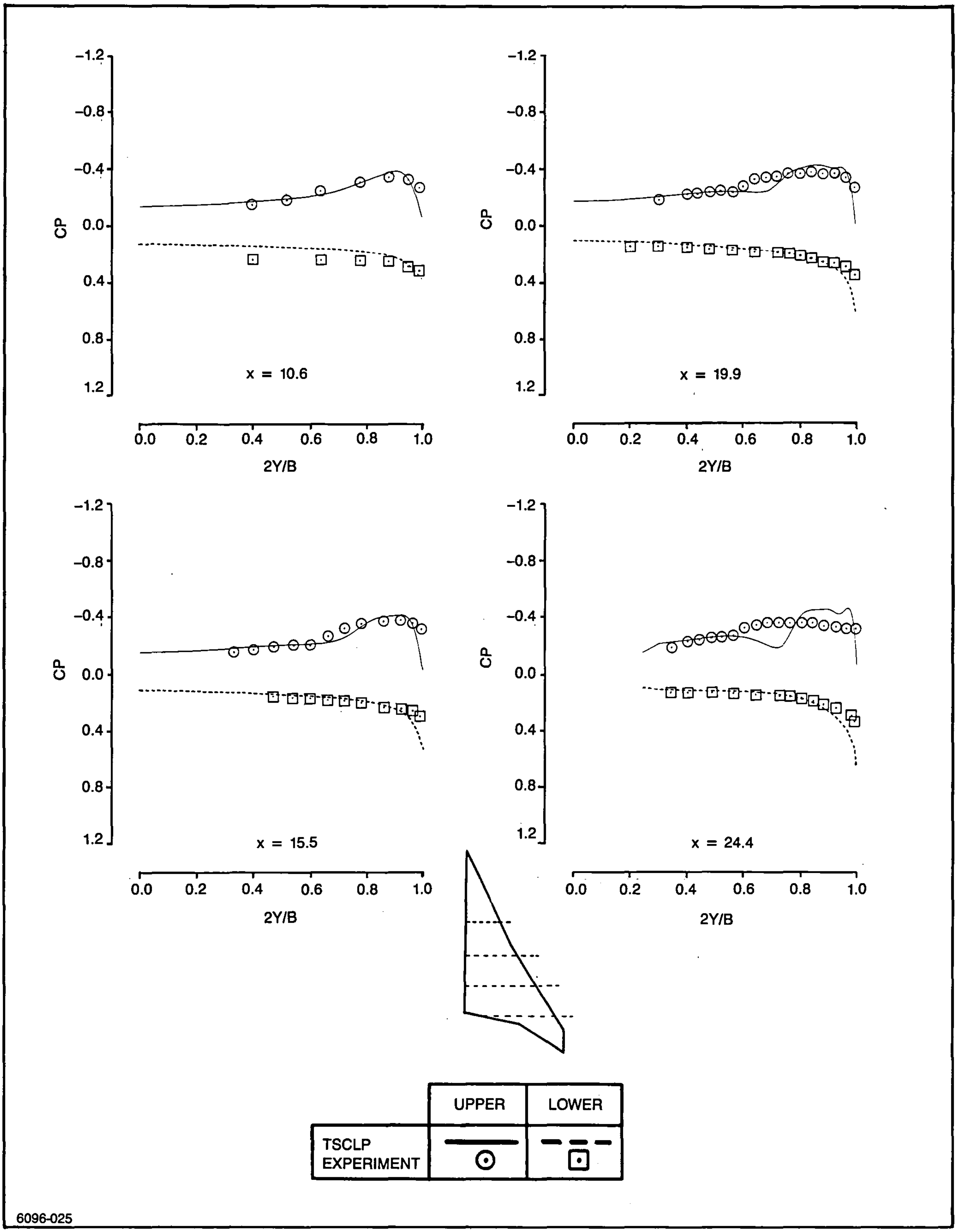

Figure 25 SC3 Demonstration Wing Pressure Distribution Correlations, M_∞ = 1.62, α = 12°

tations. This is attributed to transonic small disturbance flow equation limitations and/or to the need for higher spanwise grid density (there are only 18 grid span cuts from root to tip). The inability to resolve regions of supercritical crossflow should not pose problems when spanwise flow remains subsonic (e.g., for similar wing planforms at transonic speeds, or for less swept and tapered planforms at supersonic speeds). Even so, predictions shown in Fig. 25 are more accurate than panel method results (Ref. 25) which are also commonly employed at these flight conditions.

CONCLUDING REMARKS

Correlations indicate that the TSCLP code provides reliable prediction of external store carriage pressure/loading characteristics. Predictions for isolated stores are good, especially when coupled with simple estimates of store body loads due to viscous crossflow effects. For underwing, pylon-mounted stores, even simple 2-D or axisymmetric modelling of viscous boundary layer and flow separation effects on wing, pylon, and store surfaces would improve loads prediction accuracy. Further studies are required to fully understand the limitations of the transonic small disturbance, embedded grid formulation. Beyond these limitations, the method will still provide a fundamental understanding of complex store/airframe interactions not available by other means.

A finite difference relaxation scheme developed specifically for modified transonic small disturbance flow equations allows treatment of lower aspect ratio, more highly swept and tapered wings, and provides a supersonic freestream capability (supersonic calculations for stores met with limited success). Numerical stability and accuracy is enhanced to such a degree that wing/fuselage solutions are readily obtained even for cases where the physics of the flow are well beyond the scope of the governing flow equation. As with any computational method, the user should assess the validity of a solution for each particular application.

This Page Intentionally Left Blank

APPENDIX A

GRID GENERATION PROCEDURE

Global Coarse Grid

The Cartesian global coarse grid is arranged about the entire configuration. Initially, 71 grid points are evenly spaced in the x direction, over a finite region extending one half the total length upstream and downstream of the configuration:

$$x = A_0 + A_1 \xi \tag{13}$$

with $-1.0 \le \xi \le +1.0$. For subsonic freestreams, the first eight and the last eight mesh cells are redefined so as to stretch to upstream and downstream infinity:

$$x = A_0 + A_1 \xi + A_3 \tan \left[\frac{\pi}{2}\left(\frac{\xi - \xi_1}{\xi_2 - \xi_1}\right)^3\right] \tag{14}$$

The constant A_3 is chosen so that next-to-last grid points are located twice the total length upstream and downstream of the configuration.

For cases with a wing or fuselage, only the half space $y \ge 0$ is modelled:

$$y = \frac{1}{B_1} \tanh^{-1} (\eta) \tag{15}$$

with $0.0 \le \eta \le 1.0$, and

$$z = C_1 \tan \left(\frac{\pi}{2} \zeta\right) \tag{16}$$

with $-1.0 \le \zeta \le +1.0$. Total number of grid points is 26 in the y direction and 31 in the z direction. The constant B_1 is chosen so as to provide 18-1/2 mesh cells to the wing tip or, when no wing is present, 2-1/2 mesh cells to the fuselage side. The consant C_1 is chosen to be the smaller of two values determined by the requirements that next-to-last grid points fall five wing average chord lengths above and below the configuration, and, when a fuselage is present, that z mesh cell size at $\zeta=0$ be equal to y mesh cell size at $\eta=0$.

When a pylon is present, a small bump is added to the spanwise transformation from centerline to wing tip so as to ensure a global coarse grid line at the pylon spanwise location:

$$y = \frac{1}{B_1} \tanh^{-1} (\eta + \Delta\eta). \tag{17}$$

A combination of polynomial and exponential functions are used to define the bump:

$$\Delta\eta = 64 \left[\tanh(B_1 \cdot y_{PYLON}) - \eta_{PYLON}\right] \left(\frac{e^{k\eta/\eta_{TIP}} - 1}{e^k - 1}\right)^3 \left(\frac{e^k - e^{k\eta/\eta_{TIP}}}{e^k - 1}\right)^3 \tag{18}$$

where

Y_{PYLON} = actual pylon spanwise location

η_{PYLON} = grid line desired at that location (closet grid line after applying Eq. 15)

$\eta_{TIP} = \tanh\,(B_1 \cdot b_{WING}/2)$

and k is found by requiring that:

$$\frac{e^{k\eta_{PYLON}/\eta_{TIP}} - 1}{e^k - 1} = \frac{1}{2}$$

For isolated stores, the entire flow field is modelled:

$$y = B_1 \tan\left(\frac{\pi}{2}\eta\right) \tag{19}$$

with $-1.0 \leq \eta \leq +1.0$. In the z direction Eq. 16 is used. Total number of grid points is 25 in both the y and z directions. The constants B_1 and C_1 are chosen so as to provide 2-1/2 mesh cells to the store body maximum radius.

For supersonic freestreams, global coarse grid setup in the y and z directions is redefined, using cubic polynomials, so as to establish finite grid outer boundaries in regions inboard of, outboard of, above, and below the configuration:

$$y = b_0 + b_1\eta + b_2\eta^2 + b_3\eta^3 \qquad (20)$$

$$z = c_0 + c_1\zeta + c_2\zeta^2 + c_3\zeta^3. \qquad (21)$$

Global coarse grid setup near the configuration itself remains unchanged. Polynomial coefficients are determined by requiring continuous first and second order grid metrics where original and redefined regions abut, and by requiring a zero second order grid metric at the finite grid outer boundaries.

When a store is present, the global coarse grid inner boundary is defined by those global coarse grid y and z grid lines which just enclose the store. This rectangular boundary is defined for the total upstream and downstream extent of the grid.

Wing/Store Interaction Grid

The Cartesian Wing/Store Interaction (WSI) grid is arranged about the store. Initially, 51 grid points are evenly spaced in the x direction, over a finite region extending one half the total store length upstream and downstream of the store nose and tail. Eq. 13 is used with $-3.0 \leq \xi \leq +3.0$. For subsonic freestreams, the first eight and the last eight mesh cells are redefined using Eq. 14 so as to stretch to upstream and downstream infinity. The constants A_3 are chosen so that next-to-last WSI grid points coincide with next-to-last global coarse grid points. For supersonic freestreams, a finite transformation is employed:

$$x = A_0 + A_1\,\xi + A_3\,(\xi - \xi_1)^3. \qquad (22)$$

The constants A_3 are chosen so that upstream and downstream WSI grid boundaries coincide with global coarse grid boundaries.

In the y and z directions, the WSI grid is evenly spaced near the store, and it is stretched near its outer boundary to provide reasonable overlap with the global coarse grid. Spacing is based on the parameter BAXIS which is defined to be the greater of 3.0 times the maximum store radius, excluding fins, or 1.5 times the maximum store radius, including fins. In addition, a scaling factor is applied to BAXIS to limit its maximum value to 0.99 times the distance from wing plane to store centerline. Initially, 19 WSI grid points are evenly spaced in the y and z directions, extending a distance BAXIS inboard of, outboard of, above, and below the store centerline:

$$y = B_0 + B_1\eta \tag{23}$$

with $0.0 \leq \eta \leq 1.0$, and

$$z = C_0 + C_1\zeta \tag{24}$$

with $0.0 \leq \zeta \leq 1.0$.

WSI grid spacing in the y and z directions is then modified to provide a 1-1/2 global coarse grid mesh cell overlap between the WSI grid outer boundary and the global coarse grid inner boundary. The first three and last three WSI grid mesh cells in both the y and z directions are redefined using Eqs. 20 and 21. Polynomial coefficients are determined by requiring continuous first and second order grid metrics where original and redefined WSI grid regions abut, and by the overlap requirement.

In some instances this procedure may generate a WSI grid which extends above (or below) the wing plane. When this occurs, polynomial coefficients are instead determined by requiring that the WSI grid outer boundary coincide with the wing plane itself. A new overlap region is then provided by extending the WSI grid an additional three mesh cells above (or below) the wing, again using Eq. 21. Polynomial coefficients for the additional mesh cells are determined by requiring continuous first and second order grid metrics at the wing plane, and by requiring a 1-1/2 global coarse grid mesh cell overlap between the extended WSI grid boundary and the wing plane.

The WSI grid inner boundary is defined by those y-z grid points which just enclose the store. This boundary is defined from just upstream of the store nose to the downstream grid boundary.

Coarse Cylindrical C-Grid

Cylindrical and Cartesian coordinates are related by the following:

$$
\left.\begin{aligned}
y &= y_s + r \cos(\Theta) \\
z &= z_s + r \sin(\Theta).
\end{aligned}\right. \qquad (25)
$$

Angular spacing, Θ, employs 24 evenly spaced mesh cells about each circumference. Coarse cylindrical C-grid physical coordinates x_c and r_c are nominally generated from computational coordinates ξ and η via a series of conformal (Ref. 11) and shearing transformation:

$$
\left.\begin{aligned}
&\hat{\xi} = \xi \cdot \hat{\xi}_{MAX} \\
&\hat{\eta} = \eta \cdot \hat{\eta}_{MAX} \\
&\bar{\xi} = -\hat{\xi} \\
&\eta_1 = \hat{\eta} \\
&\eta_2 = A\hat{\eta} + B \tanh(C\hat{\eta}) \\
&\eta_{LOC} = \eta_2 + \left(\frac{R}{RMAXS}\right)^{1.1}(\eta_1 - \eta_2) \\
&\eta_D = \eta_{BODY}(\xi) + \eta_{LOC}\left[\eta_{OUTER}(\xi) - \eta_{BODY}(\xi)\right] \\
&\bar{\eta} = \pi - \eta_D \\
&\bar{z} = (\bar{x},\bar{r}) = \ln(1 - \cosh\bar{\zeta}) \text{ where } \bar{\zeta} = (\bar{\xi},\bar{\eta}) \\
&x_c = x_{SING} + \frac{L}{\Lambda}(\bar{x} - \ln 2) \\
&r_c = \frac{BAXISO}{\pi}\bar{r}
\end{aligned}\right\} \qquad (26)
$$

BAXISO is defined to be the greater of 4.0 times the store maximum radius, excluding fins, or the value of BAXIS before scaling. The scaling factor applied to BAXIS is then applied to BAXISO as well. Other parameters are $L = x_{TAIL} - x_{SING}$ and $\Lambda = 2\pi - \ln(2)$. The variables $\eta_{BODY}(\xi)$ and $\eta_{OUTER}(\xi)$ shear the grid inner and outer boundaries to the specific store body and outer boundary shapes. The outer boundary is located a distance BAXIS from the store centerline and one quarter store body length upstream of the store nose. Forward of the store nose location it is ellipsoid in shape. The coefficients A, B, and C provide a clustering of grid points towards the store body surface. The parameters $\hat{\xi}_{MAX}$ and $\hat{\eta}_{MAX}$ are chosen so that $0.0 \leq \xi \leq 1.0$ along the store body and $0.0 \leq \eta \leq 1.0$ between the store body and the outer boundary.

Singularity location x_{SING} for the conformal mapping is internally calculated. For blunt noses it is located at the center of nose curvature. For sharp noses an iterative scheme was developed which determines x_{SING} by requiring that $d(\eta_{BODY})/d(\xi)=0$ as ξ goes to zero (i.e., at the nose). An option is available to override the internal calculation of x_{SING} and to use a specified input value. All cases presented in this report use the default internal calculation.

Coarse C-grid setup uses 40 ξ mesh cells between store nose and tail. A total of 5 η mesh cells is used between the store body and the grid outer boundary. A transition region is then defined which extends from the store body tail, ξ_T, to a location approximately one quarter store body length downstream of the tail, ξ_D. At the ξ_D location a decoupled spacing $x_D(\xi)$ and $r_D(\eta)$ is derived from the nominal spacing $x_c(\xi,\eta)$ and $r_c(\xi,\eta)$:

$$x_D(\xi) = x_c(\xi_D,0) + (\xi - \xi)_D \frac{dx_c}{d\xi}(\xi_D,0) \qquad (27)$$

$$r_D(\eta) = r_c(\xi_D,\eta)$$

The coarse C-grid is required to transition from the nominal C-grid transformation x_c and r_c, at ξ_T, to the decoupled spacing x_D and r_D, at ξ_D:

$$x(\xi,\eta) = (1 - 3t^2 + 2t^3)\, x_c(\xi,\eta) + (3t^2 - 2t^3)\, x_D(\xi)$$

$$r(\xi,\eta) = (1 - 3t^2 + 2t^3)\, r_c(\xi,\eta) + (3t^2 - 2t^3)\, r_D(\eta) \qquad (28)$$

where

$$t = \frac{\xi - \xi_T}{\xi_D - \xi_T}$$

Approximately 8 ξ mesh cells are used in the transition region between ξ_T and ξ_D. For subsonic freestreams, an additional 10 ξ mesh cells and Eq. 14 are then used to stretch the coarse C-grid to downstream infinity, with next-to-last grid points in the global coarse grid and coarse C-grid being coincident. For supersonic freestreams, Eq. 22 is used to stretch the coarse C-grid to the global coarse grid downstream boundary, using that additional number (10 at most) of ξ mesh cells producing the smallest positive value of the constant A_3. A maximum total of 60 coarse C-grid ξ mesh cells is permitted.

Finally, the coarse C-grid is modified so that constant η coordinate lines closely resemble fin tip vortex streamlines. The streamline locations are derived (approximately) from the body thickness distribution and slender body theory:

$$r \frac{d\phi}{dr} = R \frac{dR}{dx} \tag{29}$$

which is integrated to give:

$$r(x) = \left\{ \begin{array}{l} [r^2(x_{FIN\ TIP\ LE}) + R^2(x) - R^2(x_{FIN\ TIP\ LE})]^{1/2};\ x<x_{FIN\ TIP\ LE} \\ b_{FIN}/2;\ x_{FIN\ TIP\ LE} \leq x \leq x_{FIN\ TIP\ TE} \\ [r^2(x_{FIN\ TIP\ TE}) + R^2(x) - R^2(x_{FIN\ TIP\ TE})]^{1/2};\ x>x_{FIN\ TIP\ TE} \end{array} \right\} \tag{30}$$

For arbitrary store body shape R(x), this fin tip vortex streamwise location will not pass smoothly along the fin tip itself. After eliminating the discontinuities in dr/dx at the fin tip leading and trailing edges, the desired grid line shape r(x) is obtained by introducing small bumps in the η transformation, along each ξ = constant grid line, using Eq. 18.

Fine Cylindrical C-Grid

The fine cylindrical C-grid uses the same angular spacing as the coarse cylindrical C-grid. In the ξ and η directions, mesh cell density in the fine C-grid is twice that of the coarse C-grid: 80 ξ mesh cells from nose to tail, approximately 16 ξ mesh cells from ξ_T to ξ_D, and 10 η mesh cells between the store body and the grid outer boundary. A maximum total of 100 fine C-grid ξ mesh cells is permitted. Rather than stretching the fine C-grid downstream boundary with Eqs. 14 or 22, it is simply truncated one quarter store body length downstream of the tail (at the end of the transition region, ξ_D).

Wing Fine Grid

As in the basic NASA/Grumman Transonic Wing-Body Code, wing fine grid arrays are set up at each global coarse grid wing spanwise station, and at two additional planes beyond the wing tip. For treatment of stores the outer boundary is redefined so as to exclude wing fine grid y-z points passing within the WSI grid inner boundary. This outer boundary modification is defined for the total upstream and downstream extent of the wing fine grid.

APPENDIX B
FINITE DIFFERENCE APPROXIMATIONS

Flow Equation Algorithm

At each grid point, finite difference approximations are substituted for terms appearing in the governing flow equations, Eqs. 1 and 2. An upwind rotated difference scheme for the full potential equation (Ref. 12) extended for transonic small disturbance applications (Ref. 3) is used. Differencing in Cartesian coordinates x-y and z is analogous to differencing in cylindrical coordinates x-r and Θ, respectively, and is omitted for brevity.

Difference approximations in the physical domain are related to those in the computational space as follows:

$$\left.\begin{aligned}
\phi_x &= \phi_\xi \xi_x + \phi_\eta \eta_x \\
\phi_r &= \phi_\xi \xi_r + \phi_\eta \eta_r \\
\phi_{xx} &= \phi_{\xi\xi}\xi_x^2 + 2\phi_{\xi\eta}\xi_x\eta_x + \phi_{\eta\eta}\eta_x^2 + \phi_\xi\xi_{xx} + \phi_\eta\eta_{xx} \\
\phi_{xr} &= \phi_{\xi\xi}\xi_x\xi_r + \phi_{\xi\eta}(\xi_x\eta_r + \xi_r\eta_x) + \phi_{\eta\eta}\eta_x\eta_r + \phi_\xi\xi_{xr} + \phi_\eta\eta_{xr} \\
\phi_{rr} &= \phi_{\xi\xi}\xi_r^2 + 2\phi_{\xi\eta}\xi_r\eta_r + \phi_{\eta\eta}\eta_r^2 + \phi_\xi\xi_{rr} + \phi_\eta\eta_{rr}
\end{aligned}\right\} \qquad (31)$$

Grid metrics are calculated with second order accurate central difference formulae, except at grid boundaries, where appropriate one-sided formulae are used.

The parameter U^2-4TV (where T, U, and V are from Eq. 2) determines whether a particular point is treated as subsonic or supersonic. At subsonic points, U^2-4TV<0, centered finite difference expressions are given by:

$$
\left.
\begin{aligned}
\phi_\xi &= (\phi_{i+1,j,k} - \phi_{i-1,j,k})/2\Delta\xi \\
\phi_\eta &= (\phi_{i,j+1,k} - \phi_{i,j-1,k})/2\Delta\eta \\
\phi_\theta &= (\phi_{i,j,k+1} - \phi_{i,j,k-1})/2\Delta\theta \\
\phi_{\xi\xi} &= (\phi_{i+1,j,k} - \tfrac{2}{\omega}\,\phi^+_{i,j,k} - (2-\tfrac{2}{\omega})\,\phi_{i,j,k} + \phi^+_{i-1,j,k})/(\Delta\xi)^2 \\
\phi_{\xi\eta} &= (\phi^+_{i-1,j-1,k} - \phi^+_{i+1,j-1,k} - \phi_{i-1,j+1,k} + \phi_{i+1,j+1,k})/4\Delta\xi\Delta\eta \\
\phi_{\eta\eta} &= (\phi_{i,j+1,k} - \tfrac{2}{\omega}\,\phi^+_{i,j,k} - (2-\tfrac{2}{\omega})\phi_{i,j,k} + \phi^+_{i,j-1,k})/(\Delta\eta)^2 \\
\phi_{\theta\theta} &= (\phi^+_{i,j,k+1} - 2\phi^+_{i,j,k} + \phi^+_{i,j,k-1})/(\Delta\theta)^2
\end{aligned}
\right\}
\qquad (32)
$$

Note that terms with the + superscript indicate new potential values, while those without it denote values from a previous grid sweep. At supersonic points, $U^2-4TV \geq 0$, the governing flow equation is recast into characteristic coordinates:

$$
(a^2 - u^2 - v^2)\,\phi_{ss} + a^2\,\phi_{nn} + \frac{1}{r}\,\phi_r + \frac{1}{r^2}\,\phi_{\theta\theta} = 0 \qquad (33)
$$

where

$$
\begin{aligned}
u^2 &= \tfrac{1}{2}\,[-\,(T-V) + \sqrt{(T-V)^2 + U^2}] \\
v^2 &= \tfrac{1}{2}\,[+\,(T-V) + \sqrt{(T-V)^2 + U^2}] \\
a^2 &= \tfrac{1}{2}\,[+\,(T+V) + \sqrt{(T-V)^2 + U^2}]
\end{aligned}
$$

and

$$
\begin{aligned}
\phi_{ss} &= (u^2\phi_{xx} + 2uv\phi_{xr} + v^2\phi_{rr})/(u^2 + v^2) \\
\phi_{nn} &= (v^2\phi_{xx} - 2uv\phi_{xr} + u^2\phi_{rr})/(u^2 + v^2)
\end{aligned}
$$

Contributions to the ϕ_{nn} term are centrally differenced using Eq. 32. Contributions to the ϕ_{ss} term are upwind differenced using formulae appropriate for local flow and grid properties. For example, at points where $u\xi_x + v\xi_r > 0$ and where $u\eta_x + v\eta_r > 0$, the following are used:

$$\left.\begin{aligned}
\phi_{\xi\xi} &= (2\phi^+_{i,j,k} - \phi_{i,j,k} - 2\phi^+_{i-1,j,k} + \phi_{i-2,j,k})/(\Delta\xi)^2 \\
\phi_{\xi\eta} &= (\phi_{i-1,j-1,k} - \phi^+_{i,j-1,k} - \phi^+_{i-1,j,k} + 2\phi^+_{i,j,k} - \phi_{i,j,k})/\Delta\xi\Delta\eta \\
\phi_{\eta\eta} &= (2\phi^+_{i,j,k} - \phi_{i,j,k} - 2\phi^+_{i,j-1,k} + \phi_{i,j-2,k})/(\Delta\eta)^2
\end{aligned}\right\} \tag{34}$$

A periodic tridiagonal matrix solver was developed to facilitate a ring relaxation scheme. The relaxation process starts with the η-surface adjacent to the body (and sting). Each constant ξ,η-ring is relaxed in succession moving from the upstream centerline to the downstream boundary. The process is repeated for each η-surface and proceeds outward until the grid outer boundary is reached.

The governing flow equation expressed in cylindrical coordinates is indeterminate along the grid centerline (r=0). Here, appropriate Cartesian formulations are employed.

Far Field and Symmetry Plane Boundary Conditions

For subsonic freestreams, various grid boundaries are stretched to correspond to infinity. The far field boundary condition imposed at $x=-\infty$, $y=\pm\infty$, and $z=\pm\infty$ is:

$$\phi = 0 \tag{35}$$

The far field boundary condition imposed at $x=+\infty$ is:

$$\phi_x = \phi_{xx} = \phi_{xy} = 0 \quad \text{(Cartesian)} \tag{36}$$

$$\phi_x = \phi_{xx} = \phi_{xr} = 0 \quad \text{(cylindrical)}$$

For supersonic freestreams, grid boundaries are located at a finite distance from the configuration. At the upstream boundary the inflow boundary condition is:

$$\phi = \phi_x = 0 \tag{37}$$

At top, bottom, and side boundaries a radiation-type boundary condition (Ref. 13) is imposed. The value of ϕ_x at the boundary is found from interior values using an extrapolation along local flow equation characteristics. The extrapolation is performed in an x-z plane directly above and below the configuration, in an x-y plane directly to the sides of the configuration, and in appropriately canted planes in between. The potential at the boundary is then set using an upwind expression for ϕ_x:

$$\phi_x = (3\phi_{i,j,k} - 4\phi_{i-1,j,k} + \phi_{i-2,j,k})\xi_x/2\Delta\xi \tag{38}$$

which can be rearranged to give:

$$\phi_{i,j,k} = (4\phi_{i-1,j,k} - \phi_{i-2,j,k} + (2\Delta\xi/\xi_x)\ \phi_x)/3 \tag{39}$$

The radiation-type boundary condition is applied repretitively while marching downstream in the x direction. At the downstream boundary the outflow boundary condition is:

$$(\phi_x)_{i-1/2,j,k} = (\phi_x)_{i-3/2,j,k} \tag{40}$$

or:

$$\phi_{i,j,k} = \phi_{i-1,j,k} + \frac{(\xi_x)_{i-1} + (\xi_x)_{i-2}}{(\xi_x)_i + (\xi_x)_{i-1}} (\phi_{i-1,j,k} - \phi_{i-2,j,k}) \tag{41}$$

When a wing or fuselage is modelled, the symmetry conditions at y=0 are given by:

$$\phi_y = \phi_{xy} = 0 \tag{42}$$

Embedded Grid Boundaries

The coarse cylindrical C-grid outer boundary is used to illustrate the Neumann-type embedded grid boundary condition. The location of each coarse C-grid outer boundary point in the WSI grid is determined once and appropriate interpolation parameters saved. The first step in updating a coarse C-grid outer boundary point is to obtain the values of ϕ_x, ϕ_y, and ϕ_z at the corresponding point in the WSI grid. These are then transformed to the coarse C-grid computational space:

$$\phi_\eta = \phi_x x_\eta + \phi_y y_\eta + \phi_z z_\eta \tag{43}$$

Then, using the relationship:

$$\phi_\eta = \frac{\phi^D_{i,j+1,k} - \phi_{i,j-1,k}}{2\Delta\eta} \tag{44}$$

a dummy point just outside the coarse C-grid outer boundary is set:

$$\phi^D_{i,j+1,k} = \phi_{i,j-1,k} + 2\Delta\eta\phi_\eta \tag{45}$$

This is sufficient treatment for most embedded grid boundaries. At the C-grid outer boundaries (and at the wing fine grid upstream boundary) it is also necessary to supply information for upwind differencing. First, upwind values of ϕ_{xx}, ϕ_{xy}, and ϕ_{xz} and centrally differenced values of ϕ_{yy}, ϕ_{yz}, and ϕ_{zz} are obtained at the corresponding WSI grid point. These are then transformed to the coarse C-grid computational space:

$$\begin{aligned}\phi_{\eta\eta} = {} & \phi_{xx}x_\eta^2 + \phi_{yy}y_\eta^2 + \phi_{zz}z_\eta^2 + 2\phi_{xy}x_\eta y_\eta + 2\phi_{xz}x_\eta z_\eta \\ & +2\phi_{yz}y_\eta z_\eta + \phi_x x_{\eta\eta} + \phi_y y_{\eta\eta} + \phi_z z_{\eta\eta}\end{aligned} \tag{46}$$

Then, using the relationship:

$$\phi_{\eta\eta} = \frac{\phi^D_{i,j+2,k} - 2\phi^D_{i,j+1,k} + \phi_{i,j,k}}{(\Delta\eta)^2} \tag{47}$$

an additional dummy point outside the coarse C-grid is set:

$$\phi^D_{i,j+2,k} = 2\phi^D_{i,j+1,k} - \phi_{i,j,k} + (\Delta\eta)^2\phi_{\eta\eta} \tag{48}$$

In addition to the Neumann-type boundary condition described above, a Dirichlet-type embedded grid boundary condition is also employed. This is used to set potentials in wing fine grid arrays beyond the wing tip, and to set the potential at a single grid point at the front of the coarse and fine cylindrical C-grids (in which the potential would otherwise vary by an indeterminate constant).

Wing and Pylon Surfaces

Wing surface boundary conditions are imposed via the ϕ_{zz} term of the governing flow equation (Ref. 1), as illustrated for wing lower surface treatment in the wing fine grid system. Using the difference expression:

$$\phi_z = (\phi^D_{k+1} - \phi_{k-1})/2\Delta z \tag{49}$$

a dummy point above the wing plane is set:

$$\phi^D_{k+1} = \phi_{k-1} + 2\Delta z\phi_z \tag{50}$$

where ϕ_z is given by Eq. 3. Dummy point values are then used in the appropriate finite difference expressions; for example:

$$\phi_{zz} = (2\phi^+_{k-1} - 2\phi^+_k + 2\Delta z\phi_z)/(\Delta z)^2 \tag{51}$$

(note that i and j subscripts have been omitted for convenience). In the wing/pylon junction, a combination of first and second order accurate expressions are used:

$$\phi_z = \frac{1}{2}\left[\frac{\phi^D_{k+1} - \phi_{k-1}}{2\Delta z} + \frac{\phi^D_{k+1} - \phi_k}{\Delta z}\right] \tag{52}$$

and the dummy point value is given by:

$$\phi^D_{k+1} = (\phi_{k-1} + 2\phi_k + 4\ \Delta z\ \phi_z)/3 \tag{53}$$

In the wake, the Kutta condition is enforced using the wing circulation Γ (the jump in potential at the trailing edge) to set the dummy point value:

$$\phi^D_{k+1} = \phi_{k+1} - \Gamma \tag{54}$$

Pylon surface boundary conditions are imposed in a similar manner. In the wing fine grid a Z-scheme (Ref. 14) is employed, as illustrated for pylon outboard surface treatment. Using the following difference expression:

$$\phi_y = \phi_\xi \xi_y + \phi_\eta \eta_y \tag{55}$$

where, for $\xi_y \lessgtr 0$,

$$\phi_\xi = \pm \left(\phi_{i\pm1,j+1} - \phi_{i,j+1} + \phi^D_{i,j-1} - \phi^D_{i\mp1,j-1}\right)/2\Delta\xi$$

$$\phi_\eta = (\phi_{i,j+1} - \phi^D_{i,j-1})/2\Delta\eta$$

a triadiagonal system of equations for dummy point values inboard of the pylon plane results:

$$\begin{aligned}&\left(\frac{\xi_y}{2\Delta\xi} \mp \frac{\eta_y}{2\Delta\eta}\right) \phi^D_{i,j-1} - \frac{\xi_y}{2\Delta\xi} \phi^D_{i\mp1,j-1} = \\ &\left(\frac{\xi_y}{2\Delta\xi} \mp \frac{\eta_y}{2\Delta\eta}\right) \phi_{i,j+1} - \frac{\xi_y}{2\Delta\xi} \phi_{i\pm1,j+1} \pm \phi_y\end{aligned} \tag{56}$$

where ϕ_y is given by Eq. 5 (note that k subscripts have been omitted for convenience). The dummy point values are then used in the appropriate finite difference expressions. In the wing/pylon junction, combined first and second order accurate expressions are used:

$$\left.\begin{aligned}&\phi_\xi = \frac{1}{2}\left[\pm(\phi_{i\pm1,j+1} - \phi_{i,j+1} + \phi^D_{i,j-1} - \phi^D_{i\mp1,j-1})/2\Delta\xi\right. \\ &\left.\pm(\phi_{i\pm1,j} - \phi_{i,j} + \phi^D_{i,j-1} - \phi^D_{i\mp1,j-1})/2\Delta\xi\right] \\ &\phi_\eta = \frac{1}{2}\left[(\phi_{i,j+1} - \phi^D_{i,j-1})/2\Delta\eta + (\phi_{i,j} - \phi^D_{i,j-1})/\Delta\eta\right]\end{aligned}\right\} \tag{57}$$

and the resulting tridiagonal system for dummy point values is given by:

$$\left(\frac{\xi_y}{2\Delta\xi} \mp \frac{3\eta_y}{4\Delta\eta}\right) \phi^D_{i,j-1} - \frac{\xi_y}{2\Delta\xi} \phi^D_{i\mp1,j-1} =$$

$$\frac{1}{2} \left[\left(\frac{\xi_y}{2\Delta\xi} \mp \frac{\eta_y}{2\Delta\eta}\right) \phi_{i,j+1} - \frac{\xi_y}{2\Delta\xi} \phi_{i\pm1,\, j+1} \right. \tag{58}$$

$$\left. + \left(\frac{\xi_y}{2\Delta\xi} \mp \frac{\eta_y}{\Delta\eta}\right) \phi_{i,j} - \frac{\xi_y}{2\Delta\xi} \phi_{i\pm1,j} \right] \pm \phi_y$$

In the wake, the pylon circulation is used to set the dummy point value:

$$\phi^D_{i,j-1} = \phi_{i,j-1} + \Gamma \tag{59}$$

Store Body and Fin Surfaces

The store body surface boundary condition, Eq. 7, is implemented using Eq. 31 and the following finite difference expressions:

$$\phi_\xi = (\phi^+_{i+1,j,k} - \phi^+_{i-1,j,k})/2\Delta\xi$$

$$\phi_\eta = (-3\phi^+_{i,j,k} + 4\phi_{i,j+1,k} - \phi_{i,j+2,k})/2\Delta\eta \tag{60}$$

to arrive at a tridiagonal system of equations for store body surface potentials:

$$\left.\begin{aligned} \phi^+_{i,j,k} = [\xi_x n_x + \xi_r n_r)\ (\phi^+_{i+1,j,k} - \phi^+_{i-1,j,k})/2\Delta\xi \\ +(\eta_x n_x + \eta_r n_r)\ (4\phi_{i,j+1,k} - \phi_{i,j+2,k})/2\Delta\eta \\ + U_\infty n_x + V_\infty n_r] \ /\ [3(\eta_x n_x + \eta_r n_r)/2\Delta\eta] \end{aligned}\right\} \tag{61}$$

Special care is required at the store nose, where for sharp noses the potential is singular and/or multivalued. To avoid numerical difficulties, the boundary condition at the nose itself is replaced by the requirement that the streamwise (ξ) derivative of the boundary condition be zero at body surface points adjacent to the nose:

$$\frac{d}{d\xi} [(U_\infty + \phi_x)n_x + (V_\infty + \phi_r)n_r] = 0 \tag{62}$$

A store nose stagnation point potential value is also computed for use in flow computations at the point just upstream of the nose:

$$U_\infty + \phi_x = 0 \tag{63}$$

or

$$\phi^+_{1,1,k} = (4\phi_{1,2,k} - \phi_{1,3,k} + \frac{2\Delta\eta}{\eta_x} U_\infty)/3 \tag{64}$$

In a store body/fin junction the potential can also be set based on the fin boundary condition, Eq. 9, as illustrated for a body/fin upper surface junction. The difference expression:

$$\frac{1}{r}\phi_\theta = (-3\phi^+_{i,j,k} + 4\phi_{i,j,k+1} - \phi_{i,j,k+2})/2r\Delta\theta \tag{65}$$

is used to arrive at:

$$\phi^+_{i,j,k} = [4\phi_{i,j,k+1} - \phi_{i,j,k+2} - 2r\Delta\theta(\phi_\theta/r)]/3 \tag{66}$$

The tridiagonal matrix for store body surface potentials is modified at body/fin junction points to use the average of the Eq. 61 and Eq. 66 right hand side expressions.

Store surface potentials are updated during each C-grid sweep using an under-relaxation factor of 0.5. Once all body surface potentials have been set, dummy potentials inside the body surface (for use by the rotated difference scheme) are set by equating two expressions for ϕ_η:

$$\phi_\eta = \frac{\phi_{i,j+1,k} - \phi^D_{i,j-1,k}}{2\Delta\eta} = \frac{-3\phi^+_{i,j,k} + 4\phi_{i,j+1,k} - \phi_{i,j+2,k}}{2\Delta\eta} \tag{67}$$

which yields:

$$\phi^+_{i,j-1,k} = 3\phi^+_{i,j,k} - 3\phi_{i,j+1,k} + \phi_{i,j+2,k} \tag{68}$$

Store fin surfaces receive a lifting-surface treatment analogous to that for wing and pylon surfaces, as illustrated for a fin upper surface. Using the following difference expression:

$$\frac{1}{r}\,\phi_\theta = (\phi_{k+1} - \phi^D_{k-1})/2r\Delta\theta \tag{69}$$

a dummy point below the fin plane is set:

$$\phi^D_{k-1} = \phi_{k+1} - 2r\Delta\theta(\phi_\theta/r) \tag{70}$$

where ϕ_θ/r is given by Eq. 9 (note that i and j subscripts have been omitted for convenience). In the wake, the fin circulation is used to set the dummy point value:

$$\phi^D_{K-1} = \phi_{k-1} + \Gamma \tag{71}$$

APPENDIX C

CALCULATION OF FORCE AND MOMENT COEFFICIENTS

Computed surface pressure and estimated skin friction coefficients are integrated to yield load distributions and force and moment coefficients. For the wing and fuselage this integration is identical to that found in the basic Transonic Wing-Body Code (Ref. 1). For cases where the wing finite difference boundary layer calculation is not activated, estimated wing upper and lower surface section skin friction coefficients are obtained in the same manner as for the fuselage, using the Prandtl-Schlichting formula (Ref. 15) corrected for compressibility effects:

$$c_{f,ave} = (1 + 0.028M_\infty)\ 0.455/[\log(Re)]^{2.58} \qquad (72)$$

where the Reynolds number is based on local chord.

In general, the pylon surface will not be represented in its entirety in any one grid system. It therefore becomes necessary to piece together pylon coefficient contributions from several grid systems. First, contributions from that portion of the pylon located in the fine C-grid are computed. Section coefficients for the almost streamwise, constant η-coordinate grid lines are defined as follows:

$$\left.\begin{aligned} c_\ell &= -\frac{1}{s}\int_{\xi_{LE}}^{\xi_{TE}} (C_{p,u} - C_{p,l})\, ds \\ c_m &= \frac{1}{s}\int_{\xi_{LE}}^{\xi_{TE}} (C_{p,u} - C_{p,l})\left(\frac{x}{c} - 0.25\right) ds \\ c_d &= -\frac{1}{s}\int_{\xi_{LE}}^{\xi_{TE}} (C_{p,u}\, n_{x,u} + C_{p,l}\, n_{x,l})\, ds \\ c_f &= \frac{2}{s}\int_{\xi_{LE}}^{\xi_{TE}} c_{f,ave}\, ds \end{aligned}\right\} \qquad (73)$$

where

$$\left.\begin{aligned} s &= \int_{\xi_{LE}}^{\xi_{TE}} ds \\ ds &= (\eta_x^2 + \eta_r^2)^{1/2}/(\xi_x\eta_r - \xi_r\eta_x)\ d\xi \end{aligned}\right\} \qquad (73)\ \text{Cont'd}$$

Contributions to total pylon force and moment coeffients in aircraft body axes are defined as follows:

$$\left.\begin{aligned} \Delta\hat{F}_p &= \Delta CX_p\hat{i} + \Delta CY_p\hat{j} + \Delta CZ_p\hat{k} \\ &= -\frac{1}{A_{REF}}\int_{\eta=0}^{\eta=1}\int_{\xi_{LE}}^{\xi_{TE}} (C_{p,u}\,\bar{n}_u + C_{p,l}\bar{n}_l)dA \\ \Delta\hat{M}_p &= \Delta CMX_p\hat{i} + \Delta CMY_p\hat{j} + \Delta CMZ_z\hat{k} \\ &= \frac{1}{A_{REF}L_{REF}}\int_{\eta=0}^{\eta=1}\int_{\xi_{LE}}^{\xi_{TE}}(C_{p,u} - C_{p,l})\hat{j} \times (\bar{x} - \bar{x}_{REF})dA \end{aligned}\right\} \qquad (74)$$

where

$$\bar{n} = n_x\hat{i} + n_y\hat{j} + n_z\hat{k}$$

$$\bar{x} - \bar{x}_{REF} = (x - x_{REF})\ \hat{i} + y\hat{j} + (z - z_{wing})\ \hat{k}$$

$$dA = 1/(\xi_x\eta_r - \xi_r\eta_x)\ d\xi d\eta$$

A separate skin friction value is also calculated:

$$\Delta C_{F,p} = \frac{2}{A_{REF}}\int_{\eta=0}^{\eta=1}\int_{\xi_{LE}}^{\xi_{TE}} c_{f,ave}\ dA \qquad (75)$$

Next, contributions from that portion of the pylon surface located in the wing fine grid (but not in the fine C-grid) are considered. Contributions are computed using expressions analogous to Eqs. 73-75. Similarly, contributions from portions of the pylon surface in the global coarse grid and WSI grid are considered, as required, until the entire pylon surface has been accounted for.

Once the total pylon force and moment coefficients in aircraft body axes have been calculated, coefficients in aircraft stability axes are given by the following transformation:

$$\bar{F}_p = C_{D,p}\hat{i} + C_{y,p}\hat{j} + C_{L,p}\hat{k} = \hat{F}_p - \hat{F}_p \times \alpha\hat{j} \tag{76}$$

$$\bar{M}_p = C_{\ell,p}\hat{i} + C_{m,p}\hat{j} + C_{n,p}\hat{k} = \hat{M}_p - \hat{M}_p \times \alpha\hat{j}$$

The skin friction coefficient remains unchanged. Finally, combined left- and right-hand pylon surface contributions to total configuration force and moment coefficients are given by:

$$\left.\begin{aligned} \Delta C_D &= 2C_{D,p} \\ \Delta C_L &= 2C_{L,p} \\ \Delta C_m &= 2C_{m,p} \\ \Delta C_F &= 2C_{F,p} \end{aligned}\right\} \tag{77}$$

Store body loads are calculated as follows. Cross-section force coefficients, in grid system axes and based on local diameter, are defined as:

$$\bar{f} = c_x\hat{i} + c_y\hat{j} + c_z\hat{k} = -\frac{1}{2}\int_0^{2\pi} C_p\bar{n}\, d\theta$$

where (78)

$$\bar{n} = n_x\hat{i} + n_r\cos\theta\hat{j} + n_r\sin\theta\hat{k}$$

Store body viscous crossflow effects (Refs. 16, 17) are then estimated. First, a crossflow Reynolds number is defined at each store body cross-section in the fine C-grid:

$$Re_c = \rho V_c 2r/\mu \qquad (79)$$

where

$$V_c = V_\infty \, [(\alpha + \alpha_s)^2 + \beta_s^2]^{1/2}$$

The viscous crossflow drag coefficient for an infinite cylinder placed normal to the flow, $c_{d,c}$, is then calculated as a function of Re_c, via a curve fit to experimental data (see Ref. 16, Fig. 10). Next, the store fineness ratio is defined:

$$L/d = (X_{TAIL} - X_{NOSE})/(2 \cdot RMAXS) \qquad (80)$$

The ratio of crossflow drag for a finite cylinder to that for an infinite cylinder, η_c, is then calculated as a function of L/d, again via a curve fit to experimental data (see Ref. 16, Fig. 11). The estimated viscous crossflow drag coefficient value, referenced to freestream flow conditions, is given by:

$$|\tilde{f}_c| = \eta_c \, c_{d,c} \, (V_c/V_\infty)^2 \qquad (81)$$

This is broken down into cross-section viscous side and normal force coefficients:

$$\left.\begin{aligned} c_{y,c} &= |\tilde{f}_c| \cos\Theta \\ c_{z,c} &= |\tilde{f}_c| \sin\Theta \\ &\text{where} \\ \Theta_c &= \tan^{-1} [(\alpha + \alpha_s)/\beta_s] \end{aligned}\right\} \qquad (82)$$

which can be added to cross-section coefficients calculated with Eq. 78. All loads, forces, and moments are subsequently calculated both with and without estimated viscous crossflow effects.

To calculate total store body force and moment coefficients the following quantities, in grid system axes, are first computed:

$$
\left.\begin{aligned}
\tilde{F}_b &= C\tilde{X}_b\hat{i} + C\tilde{Y}_b\hat{j} + C\tilde{Z}_b\hat{k} \\
&= \frac{1}{A_{REFS}} \int_{\xi_{NOSE}}^{\xi_{TAIL}} 2r\tilde{f}\ ds \\
\tilde{M}_b &= CM\tilde{X}\hat{i} + CM\tilde{Y}\hat{j} + CM\tilde{Z}\hat{k} \\
&= -\frac{1}{A_{REFS}\ L_{REFS}} \int_{\xi_{NOSE}}^{\xi_{TAIL}} 2r\tilde{f} \times (x - x_{REFS})\hat{i}\ ds
\end{aligned}\right\} \quad (83)
$$

where ds is as defined for Eq. 73. Store body forces and moments in store body axes are then defined as:

$$
\left.\begin{aligned}
\hat{F}_b &= CX_b\hat{i} + CY_b\hat{j} + CZ_b\hat{k} \\
&= C\tilde{X}_b\hat{i} + (C\tilde{Y}_b\cos\phi_s + C\tilde{Z}_b\sin\phi_s)\hat{j} + (C\tilde{Z}_b\cos\phi_s - C\tilde{Y}_b\sin\phi_s)\hat{k} \\
\hat{M}_b &= CMX_b\hat{i} + CMY_b\hat{j} + CMZ_b\hat{k} \\
&= CM\tilde{X}_b\hat{i} + (CM\tilde{Y}_b\cos\phi_s + CM\tilde{Z}_b\sin\phi_s)\hat{j} + (CM\tilde{Z}_b\cos\phi_s - CM\tilde{Y}_b\sin\phi_s)\hat{k}
\end{aligned}\right\} \quad (84)
$$

where ϕ_s is the store roll angle. Forces and moments in store stability axes are defined as:

$$
\left.\begin{aligned}
\bar{F}_b &= C_{D,b}\hat{i} + C_{Y,b}\hat{j} + C_{L,b}\hat{k} \\
&= \tilde{F}_b - \tilde{F}_b \times [(\alpha + \alpha_s)\hat{j} - \beta_s\hat{k}] \\
\bar{M}_b &= C_{\ell,b}\hat{i} + C_{m,b}\hat{j} + C_{n,b}\hat{k} \\
&= \tilde{M}_b - \tilde{M}_b \times [(\alpha + \alpha_s)\hat{j} - \beta_s\hat{k}]
\end{aligned}\right\} \quad (85)
$$

A separate skin friction value is also calculated using Eq. 72, with a Reynolds number based on store body length, and the following:

$$C_{F,b} = \frac{S_{b,wet}}{A_{REFS}} c_{f,ave} \tag{86}$$

Store fin section coefficients are calculated using Eq. 73. To calculate total store fin force and moment coefficients the following quantities, in grid system axes, are first computed:

$$\left.\begin{aligned}
\tilde{F}_f &= C\tilde{X}_f\hat{i} + C\tilde{Y}_f\hat{j} + C\tilde{Z}_f\hat{k} \\
&= -\frac{1}{A_{REFS}}\int_{\eta_{root}}^{\eta_{tip}}\int_{\xi_{LE}}^{\xi_{TE}} (C_{p,u}\bar{n}_u + C_{p,l}\bar{n}_l)dA \\
\tilde{M}_f &= CM\tilde{X}_f\hat{i} + CM\tilde{Y}_f\hat{j} + CM\tilde{Z}_f\hat{k} \\
&= \frac{1}{A_{REFS}\,L_{REFS}}\int_{\eta_{root}}^{\eta_{tip}}\int_{\xi_{LE}}^{\xi_{TE}} (C_{p,u} - C_{p,l})(-\sin\theta\hat{j} + \cos\theta\hat{k}) \\
&\quad x(\bar{x} - \bar{x}_{REFS})dA
\end{aligned}\right\} \tag{87}$$

where

$$\bar{n} = n_x\hat{i} + (n_r\cos\theta - n_\theta\sin\theta)\hat{j} + (n_\theta\cos\theta + n_r\sin\theta)\hat{k}$$

$$\bar{x} - \bar{x}_{REFS} = (x - x_{REFS})\hat{i} + r\cos\theta\hat{j} + r\sin\theta\,\hat{k}$$

and dA is as defined for Eq. 74. Fin forces and moments in store body axes are then defined as:

$$\left.\begin{aligned}
\hat{F}_f &= CX_f\hat{i} + CY_f\hat{j} + CZ_f\hat{k} \\
&= C\tilde{X}_f\hat{i} + (C\tilde{Y}_f\cos\phi_s + C\tilde{Z}_f\sin\phi_s)\hat{j} + (C\tilde{Z}_f\cos\phi_s - C\tilde{Y}_f\sin\phi_s)\hat{k} \\
\hat{M}_f &= CMX_f\hat{i} + CMY_f\hat{j} + CMZ_f\hat{k} \\
&= CM\tilde{X}_f\hat{i} + (CM\tilde{Y}_f\cos\phi_s + CM\tilde{Z}_f\sin\phi_s)\hat{j} + (CM\tilde{Z}_f\cos\phi_s - CM\tilde{Y}_f\sin\phi_s)\hat{k}
\end{aligned}\right\} \tag{88}$$

Fin forces and moments in store stability axes are defined as:

$$\left.\begin{aligned}
\bar{F}_f &= C_{D,f}\hat{i} + C_{Y,f}\hat{j} + C_{L,f}\hat{k} \\
&= \tilde{F}_f - \tilde{F}_f \times \left[(\alpha + \alpha_s)\hat{j} - \beta_s\hat{k}\right] \\
\bar{M}_f &= C_{\ell,f}\hat{i} + C_{m,f}\hat{j} + C_{n,f}\hat{k} \\
&= \tilde{M}_f - \tilde{M}_f \times \left[(\alpha + \alpha_s)\hat{j} - \beta_s\hat{k}\right]
\end{aligned}\right\} \tag{89}$$

A separate skin friction value is also calculated:

$$C_{F,f} = \frac{2}{A_{REFS}} \int_{\eta_{root}}^{\eta_{tip}} \int_{\xi_{LE}}^{\xi_{TE}} c_{f,ave}\, ds \tag{90}$$

Total store forces and moments are obtained by summing contributions from the body and fins:

$$\left.\begin{aligned}
\hat{F}_s &= CX_s\hat{i} + CY_s\hat{j} + CZ_s\hat{k} = \hat{F}_b + \Sigma\,\hat{F}_f \\
\hat{M}_s &= CMX_s\hat{i} + CMY_s\hat{j} + CMZ_s\hat{k} = \hat{M}_b + \Sigma\,\hat{M}_f \\
\bar{F}_s &= C_{D,s}\hat{i} + C_{Y,s}\hat{j} + C_{L,s}\hat{k} = \bar{F}_b + \Sigma\,\bar{F}_f \\
\bar{M}_s &= C_{\ell,s}\hat{i} + C_{m,s}\hat{j} + C_{n,s}\hat{k} = \bar{M}_b + \Sigma\,\bar{M}_f \\
C_{F,s} &= C_{F,b} + \Sigma\, C_{F,f}
\end{aligned}\right\} \tag{91}$$

Finally, combined left- and right-hand store contributions to total configuration force and moment coefficients are given by:

$$\left.\begin{aligned}
\Delta C_D &= 2\,\frac{A_{REFS}}{A_{REF}}\, C_{D,s} \\
\Delta C_L &= 2\,\frac{A_{REFS}}{A_{REF}}\, C_{L,s}
\end{aligned}\right\} \tag{92}$$

$$\left.\begin{aligned}
\Delta C_m &= 2\,\frac{A_{REFS}\,L_{REFS}}{A_{REF}\,L_{REF}}\left[C_{m,s} + \frac{C_{D,s}(Z_s - Z_{wing}) - C_{L,s}(x_{REFS} - x_{REF})}{L_{REFS}}\right] \\
\Delta C_F &= 2\,\frac{A_{REFS}}{A_{REF}}\,C_{F,s}
\end{aligned}\right\} \quad \begin{array}{c}(92)\\ \text{Cont'd}\end{array}$$

APPENDIX D

COMPUTER CODE DESCRIPTION

CONTENTS

GENERAL COMPUTER CODE DESCRIPTION

The TSCLP computer code is operational on both CRAY XMP and CDC VPS-32 computers. After main program execution, a second auxiliary program is used to generate the plotted output. Disk unit numbers 87 and 88 are used to pass information from the main program to the auxiliary plotting program.

On the CRAY XMP, the second program module generates DISSPLA plotted output. On the CDC VPS-32, the second module does not actually call any plotting subroutines. Instead, it places all plotting subroutine call data on disc unit number 89 for transfer to the CDC NOS environment. On the NOS side, a small program module then generates Langley CALCOMP plotted output.

Program execution requires approximately $780K_{10}$ words of memory. In-core storage of data reduces I/O time and minimizes use of temporary disk storage units. In addition to the disk unit numbers discussed above, disk unit number 1 is used to store a copy of the input data set, and disk unit number 8 is used for quick geometry problem diagnosis output. Total CRAY execution time for various options are shown below.

Case	Iteration Count (Crude/Intermediate/Fine)	Time (CPU seconds)
Geometry verification	0/0/0	12
Isolated store body	0/200/200	186
Store with 8 fins	0/200/200	224
Wing/fuselage/pylon	200/0/200	281
Wing/fuselage/pylon/store	200/200/200	400
Wing/fuselage (supersonic)	200/0/200	325

Typical CDC execution time is approximately 19 CRUs for each Cray CPU second.

INPUT DATA FORMAT

Excluding literal cards, all input data cards are punched in seven-field ten-digit format (7F10.0).

Wing/fuselage/pylon geometry is input in the aircraft coordinate system.

Store body and fin geometry may be input in a separate store coordinate system. Parameters on Card 2-S are used to translate, rotate, and scale store geometry as desired within the aircraft coordinate system.

Card Number	Card Column	Variable Name	Description
Card 1-A	1-60	TITLE	Configuration or run title.
Card 2-A	1-10	AMACH	Freestream Mach number.
	11-20	AOA	Aircraft or isolated store angle-of-attack (degrees).
	21-30	RE	Reynolds number X 1.0E-06 based on REFL (based on REFLS for isolated store).
	31-40	AXITC	Number of coarse grid iterations (global coarse grid only). Use 0.0 for isolated store.
	41-50	AXITM	Number of intermediate grid iterations (global coarse grid, wing/store interaction grid, and coarse C-grid).
	51-60	AXITF	Number of fine grid iterations (global coarse grid, wing/store interaction grid, coarse C-grid, wing fine grid, and fine C-grid).
	61-70	VISMOD	=1.0 No boundary layer effects. =2.0 Wing boundary layer effects computed at end of inviscid analysis. =3.0 Wing inviscid/boundary layer interactive solution.

Card 3-A	1-10	WING	=0.0 No wing input. =+1.0 Wing input follows. =-1.0 Wing input follows. Wing included in grid setup, but not in solution process.
	11-20	BODY	=0.0 No fuselage input. =+1.0 Fuselage input follows. =-1.0 Fuselage input follows. Fuselage included in grid setup, but not in solution process.
	21-30	STOR	=0.0 No store input. =+1.0 Store input follows. =-1.0 Store input follows. Store included in grid setup, but not in solution process.

NOTE: Omit card 4-A for WING = BODY = 0.0

Card 4-A	1-10	REFA	Aircraft reference area.
	11-20	REFL	Aircraft reference length.
	21-30	REFX	Aircraft reference X-position (for force and moment calculations).

NOTE: Omit card set -W for WING=0.0

Card Number	Card Column	Variable Name	Description
Card 1-W	1-10	ASECT	Number of streamwise sections defining wing planform ($2.0 \le ASECT \le 20.0$).
	11-20	ANIN	Number of ordinates defining each wing section ($ANIN \le 60.0$).
	21-30	ANOSW	=0.0 Sharp nose wing sections. =1.0 Blunt nose wing sections.
	31-40	ZWING	Wing Z-position.
	41-50	WS	Wing C_p distribution plot scaling per inch (typically 0.4 or 0.8).
	51-60	PYLS	=0.0 No store pylon input. =1.0 Store pylon input follows.

NOTE: Card set 2-W through 5-W is repeated ASECT times (sections will be extrapolated towards aircraft centerline as required)

Card Number	Card Column	Variable Name	Description
Card 2-W	1-10	XPL	Wing section leading edge X-value.
	11-20	YP	Wing section Y-value.
	21-30	XPT	Wing section trailing edge X-value.
	31-40	TWIST	Wing section twist angle (degrees, positive leading edge up).
	41-50	AKODE	=0.0 Section ordinates identical to preceding section (omit cards 4-W and 5-W). =1.0 New section definition expected on cards 4-W and 5-W.
Card 3-W	1-70	XINW	Wing section x/c coordinates (card 3-W defined only for first wing section, ANIN values).
Card 4-W	1-70	YINU	Wing section upper surface y/c coordinates (ANIN values).
Card 5-W	1-70	YINL	Wing section lower surface y/c coordinates (ANIN values).

NOTE: Omit card set -B for BODY=0.0

Card Number	Card Column	Variable Name	Description
Card 1-B	1-10	BKOD	=2.0 Axisymmetric fuselage definition. =3.0 Quick-Geometry model fuselage definition.
	11-20	BNOSE	Fuselage nose X-value.
	21-30	BTAIL	Fuselage tail X-value.
	31-40	BNIN	Number of axisymmetric fuselage coordinates to be input (BNIN ≤ 60.0). (BKOD=2.0 only)
	41-50	ANOSB	=0.0 Sharp nose fuselage. =1.0 Blunt nose fuselage. (BKOD=2.0 only)
	51-60	ZBODY	Fuselage axis Z-value. (BKOD=2.0 only)
	61-70	BS	Fuselage C_p plot scaling per inch (typically 0.08).

NOTE: Omit cards 2-B and 3-B for BKOD=3.0

Card 2-B	1-70	XINB	Axisymmetric fuselage X-coordinates (BNIN values).
Card 3-B	1-70	RIN	Axisymmetric fuselage radii (BNIN values).

NOTE: Omit cards 4-B through 13-B for BKOD=2.0

Card 4-B	1-70	VTITLE	Quick-Geometry model title.
Card 5-B	1-10	ACSM	Number of distinct cross-section models (ACSM card sets 6-B and 7-B will follow).
Card 6-B	1-10	ADUM	Running count of current cross-section model (1-ACSM).

	11-20	AARC	Number of arcs in current cross-section model (AARC Cards 7-B will follow).
	21-60	CTITLE	Title or descriptor of current cross-section model.
Card 7-B	1-8	ARCNAM	Arc or component name.
	11-14	ASHAPE	Arc or component shape.
	21-28	PNTNAM(1)	Control point name for beginning of this arc.
	31-38	PNTNAM(2)	Control point name for termination of this arc.
	41-48	PNTNAM(3)	Slope control point name for this arc, if required.
Card 8-B	1-10	ANTCSM	Number of cross-section models to define entire fuselage (ANTCSM cards 9-B will follow).
Card 9-B	1-10	ADUM	Running count of current cross-section model (1-ANTCSM).
	11-20	AMODEL	Index corresponding to already defined cross-section models (between 1 and ACSM).
	21-30	XCSMS1	Starting X-value for current cross-section model.
	31-40	XCSMS2	Ending X-value for current cross-section model.
Card 10-B	1-10	BLINE	Number of fuselage line models to be defined (BLINE card sets 11-B and 12-B follow).
	11-20	ALIAS	Number of fuselage line models to be aliased (ALIAS cards 13-B follow).

NOTE: Card set 11-B and 12-B is repeated BLINE times

Card 11-B	1-10	BLSEG	Number of segments defining fuselage line model.
	11	BYORZ	The letter Y or Z indicates which data definition is to follow.
	12-19	BNAME	Fuselage line name to be defined.
Card 12-B	1-4	SSHAPE	Segment shape.
	11-20	D(1)	X-value for beginning of segment.

	21-30	D(2)	Y or Z value at D(1).
	31-40	D(3)	X-value for termination of segment.
	41-50	D(4)	Y or Z value at D(3).
	51-60	D(5)	X-value for segment slope control point.
	61-70	D(6)	Y or Z value at D(5).

NOTE: Card 13-B is repeated ALIAS times

Card 13-B	11	BYORZ	The letter Y or Z indicates which data definition is to follow.
	12-19	BNAME	Fuselage line name to be defined.
	21	AYORZ	The letter Y or Z indicates which definition is to be used for aliasing.
	22-29	ANAME	Fuselage line name to which BNAME is aliased.

NOTE: Omit card set -P for WING=0.0 or PYLS=0.0

Card Number	Card Column	Variable Name	Description
Card 1-P	1-10	PSEC	Number of streamwise sections defining pylon planform ($2.0 \leq PSEC \leq 10.0$). PSEC < 0.0; pylon included in grid setup but not in solution process.
	11-20	PNIN	Number of ordinates defining each pylon section ($PNIN \leq 61.0$).
	21-30	PNOSE	=0.0 Sharp nose pylon sections. =1.0 Blunt nose pylon sections.
	31-40	YPYLS	Pylon Y-position.
	41-50	BETAP	Pylon yaw angle (degrees, positive leading edge outboard).
	51-60	PS	Pylon C_p distribution plot scaling per inch.

NOTE: Card set 2-P through 4-P is repeated PSEC times. Input sections in order of increasing distance from wing plane. Sections will be extrapolated towards wing plane and store (if present) as required.

Card Number	Card Column	Variable Name	Description
Card 2-P	1-10	XPLP	Pylon section leading edge X-value.
	11-20	YPP	Pylon section Z-value.
	21-30	XPTP	Pylon section trailing edge X-value.
	31-40	PKODE	=0.0 Section ordinates identical to preceding section (omit card 4-P). =1.0 New section definition expected on card 4-P.
Card 3-P	1-70	XINP	Pylon section x/c coordinates (card 3-P defined only for first pylon section, PNIN values).
Card 4-P	1-70	YINP	Pylon section upper/lower surface y/c coordinates (PNIN values).

NOTE: Omit card set -S for STOR=0.0

Card Number	Card Column	Variable Name	Description
Card 1-S	1-60	TITLES	Store identifying title.
Card 2-S	1-10	SNOSE	Store nose X-value in aircraft coordinate system.
	11-20	STAIL	Store tail X-value in aircraft coordinate system.
	21-30	YSTOR	Store axis Y-value in aircraft coordinate system.
	31-40	ZSTOR	Store axis Z-value in aircraft coordinate system.
	41-50	ALPAS	Store pitch angle with respect to aircraft (degrees, positive nose up).
	51-60	BETAS	Store yaw angle with respect to aircraft (degrees, positive nose outboard).
	61-70	ROLLS	Store roll angle (degrees, positive counterclockwise looking upstream).

NOTE: Remaining geometry may be input in a separate store coordinate system.

Card Number	Card Column	Variable Name	Description
Card 3-S	1-10	SNIN	Number of coordinates defining axisymmetric store body (SNIN $\leq$ 61.0).
	11-20	ANOSES	=0.0 Sharp nosed store. =1.0 Blunt nosed store.
	21-30	ASING	=0.0 C-grid singularity location XSING calculated internally. =1.0 C-grid singularity location XSING to be input.
	31-40	XSING	C-grid singularity location (ASING=1.0 only).
	41-50	FINS	=0.0 No store fins. =1.0 One set of store fins to be input. =2.0 Two sets of store fins to be input.
	51-60	SS	Store C_p plot scaling per inch.

Card 4-S	1-10	REFAS	Store reference area.
	11-20	REFLS	Store reference length.
	21-30	REFXS	Store reference X-position.
	31-40	OMEGAS	Store roll rate, p/V_∞ (rad/unit length). Positive counterclockwise looking upstream.
Card 5-S	1-70	XINS	Store body X-coordinates (SNIN values).
Card 6-S	1-70	RINS	Store body radii (SNIN values).

NOTE: Omit card set -F for STOR=0.0 or FINS=0.0

Card Number	Card Column	Variable Name	Description
Card 1-F	1-10	FANG	Number of fin angular positions ($1.0 \leq FANG \leq 4.0$).
	11-20	FS	Fin C_p distribution plot scaling per inch.
	21-30	DFIN	=0.0 No fin deflections (omit cards 3-F). =1.0 Fins deflected (include cards 3-F).
Card 2-F	1-40	ANGF	Fin angular positions (degrees, positive counterclockwise from outboard horizontal looking upstream). FANG values. Fins cannot be in same plane as pylon.

NOTE: Card set 3-F through 7-F is repeated FINS times (fore-fin input followed by aft-fin input for FINS=2.0)

NOTE: Omit card 3-F for DFIN=0.0

Card Number	Card Column	Variable Name	Description
Card 3-F	1-40	DELTAF	Fin deflection angles (degrees, positive leading edge counterclockwise looking upstream). FANG values.
Card 4-F	1-10	FSEC	Number of streamwise sections defining fin planform ($2.0 \leq FSEC \leq 10.0$). FSEC < 0.0; fin included in grid setup but not in solution process.
	11-20	FNIN	Number of ordinates defining each fin section ($FNIN \leq 61.0$).
	21-30	FNOSE	=0.0 Sharp nose fin sections. =1.0 Blunt nose fin sections.

NOTE: Card set 5-F through 7-F is repeated FSEC times (sections will be extrapolated towards store axis as required)

Card 5-F	1-10	XPLF	Fin section leading edge X-value.
	11-20	YPF	Fin section radial location.
	21-30	XPTF	Fin section trailing edge X-value.
	31-40	FKODE	=0.0 Section ordinates identical to preceding section (omit card 7-F). =1.0 New section definition expected on card 7-F.
Card 6-F	1-70	XINF	Fin section x/c coordinates (card 6-F defined only for first fin section, FNIN values).
Card 7-F	1-70	YINF	Fin section upper/lower surface y/c coordinates (FNIN values).

SAMPLE INPUT DATA SETS

```
NTF 5 DEG TEST CONE
    0.60000   0.00000   0.87489   0.00000 200.00000 200.00000   1.00000
    0.00000   0.00000   1.00000
ANALYSIS : BODY ALONE
    0.00000 100.00000   0.00000   0.00000   0.00000   0.00000   0.00000
   15.00000   0.00000   0.00000   0.00000   0.00000   0.04000   0.00000
   60.11638   8.74886  50.00000
    0.00000   5.00000  10.00000  20.00000  30.00000  40.00000  45.00000
   48.00000  52.00000  55.00000  60.00000  70.00000  80.00000  90.00000
  100.00000
    0.00000   0.43744   0.87489   1.74977   2.62466   3.49955   3.93699
    4.19946   4.37443   4.37443   4.37443   4.37443   4.37443   4.37443
    4.37443
```

```
PATHFINDER I NOSECONE
    0.84000   0.00000   1.43750   0.00000 200.00000 200.00000   1.00000
    0.00000   0.00000   1.00000
ANALYSIS : BODY ALONE
    0.00000 100.00000   0.00000   0.00000   0.00000   0.00000   0.00000
   41.00000   1.00000   0.00000   0.00000   0.00000   0.20000   0.00000
  162.29517  14.37500  50.00000
    0.00000   0.12500   0.25000   0.37500   0.50000   0.62500   0.75000
    0.87500   1.00000   1.12500   1.25000   1.37500   1.50000   1.62500
    2.50000   3.75000   5.00000   6.25000   7.50000   8.75000  10.00000
   11.25000  12.50000  13.75000  15.00000  16.25000  17.50000  18.75000
   20.00000  21.25000  22.50000  23.75000  25.00000  26.25000  27.50000
   37.50000  50.00000  62.50000  75.00000  87.50000 100.00000
    0.00000   0.61250   0.84750   1.01500   1.14620   1.25000   1.33620
    1.42000   1.50250   1.58370   1.66500   1.74500   1.82500   1.90370
    2.43370   3.13250   3.76630   4.33750   4.85000   5.30750   5.71000
    6.06250   6.36500   6.61870   6.82370   6.98370   7.09750   7.16500
    7.18750   7.18750   7.18750   7.18750   7.18750   7.18750   7.18750
    7.18750   7.18750   7.18750   7.18750   7.18750   7.18750
```

```
NACA RM L53F07 100 INCH BODY
    0.99000   8.00000  3.167000   0.00000 200.00000 200.00000   0.00000
    0.00000   0.00000   1.00000
ANALYSIS : BODY ALONE
    0.00000 100.00000   0.00000   0.00000   0.00000   0.00000   0.00000
   30.00000   1.00000   0.00000   0.00000   0.00000   0.08000   0.00000
   78.53982  10.00000  50.00000
    0.00000   0.00248   0.00995   0.03939   0.08800   0.15504   0.24042
    0.34317   0.60000   0.90000   1.50000   3.00000   6.00000   9.00000
   12.00000  18.00000  24.00000  30.00000  36.00000  42.00000  48.00000
   54.00000  60.00000  66.00000  72.00000  78.00000  84.00000  90.00000
   96.00000 100.00000
    0.00000   0.01726   0.03458   0.06883   0.10292   0.13668   0.17049
    0.20454   0.27720   0.35760   0.51360   0.86640   1.44600   1.93600
    2.36500   3.11200   3.70800   4.15800   4.48900   4.72000   4.87600
    4.97200   5.00000   4.95600   4.82900   4.61000   4.27400   3.75400
    3.03100   2.50000
```

```
GBU-15 CWW STORE WINGS CANARDS
   0.95000   6.00000   0.93750   0.00000 200.00000 200.00000   1.00000
   0.00000   0.00000  +1.00000
WINGS ON : CANARDS ON
   0.00000  38.62500   0.00000   0.00000   0.00000   0.00000   0.00000
  51.00000   1.00000   0.00000   0.00000   2.00000   0.40000   0.00000
  16.92000   4.50000  21.75000
   0.0       0.03810   0.15230   0.34210   0.60675   0.94520   1.35620
   1.83805   2.38885   3.00640   3.68835   4.43195   5.23430   6.09220
   7.00225   7.96090   8.96435  10.00865  11.08965  12.20310  13.34460
  14.50970  15.69370  16.89200  18.09985  19.31250  20.52515  21.73300
  22.93130  24.11530  25.28040  26.42190  27.53535  28.61635  29.66065
  30.66410  31.62275  32.53280  33.39070  34.19305  34.93665  35.61860
  36.23615  36.78695  37.26880  37.67980  38.01825  38.28290  38.47270
  38.58690  38.62500
   0.0       0.30505   0.59540   0.85520   1.07330   1.29165   1.50395
   1.68970   1.82880   1.87500   1.87500   1.87500   1.87500   1.87500
   1.87500   1.87500   1.87500   1.87500   1.87500   1.87500   1.88135
   1.98985   2.08900   2.17145   2.22805   2.25000   2.25000   2.25000
   2.25000   2.25000   2.25000   2.23365   2.19975   2.15050   2.09390
   2.02345   2.00000   2.00000   2.00000   2.00000   2.00000   2.00000
   2.00000   2.00000   1.99920   1.91185   1.83990   1.78365   1.74330
   1.71900   1.71090
   4.00000   0.40000
  45.00000 135.00000 225.00000 315.00000
  +2.00000  36.00000   1.00000
   2.72500   1.87500  13.24000   1.00000
   0.00000   0.00028   0.00111   0.00247   0.00432   0.00660   0.00924
   0.01215   0.01527   0.01847   0.02000   0.05000   0.10000   0.15000
   0.20000   0.25000   0.30000   0.35000   0.40000   0.45000   0.50000
   0.55000   0.60000   0.65000   0.67857   0.70000   0.73000   0.76000
   0.79000   0.82000   0.85000   0.88000   0.91000   0.94000   0.97000
   1.00000
   0.00000   0.00074   0.00146   0.00217   0.00284   0.00349   0.00410
   0.00467   0.00520   0.00569   0.00590   0.00889   0.01171   0.01336
   0.01434   0.01485   0.01501   0.01487   0.01451   0.01395   0.01324
   0.01238   0.01141   0.01033   0.00968   0.00916   0.00842   0.00764
   0.00684   0.00600   0.00514   0.00424   0.00331   0.00235   0.00135
   0.00032
   3.72700   3.61000   4.53900   1.00000
   0.00000   0.00320   0.00632   0.00924   0.01187   0.01415   0.01600
   0.01736   0.01819   0.01847   0.01847   0.01847   0.01847   0.01847
   0.01847   0.01847   0.01847   0.01847   0.01847   0.01847   0.01847
   0.01847   0.01847   0.01847   0.01847   0.01839   0.01800   0.01729
   0.01626   0.01488   0.01321   0.01122   0.00889   0.00626   0.00329
   0.00000
  +5.00000  58.00000   1.00000
  21.41972   2.00000  38.46027   1.00000
   0.0       0.00500   0.01000   0.01500   0.02000   0.02500   0.03000
   0.03500   0.04000   0.04500   0.05000   0.10000   0.15000   0.20000
   0.25000   0.30000   0.35000   0.40000   0.45000   0.50000   0.55000
   0.60000   0.65000   0.66000   0.67000   0.68000   0.69000   0.70000
   0.71000   0.72000   0.73000   0.74000   0.75000   0.76000   0.77000
   0.78000   0.79000   0.80000   0.81000   0.82000   0.83000   0.84000
   0.85000   0.86000   0.87000   0.88000   0.89000   0.90000   0.91000
   0.92000   0.93000   0.94000   0.95000   0.96000   0.97000   0.98000
   0.99000   1.00000
   0.0       0.00308   0.00424   0.00517   0.00591   0.00654   0.00710
   0.00761   0.00808   0.00850   0.00889   0.01172   0.01338   0.01436
   0.01487   0.01502   0.01489   0.01453   0.01402   0.01372   0.01372
   0.01372   0.01372   0.01372   0.01371   0.01370   0.01371   0.01373
   0.01376   0.01376   0.01367   0.01355   0.01354   0.01378   0.01422
   0.01432   0.01344   0.01093   0.00800   0.00506   0.00207   0.00107
   0.00320   0.00510   0.00652   0.00746   0.00790   0.00787   0.00768
   0.00752   0.00735   0.00718   0.00701   0.00684   0.00667   0.00650
   0.00633   0.00616
  22.92933   3.05700  38.46027   1.00000
   0.0       0.00308   0.00424   0.00517   0.00591   0.00654   0.00710
   0.00761   0.00808   0.00850   0.00889   0.01172   0.01338   0.01436
   0.01487   0.01503   0.01490   0.01453   0.01401   0.01371   0.01372
   0.01372   0.01372   0.01372   0.01372   0.01372   0.01371   0.01371
   0.01372   0.01370   0.01345   0.01275   0.01143   0.00995   0.00849
   0.00703   0.00557   0.00412   0.00264   0.00123   0.00101   0.00303
```

0.00499	0.00645	0.00740	0.00784	0.00781	0.00761	0.00745
0.00728	0.00711	0.00694	0.00677	0.00660	0.00643	0.00626
0.00609	0.00592					
24.25470	3.98500	38.46027	1.00000			
0.0	0.00308	0.00424	0.00517	0.00591	0.00654	0.00710
0.00761	0.00808	0.00850	0.00890	0.01172	0.01338	0.01436
0.01487	0.01503	0.01490	0.01454	0.01402	0.01371	0.01372
0.01372	0.01372	0.01372	0.01372	0.01372	0.01371	0.01372
0.01369	0.01344	0.01274	0.01143	0.00995	0.00850	0.00705
0.00560	0.00415	0.00269	0.00127	0.00097	0.00298	0.00497
0.00643	0.00737	0.00779	0.00773	0.00753	0.00737	0.00720
0.00703	0.00686	0.00669	0.00652	0.00635	0.00618	0.00601
0.00584	0.00567					
24.25471	3.98500	37.58527	1.00000			
0.0	0.00319	0.00438	0.00535	0.00612	0.00677	0.00735
0.00789	0.00837	0.00882	0.00923	0.01220	0.01399	0.01510
0.01573	0.01599	0.01597	0.01571	0.01525	0.01476	0.01462
0.01462	0.01462	0.01462	0.01462	0.01462	0.01462	0.01462
0.01462	0.01462	0.01461	0.01462	0.01462	0.01454	0.01419
0.01336	0.01196	0.01050	0.00905	0.00759	0.00614	0.00468
0.00325	0.00174	0.00092	0.00203	0.00434	0.00608	0.00731
0.00807	0.00824	0.00776	0.00714	0.00652	0.00590	0.00529
0.00467	0.00405					
29.09632	7.37500	37.58527	1.00000			
0.0	0.00326	0.00447	0.00545	0.00624	0.00690	0.00750
0.00804	0.00854	0.00899	0.00941	0.01248	0.01434	0.01552
0.01621	0.01654	0.01658	0.01637	0.01597	0.01543	0.01514
0.01515	0.01515	0.01515	0.01515	0.01514	0.01515	0.01516
0.01515	0.01503	0.01466	0.01386	0.01252	0.01108	0.00968
0.00827	0.00686	0.00545	0.00405	0.00260	0.00127	0.00101
0.00323	0.00537	0.00690	0.00783	0.00823	0.00845	0.00871
0.00900	0.00927	0.00955	0.00983	0.01011	0.01039	0.01067
0.01095	0.01123					

```
DAS WING PYLON STORE FINS
   0.75000   4.00000   3.69500 200.00000 200.00000 200.00000   1.00000
  +1.00000   0.00000  +1.00000
1679.04000  20.40000  15.16000
   2.00000  43.00000   1.00000   0.00000   0.40000   1.00000
  10.06000   0.00000  30.46000   0.00000   1.00000
   0.00000   0.00100   0.00300   0.00500   0.00700   0.01000   0.02000
   0.03000   0.04000   0.05000   0.06000   0.08000   0.10000   0.12000
   0.14000   0.16000   0.18000   0.20000   0.25000   0.30000   0.35000
   0.40000   0.45000   0.50000   0.55000   0.60000   0.65000   0.70000
   0.75000   0.80000   0.82000   0.84000   0.86000   0.88000   0.90000
   0.92000   0.94000   0.95000   0.96000   0.97000   0.98000   0.99000
   1.00000
   0.00000   0.00429   0.00730   0.00931   0.01091   0.01288   0.01767
   0.02116   0.02400   0.02643   0.02859   0.03232   0.03554   0.03840
   0.04100   0.04339   0.04560   0.04765   0.05213   0.05565   0.05812
   0.05937   0.05923   0.05769   0.05491   0.05105   0.04627   0.04073
   0.03460   0.02802   0.02531   0.02256   0.01979   0.01700   0.01422
   0.01144   0.00867   0.00730   0.00594   0.00459   0.00324   0.00191
   0.00060
   0.00000  -0.00429  -0.00730  -0.00931  -0.01091  -0.01288  -0.01767
  -0.02116  -0.02400  -0.02643  -0.02859  -0.03232  -0.03554  -0.03840
  -0.04100  -0.04339  -0.04560  -0.04765  -0.05213  -0.05565  -0.05812
  -0.05937  -0.05923  -0.05769  -0.05491  -0.05105  -0.04627  -0.04073
  -0.03460  -0.02802  -0.02531  -0.02256  -0.01979  -0.01700  -0.01422
  -0.01144  -0.00867  -0.00730  -0.00594  -0.00459  -0.00324  -0.00191
  -0.00060
  10.06000  41.75000  30.46000   0.00000   0.00000
  +2.00000  21.00000   0.00000  20.87500   0.00000   0.40000
  10.90000  -0.68000  21.01401   1.00000
   0.0       0.02500   0.05000   0.07500   0.10000   0.12500   0.15000
   0.21250   0.27500   0.33750   0.40000   0.46250   0.52500   0.58750
   0.65000   0.70000   0.76000   0.82000   0.88000   0.94000   1.00000
   0.0       0.01434   0.02468   0.03164   0.03584   0.03791   0.03846
   0.03846   0.03846   0.03846   0.03846   0.03846   0.03846   0.03846
   0.03846   0.03756   0.03409   0.02833   0.02055   0.01101   0.0
  10.90000  -3.61000  21.01401   0.00000
DAS STORE
   0.00000  36.00000  20.87500  -5.71000   0.00000   0.00000   0.00000
  61.00000   0.00000   0.00000   0.00000   1.00000   0.40000   0.00000
  13.85442  36.00000  15.30000
   0.00000   0.60000   1.20000   1.80000   2.40000   3.00000   3.60000
   4.20000   4.80000   5.40000   6.00000   6.60000   7.20000   7.80000
   8.40000   9.00000   9.60000  10.20000  10.80000  11.40000  12.00000
  12.60000  13.20000  13.80000  14.40000  15.00000  15.60000  16.20000
  16.79999  17.39999  18.00000  18.59999  19.20000  19.79999  20.39999
  20.99998  21.59999  22.20000  22.79999  23.39999  23.99998  24.59999
  25.20000  25.79999  26.39999  27.00000  27.59999  28.20000  28.79999
  29.39999  29.99998  30.59999  31.20000  31.79999  32.39999  32.99998
  33.59999  34.20000  34.79999  35.39999  36.00000
   0.00000   0.29557   0.54896   0.76566   0.95075   1.10887   1.24424
   1.36064   1.46144   1.54955   1.62748   1.69732   1.76069   1.81882
   1.87249   1.92207   1.96749   2.00826   2.04343   2.07168   2.09121
   2.09981   2.10000   2.10000   2.10000   2.10000   2.10000   2.10000
   2.10000   2.10000   2.09992   2.09620   2.08700   2.07251   2.05287
   2.02826   1.99885   1.96482   1.92636   1.88366   1.83690   1.78629
   1.73202   1.67431   1.61337   1.54941   1.48266   1.41334   1.34168
   1.26793   1.19231   1.11508   1.03648   0.95677   0.87621   0.79506
   0.71359   0.63208   0.55079   0.47003   0.39007
   4.00000   0.40000
  45.00000 135.00000 225.00000 315.00000
  +3.00000  21.00000   0.00000
  28.40000   0.00000  32.80000   1.00000
   0.00000   0.05000   0.10000   0.15000   0.20000   0.25000   0.30000
   0.35000   0.40000   0.45000   0.50000   0.55000   0.60000   0.65000
   0.70000   0.75000   0.80000   0.85000   0.90000   0.95000   1.00000
   0.00000   0.00000   0.00000   0.00000   0.00000   0.00000   0.00000
   0.00000   0.00000   0.00000   0.00000   0.00000   0.00000   0.00000
   0.00000   0.00000   0.00000   0.00000   0.00000   0.00000   0.00000
  30.50000   2.10000  34.90000   0.00000
  32.70000   4.30000  34.90000   0.00000
```

```
NIELSEN WING/BODY PYLON STORE
   0.92500   5.00000   1.33600 200.00000 200.00000 200.00000   1.00000
  +1.00000  +1.00000  +1.00000
  63.93600   5.34400   14.0920
   2.00000  23.00000   0.00000   0.00000   0.40000   1.00000
   9.40000   0.00000  18.10000   0.00000   1.00000
   0.00000   0.02500   0.05000   0.07500   0.10000   0.15000   0.20000
   0.25000   0.30000   0.35000   0.40000   0.45000   0.50000   0.55000
   0.60000   0.65000   0.70000   0.75000   0.80000   0.85000   0.90000
   0.95000   1.00000
   0.00000   0.00325   0.00548   0.00736   0.00900   0.01175   0.01399
   0.01576   0.01726   0.01837   0.01921   0.01974   0.01998   0.01989
   0.01955   0.01885   0.01777   0.01620   0.01406   0.01085   0.00738
   0.00369   0.00000
   0.00000  -0.00325  -0.00548  -0.00736  -0.00900  -0.01175  -0.01399
  -0.01576  -0.01726  -0.01837  -0.01921  -0.01974  -0.01998  -0.01989
  -0.01955  -0.01885  -0.01777  -0.01620  -0.01406  -0.01085  -0.00738
  -0.00369   0.00000
  16.10000   8.00000  18.10000   0.00000   0.00000
   2.00000   0.00000  24.00000  18.00000   0.00000   0.00000   0.40000
   0.00000   0.50000   1.00000   1.50000   2.00000   2.50000   3.00000
   3.50000   4.00000   4.50000   5.00000   5.50000   6.00000   6.50000
   7.00000   7.50000   8.00000  24.0000
   0.00000   0.16200   0.31300   0.45300   0.58300   0.70300   0.81300
   0.91200   1.00000   1.07800   1.14600   1.20300   1.25000   1.28700
   1.31300   1.32800   1.33300   1.33300
  +2.00000  21.00000   0.00000   3.50000   0.00000   0.40000
  14.25223  -0.07500  16.77100   1.00000
   0.0       0.05000   0.10000   0.15000   0.20000   0.25000   0.30000
   0.35000   0.40000   0.45000   0.50000   0.55000   0.60000   0.65000
   0.70000   0.75000   0.80000   0.85000   0.90000   0.95000   1.00000
   0.0       0.01353   0.02446   0.03284   0.03875   0.04223   0.04338
   0.04338   0.04338   0.04338   0.04338   0.04338   0.04338   0.04338
   0.04338   0.04223   0.03875   0.03284   0.02446   0.01353   0.0
  13.53632  -0.82500  16.77100   1.00000
   0.0       0.01054   0.01905   0.02558   0.03017   0.03289   0.03378
   0.03378   0.03378   0.03378   0.03378   0.03378   0.03378   0.03378
   0.03378   0.03289   0.03017   0.02558   0.01905   0.01054   0.0
NIELSEN STORE
  12.02300  18.39800   3.50000   -1.2000   0.00000   0.00000   0.00000
  21.00000   0.00000   0.00000   0.00000   0.00000   0.40000   0.00000
 108.70563  11.76471  50.00000
   0.00000   2.35290   4.70590   7.05880   9.41180  11.75470  14.11760
  16.47060  18.82350  21.17650  23.52940  25.88240  28.23531  30.00000
  40.00000  60.00000  80.00000  90.00000  95.00000  98.00000 100.00000
   0.00000   1.17800   2.20390   3.09180   3.84780   4.47840   4.98820
   5.38040   5.65960   5.82590   5.88235   5.88235   5.88235   5.88235
   5.88235   5.88235   5.88235   5.88235   5.88235   5.88235   5.88235
```

```
F-14 WING/BODY/GLOVE (68 DEGREE LE) - MD
1.3        5.0        10.0       200.0      0.0        200.0      1.0
1.0        1.0        0.0
81360.0    117.618    532.5
10.0       50.0       1.0        160.06     0.4
   163.735      0.0      558.073      0.0        1.0                             160.55203
   0.0        0.00191   0.00491   0.00995   0.02000   0.03993   0.06000
   0.08000    0.10000   0.12000   0.14000   0.16000   0.18000   0.20000
   0.22000    0.24000   0.26000   0.28000   0.30000   0.32000   0.34000
   0.36000    0.38000   0.40000   0.42000   0.44000   0.46000   0.48000
   0.50000    0.52000   0.56000   0.60000   0.64000   0.68000   0.70000
   0.72000    0.74000   0.76000   0.78000   0.80000   0.82000   0.84000
   0.86000    0.88000   0.90000   0.92000   0.94000   0.96000   0.98000
   1.00000
  -0.00081    0.00141   0.00263   0.00391   0.00568   0.00826   0.01043
   0.01250    0.01453   0.01648   0.01835   0.02009   0.02168   0.02314
   0.02445    0.02562   0.02663   0.02750   0.02822   0.02881   0.02927
   0.02959    0.02981   0.02991   0.02993   0.02985   0.02970   0.02950
   0.02924    0.02893   0.02820   0.02733   0.02632   0.02510   0.02437
   0.02355    0.02260   0.02149   0.02020   0.01871   0.01702   0.01517
   0.01322    0.01125   0.00937   0.00761   0.00595   0.00432   0.00267
   0.00094
  -0.00081   -0.00209  -0.00280  -0.00360  -0.00474  -0.00623  -0.00736
  -0.00835   -0.00924  -0.01002  -0.01072  -0.01131  -0.01182  -0.01223
  -0.01256   -0.01281  -0.01299  -0.01310  -0.01313  -0.01311  -0.01304
  -0.01290   -0.01272  -0.01249  -0.01222  -0.01192  -0.01158  -0.01122
  -0.01083   -0.01043  -0.00959  -0.00872  -0.00784  -0.00698  -0.00655
  -0.00613   -0.00570  -0.00526  -0.00482  -0.00437  -0.00391  -0.00343
  -0.00293   -0.00243  -0.00192  -0.00140  -0.00088  -0.00036   0.00015
   0.00067
   349.598     68.500    641.342      0.0        1.0                             160.31653
  -0.00109    0.00191   0.00355   0.00528   0.00768   0.01116   0.01410
   0.01690    0.01964   0.02228   0.02480   0.02715   0.02931   0.03128
   0.03305    0.03463   0.03600   0.03717   0.03815   0.03894   0.03956
   0.04000    0.04029   0.04043   0.04045   0.04035   0.04015   0.03987
   0.03952    0.03911   0.03812   0.03694   0.03557   0.03392   0.03294
   0.03183    0.03055   0.02905   0.02730   0.02529   0.02301   0.02051
   0.01787    0.01521   0.01267   0.01028   0.00804   0.00584   0.00361
   0.00127
  -0.00109   -0.00282  -0.00378  -0.00487  -0.00641  -0.00842  -0.00995
  -0.01129   -0.01249  -0.01355  -0.01449  -0.01529  -0.01597  -0.01653
  -0.01698   -0.01732  -0.01756  -0.01770  -0.01775  -0.01772  -0.01762
  -0.01744   -0.01719  -0.01688  -0.01652  -0.01611  -0.01565  -0.01516
  -0.01464   -0.01410  -0.01296  -0.01178  -0.01060  -0.00943  -0.00885
  -0.00828   -0.00770  -0.00711  -0.00652  -0.00591  -0.00528  -0.00463
  -0.00396   -0.00328  -0.00259  -0.00189  -0.00119  -0.00049   0.00020
   0.00090
   432.354     99.000    678.418      0.0        1.0                             160.21167
   0.00048    0.00644   0.00972   0.01330   0.01832   0.02499   0.02969
   0.03340    0.03647   0.03909   0.04132   0.04320   0.04476   0.04600
   0.04694    0.04759   0.04799   0.04814   0.04808   0.04781   0.04737
   0.04676    0.04601   0.04512   0.04412   0.04302   0.04182   0.04054
   0.03920    0.03780   0.03490   0.03193   0.02895   0.02597   0.02446
   0.02295    0.02141   0.01985   0.01825   0.01662   0.01496   0.01327
   0.01157    0.00987   0.00816   0.00645   0.00475   0.00305   0.00134
  -0.00036
   0.00048   -0.00445  -0.00707  -0.00973  -0.01319  -0.01743  -0.02013
  -0.02210   -0.02361  -0.02478  -0.02569  -0.02638  -0.02688  -0.02723
  -0.02745   -0.02756  -0.02757  -0.02750  -0.02735  -0.02713  -0.02684
  -0.02648   -0.02603  -0.02549  -0.02486  -0.02413  -0.02330  -0.02238
  -0.02137   -0.02029  -0.01800  -0.01569  -0.01352  -0.01163  -0.01080
  -0.01006   -0.00938  -0.00876  -0.00817  -0.00760  -0.00703  -0.00644
  -0.00583   -0.00518  -0.00450  -0.00378  -0.00301  -0.00222  -0.00141
  -0.00061
   502.209    127.220    712.723      0.0        1.0                             160.16689
   0.00270    0.00855   0.01162   0.01513   0.02003   0.02682   0.03151
   0.03435    0.03572   0.03615   0.03606   0.03575   0.03539   0.03507
   0.03483    0.03468   0.03459   0.03456   0.03455   0.03455   0.03455
   0.03452    0.03442   0.03428   0.03406   0.03376   0.03337   0.03288
   0.03229    0.03160   0.02995   0.02793   0.02560   0.02298   0.02158
   0.02013    0.01863   0.01709   0.01552   0.01391   0.01228   0.01064
   0.00899    0.00734   0.00569   0.00404   0.00239   0.00074  -0.00091
  -0.00256
```

0.00270	-0.00238	-0.00521	-0.00783	-0.01124	-0.01510	-0.01730	
-0.01860	-0.01912	-0.01897	-0.01838	-0.01759	-0.01680	-0.01614	
-0.01564	-0.01531	-0.01509	-0.01497	-0.01491	-0.01489	-0.01488	
-0.01490	-0.01492	-0.01495	-0.01499	-0.01504	-0.01509	-0.01515	
-0.01521	-0.01527	-0.01536	-0.01535	-0.01519	-0.01482	-0.01453	
-0.01418	-0.01375	-0.01324	-0.01266	-0.01201	-0.01129	-0.01051	
-0.00968	-0.00880	-0.00787	-0.00691	-0.00591	-0.00490	-0.00387	
-0.00285							
502.098	127.240	712.747	0.0	1.0			160.21803
0.00295	0.00573	0.00745	0.00946	0.01237	0.01650	0.01960	
0.02212	0.02422	0.02602	0.02756	0.02888	0.03003	0.03100	
0.03184	0.03254	0.03311	0.03357	0.03393	0.03418	0.03434	
0.03441	0.03437	0.03425	0.03403	0.03371	0.03329	0.03278	
0.03217	0.03146	0.02976	0.02772	0.02537	0.02275	0.02135	
0.01989	0.01840	0.01686	0.01527	0.01367	0.01204	0.01040	
0.00874	0.00709	0.00544	0.00379	0.00214	0.00050	-0.00115	
-0.00280							
0.00295	-0.00016	-0.00213	-0.00413	-0.00667	-0.00961	-0.01141	
-0.01269	-0.01364	-0.01435	-0.01486	-0.01523	-0.01547	-0.01561	
-0.01569	-0.01570	-0.01566	-0.01560	-0.01551	-0.01542	-0.01533	
-0.01524	-0.01517	-0.01512	-0.01511	-0.01513	-0.01516	-0.01523	
-0.01531	-0.01541	-0.01557	-0.01564	-0.01551	-0.01515	-0.01485	
-0.01449	-0.01404	-0.01352	-0.01292	-0.01226	-0.01154	-0.01075	
-0.00991	-0.00903	-0.00811	-0.00715	-0.00615	-0.00514	-0.00411	
-0.00309							
551.010	147.000	736.767	0.0	1.0			159.90466
0.00349	0.00662	0.00828	0.01020	0.01293	0.01673	0.01954	
0.02180	0.02371	0.02535	0.02676	0.02797	0.02899	0.02984	
0.03053	0.03109	0.03151	0.03181	0.03201	0.03211	0.03213	
0.03206	0.03191	0.03169	0.03140	0.03104	0.03061	0.03011	
0.02954	0.02890	0.02740	0.02561	0.02352	0.02115	0.01986	
0.01851	0.01710	0.01563	0.01412	0.01258	0.01100	0.00941	
0.00781	0.00621	0.00461	0.00302	0.00144	-0.00015	-0.00173	
-0.00332							
0.00349	0.00058	-0.00114	-0.00301	-0.00529	-0.00785	-0.00937	
-0.01043	-0.01121	-0.01180	-0.01226	-0.01265	-0.01302	-0.01341	
-0.01382	-0.01426	-0.01473	-0.01521	-0.01570	-0.01617	-0.01663	
-0.01707	-0.01748	-0.01786	-0.01820	-0.01851	-0.01878	-0.01900	
-0.01918	-0.01931	-0.01941	-0.01929	-0.01892	-0.01829	-0.01787	
-0.01738	-0.01682	-0.01618	-0.01546	-0.01466	-0.01379	-0.01284	
-0.01183	-0.01077	-0.00965	-0.00849	-0.00729	-0.00608	-0.00486	
-0.00365							
598.080	166.000	759.864	0.0	1.0			159.33997
0.00253	0.00557	0.00715	0.00897	0.01141	0.01476	0.01718	
0.01910	0.02071	0.02209	0.02329	0.02436	0.02530	0.02612	
0.02685	0.02746	0.02798	0.02840	0.02873	0.02897	0.02911	
0.02918	0.02917	0.02908	0.02892	0.02869	0.02840	0.02804	
0.02761	0.02711	0.02592	0.02444	0.02267	0.02059	0.01944	
0.01822	0.01693	0.01557	0.01416	0.01270	0.01122	0.00971	
0.00819	0.00667	0.00516	0.00366	0.00216	0.00066	-0.00084	
-0.00234							
0.00253	-0.00040	-0.00221	-0.00410	-0.00637	-0.00912	-0.01093	
-0.01235	-0.01353	-0.01453	-0.01537	-0.01608	-0.01670	-0.01724	
-0.01774	-0.01821	-0.01866	-0.01909	-0.01951	-0.01992	-0.02030	
-0.02067	-0.02101	-0.02131	-0.02158	-0.02182	-0.02200	-0.02214	
-0.02222	-0.02225	-0.02213	-0.02177	-0.02116	-0.02029	-0.01975	
-0.01914	-0.01845	-0.01767	-0.01681	-0.01586	-0.01481	-0.01367	
-0.01245	-0.01116	-0.00982	-0.00843	-0.00702	-0.00558	-0.00415	
-0.00273							
650.151	187.000	785.392	0.0	1.0			158.37964
-0.00139	0.00167	0.00328	0.00511	0.00765	0.01107	0.01356	
0.01555	0.01722	0.01866	0.01993	0.02105	0.02206	0.02296	
0.02377	0.02449	0.02512	0.02566	0.02613	0.02651	0.02681	
0.02704	0.02719	0.02727	0.02728	0.02722	0.02710	0.02692	
0.02667	0.02637	0.02557	0.02452	0.02320	0.02161	0.02070	
0.01972	0.01866	0.01752	0.01632	0.01504	0.01371	0.01234	
0.01094	0.00954	0.00814	0.00678	0.00546	0.00417	0.00290	
0.00163							
-0.00139	-0.00444	-0.00621	-0.00802	-0.01027	-0.01292	-0.01464	
-0.01598	-0.01707	-0.01797	-0.01872	-0.01934	-0.01989	-0.02039	
-0.02085	-0.02129	-0.02171	-0.02210	-0.02248	-0.02282	-0.02314	
-0.02341	-0.02365	-0.02383	-0.02397	-0.02405	-0.02408	-0.02405	
-0.02396	-0.02381	-0.02334	-0.02263	-0.02168	-0.02045	-0.01973	

```
  -0.01893  -0.01805  -0.01707  -0.01598  -0.01478  -0.01347  -0.01206
  -0.01055  -0.00897  -0.00733  -0.00565  -0.00395  -0.00224  -0.00053
   0.00116
   699.743   207.000   808.049     0.0       1.0                          157.43750
  -0.00675  -0.00368  -0.00195  -0.00006   0.00256   0.00615   0.00874
   0.01084   0.01262   0.01416   0.01552   0.01674   0.01783   0.01883
   0.01974   0.02057   0.02133   0.02202   0.02263   0.02318   0.02366
   0.02408   0.02444   0.02472   0.02495   0.02512   0.02522   0.02527
   0.02526   0.02519   0.02488   0.02434   0.02359   0.02261   0.02203
   0.02140   0.02070   0.01994   0.01912   0.01822   0.01727   0.01624
   0.01517   0.01407   0.01296   0.01188   0.01086   0.00992   0.00902
   0.00813
  -0.00675  -0.00985  -0.01167  -0.01348  -0.01565  -0.01818  -0.01979
  -0.02100  -0.02195  -0.02271  -0.02333  -0.02386  -0.02433  -0.02476
  -0.02516  -0.02552  -0.02584  -0.02613  -0.02637  -0.02655  -0.02669
  -0.02677  -0.02679  -0.02676  -0.02667  -0.02653  -0.02634  -0.02609
  -0.02579  -0.02544  -0.02459  -0.02351  -0.02218  -0.02058  -0.01965
  -0.01863  -0.01751  -0.01628  -0.01492  -0.01345  -0.01185  -0.01015
  -0.00837  -0.00652  -0.00461  -0.00267  -0.00069   0.00132   0.00335
   0.00537
   754.789   229.200   833.199     0.0       1.0                          156.39172
  -0.01701  -0.01392  -0.01196  -0.00996  -0.00718  -0.00327  -0.00049
   0.00182   0.00381   0.00554   0.00708   0.00849   0.00973   0.01092
   0.01202   0.01307   0.01407   0.01505   0.01593   0.01680   0.01763
   0.01841   0.01918   0.01984   0.02049   0.02110   0.02162   0.02211
   0.02256   0.02293   0.02356   0.02400   0.02434   0.02452   0.02458
   0.02462   0.02461   0.02457   0.02448   0.02431   0.02409   0.02371
   0.02327   0.02274   0.02219   0.02164   0.02120   0.02093   0.02074
   0.02057
  -0.01701  -0.02021  -0.02212  -0.02393  -0.02595  -0.02825  -0.02965
  -0.03061  -0.03129  -0.03178  -0.03216  -0.03251  -0.03283  -0.03313
  -0.03341  -0.03362  -0.03375  -0.03385  -0.03382  -0.03369  -0.03349
  -0.03320  -0.03280  -0.03237  -0.03184  -0.03128  -0.03067  -0.03000
  -0.02929  -0.02856  -0.02698  -0.02519  -0.02314  -0.02083  -0.01950
  -0.01806  -0.01648  -0.01477  -0.01289  -0.01090  -0.00875  -0.00649
  -0.00420  -0.00183   0.00060   0.00304   0.00555   0.00814   0.01078
   0.01343
3.         93.0      780.0                                   0.16
F-14 FUSELAGE MODEL
8.
1.        2.        NOSE
BLO       ELLI      BCL       MHB       SCPLO
BUP       ELLI      MHB       TCL       SCPUP
2.        4.        NOSE WITH CANOPY
BLO       ELLI      BCL       MHB       SCPLO
BSI       LINE      MHB       FUP
BUP       ELLI      FUP       CREASE    SCPUP
CAN       ELLI      CREASE    TCL       SCPCAN
3.        7.        INLET
BLO       ELLI      BCL       MHB       SCPLO
BSI       LINE      MHB       FLO
NACLO     LINE      FLO       INLTLO
NACSI     LINE      INLTLO    INLTUP
NACUP     LINE      INLTUP    FUP
BUP       ELLI      FUP       CREASE    SCPUP
CAN       ELLI      CREASE    TCL       SCPCAN
4.        6.        INLET TO NACELLE FOWARD FAIRING
BLO       ELLI      BCL       FLO       SCPLO
NACLO     LINE      FLO       INLTLO
NACSI     LINE      INLTLO    INLTUP
NACUP     LINE      INLTUP    FUP
BUP       ELLI      FUP       CREASE    SCPUP
CAN       ELLI      CREASE    TCL       SCPCAN
5.        6.        INLET TO NACELLE AFT FAIRING
BLO       LINE      BCL       FLO
NACLO     LINE      FLO       INLTLO
NACSI     LINE      INLTLO    INLTUP
NACUP     LINE      INLTUP    FUP
BUP       ELLI      FUP       CREASE    SCPUP
CAN       ELLI      CREASE    TCL       SCPCAN
6.        7.        FOWARD NACELLE
BLO       LINE      BCL       FLO
NACLO     LINE      FLO       INLTLO
```

```
NACLS   ELLI    INLTLO   MHB      SCPLO
NACSI   LINE    MHB      INLTUP
NACUP   LINE    INLTUP   FUP
BUP     ELLI    FUP      CREASE   SCPUP
CAN     ELLI    CREASE   TCL      SCPCAN
7.      6.      MID NACELLE
BLO     LINE    BCL      FLO
NACLO   LINE    FLO      INLTLO
NACLS   ELLI    INLTLO   MHB      SCPLO
NACSI   LINE    MHB      INLTUP
NACUP   LINE    INLTUP   FUP
BUP     ELLI    FUP      TCL      SCPUP
8.      6.      AFT NACELLE
BLO     LINE    BCL      FLO
NACLO   LINE    FLO      INLTLO
NACLS   ELLI    INLTLO   CREASE   SCPCAN
NACSI   LINE    CREASE   INLTUP
NACUP   LINE    INLTUP   FUP
BUP     LINE    FUP      TCL
8.
1.      1.      93.0     205.0
2.      2.      205.0    352.0
3.      3.      352.0    414.5
4.      4.      414.5    425.0
5.      5.      425.0    433.0
6.      6.      433.0    497.0
7.      7.      497.0    650.0
8.      8.      650.0    780.0
22.0    2.0
10.0    ZTCL
ELLX    93.0    131.45   205.0    171.0    127.5    152.0
LINE    205.0   171.0    241.0    191.65
ELLY    241.0   191.65   313.0    203.0    274.0    203.0
ELLY    313.0   203.0    352.0    199.5    331.0    203.0
LINE    352.0   199.5    497.0    174.5
LINE    497.0   174.5    546.0    169.5
LINE    546.0   169.5    600.0    165.0
LINE    600.0   165.0    650.0    160.5
LINE    650.0   160.5    697.0    165.5
LINE    697.0   165.5    780.0    162.75
10.0    ZBCL
ELLX    93.0    131.45   176.0    116.5    129.5    116.5
LINE    176.0   116.5    205.0    118.0
LINE    205.0   118.0    352.0    121.75
LINE    352.0   121.75   425.0    123.43
LINE    425.0   123.43   433.0    117.0
LINE    433.0   117.0    497.0    107.8
LINE    497.0   107.8    546.0    104.7
LINE    546.0   104.7    600.0    103.0
LINE    600.0   103.0    650.0    104.0
LINE    650.0   104.0    780.0    113.0
7.0     YMHB
ELLY    93.0    0.0      352.0    31.0     164.0    31.0
LINE    352.0   31.0     414.5    29.5
LINE    414.5   29.5     433.0    75.0
LINE    433.0   75.0     497.0    74.0
LINE    497.0   74.0     546.0    73.0
LINE    546.0   73.0     600.0    76.5
LINE    600.0   76.5     650.0    79.0
9.0     ZMHB
LINE    93.0    131.45   164.0    138.0
LINE    164.0   138.0    205.0    138.5
LINE    205.0   138.5    352.0    130.5
LINE    352.0   130.5    414.5    127.93
LINE    414.5   127.93   433.0    119.0
LINE    433.0   119.0    497.0    125.5
LINE    497.0   125.5    546.0    139.0
LINE    546.0   139.0    600.0    139.5
LINE    600.0   139.5    650.0    140.0
9.0     YCREASE
LINE    205.0   0.0      221.0    15.5
LINE    221.0   15.5     283.0    16.0
LINE    283.0   16.0     328.0    16.5
```

LINE	328.0	16.5	352.0	16.0		
LINE	352.0	16.0	405.0	13.0		
LINE	405.0	13.0	497.0	0.0		
LINE	497.0	0.0	650.0	79.0		
LINE	650.0	79.0	697.0	80.5		
LINE	697.0	80.5	780.0	81.0		
9.0	ZCREASE					
LINE	205.0	171.0	221.0	169.0		
LINE	221.0	169.0	283.0	179.0		
LINE	283.0	179.0	328.0	183.0		
LINE	328.0	183.0	352.0	183.5		
LINE	352.0	183.5	405.0	182.0		
LINE	405.0	182.0	497.0	174.5		
LINE	497.0	174.5	650.0	140.0		
LINE	650.0	140.0	697.0	140.0		
LINE	697.0	141.0	780.0	140.0		
7.0	YFUP					
ELLY	93.0	0.0	352.0	31.0	164.0	31.0
LINE	352.0	31.0	497.0	19.5		
LINE	497.0	19.5	546.0	14.0		
LINE	546.0	14.0	600.0	11.0		
LINE	600.0	11.0	650.0	0.0		
LINE	650.0	0.0	697.0	49.5		
LINE	697.0	49.5	780.0	51.0		
8.0	ZFUP					
LINE	93.0	131.45	205.0	138.5		
LINE	205.0	138.5	352.0	155.0		
LINE	352.0	155.0	497.0	163.0		
LINE	497.0	163.0	546.0	163.5		
LINE	546.0	163.5	600.0	163.0		
LINE	600.0	163.0	650.0	160.5		
LINE	650.0	160.5	697.0	165.5		
LINE	697.0	165.5	780.0	162.75		
6.0	YSCPUP					
ELLY	93.0	0.0	352.0	31.0	164.0	31.0
LINE	352.0	31.0	405.0	23.5		
LINE	405.0	23.5	497.0	14.0		
LINE	497.0	14.0	546.0	7.5		
LINE	546.0	7.5	600.0	5.0		
LINE	600.0	5.0	650.0	0.0		
7.0	ZSCPUP					
ELLX	93.0	131.45	205.0	171.0	127.5	152.0
LINE	205.0	171.0	221.0	158.0		
LINE	221.0	158.0	352.0	173.0		
LINE	352.0	173.0	497.0	174.5		
LINE	497.0	174.5	546.0	169.5		
LINE	546.0	169.5	600.0	165.0		
LINE	600.0	165.0	650.0	160.5		
9.0	YSCPCAN					
LINE	205.0	0.0	221.0	12.5		
LINE	221.0	12.5	283.0	16.0		
LINE	283.0	16.0	328.0	16.5		
LINE	328.0	16.5	352.0	16.0		
LINE	352.0	16.0	405.0	9.5		
LINE	405.0	9.5	497.0	0.0		
LINE	497.0	0.0	650.0	81.5		
LINE	650.0	81.5	697.0	82.5		
LINE	697.0	82.5	780.0	83.0		
7.0	ZSCPCAN					
LINE	205.0	171.0	241.0	191.65		
ELLY	241.0	191.65	313.0	203.0	274.0	203.0
ELLY	313.0	203.0	352.0	199.5	331.0	203.0
LINE	352.0	199.5	497.0	174.5		
LINE	497.0	174.5	650.0	105.5		
LINE	650.0	105.5	697.0	110.0		
LINE	697.0	110.0	780.0	116.0		
9.0	ZSCPLO					
ELLX	93.0	131.45	176.0	116.5	129.5	116.5
LINE	176.0	116.5	205.0	118.0		
LINE	205.0	118.0	352.0	121.75		
LINE	352.0	121.75	425.0	123.43		
LINE	425.0	123.43	433.0	119.0		
LINE	433.0	119.0	497.0	113.0		

```
LINE    497.0    113.0    546.0    110.0
LINE    546.0    110.0    600.0    105.0
LINE    600.0    105.0    650.0    105.5
8.0     YSCPLO
ELLY    93.0     0.0      352.0    31.0     164.0    31.0
LINE    352.0    31.0     414.5    29.5
LINE    414.5    29.5     425.0    39.79
LINE    425.0    39.79    433.0    75.0
LINE    433.0    75.0     497.0    76.2
LINE    497.0    76.2     546.0    77.7
LINE    546.0    77.7     600.0    79.0
LINE    600.0    79.0     650.0    81.5
1.0     YMAPAXIS
LINE    93.0     0.0      780.0    0.0
2.0     ZMAPAXIS
LINE    93.0     131.45   352.0    146.0
LINE    352.0    146.0    780.0    147.0
9.0     YFLO
LINE    352.0    31.0     414.5    29.5
LINE    414.5    29.5     425.0    39.79
LINE    425.0    39.79    433.0    42.0
LINE    433.0    42.0     497.0    46.3
LINE    497.0    46.3     546.0    47.5
LINE    546.0    47.5     600.0    48.5
LINE    600.0    48.5     650.0    49.5
LINE    650.0    49.5     697.0    49.75
LINE    697.0    49.75    780.0    51.0
9.0     ZFLO
LINE    352.0    150.0    414.5    127.93
LINE    414.5    127.93   425.0    123.43
LINE    425.0    123.43   433.0    117.0
LINE    433.0    117.0    497.0    107.8
LINE    497.0    107.8    546.0    104.7
LINE    546.0    104.7    600.0    103.0
LINE    600.0    103.0    650.0    104.0
LINE    650.0    104.0    697.0    107.0
LINE    697.0    107.0    780.0    113.0
7.0     YINLTUP
LINE    352.0    66.5     433.0    66.5
LINE    433.0    66.5     497.0    66.5
LINE    497.0    66.5     546.0    68.0
LINE    546.0    68.0     600.0    74.5
LINE    600.0    74.5     650.0    77.0
LINE    650.0    77.0     697.0    78.5
LINE    697.0    78.5     780.0    80.0
7.0     ZINLTUP
LINE    352.0    162.5    433.0    169.0
LINE    433.0    169.0    497.0    171.5
LINE    497.0    171.5    546.0    170.0
LINE    546.0    170.0    600.0    165.0
LINE    600.0    165.0    650.0    162.0
LINE    650.0    162.0    697.0    160.0
LINE    697.0    160.0    780.0    155.5
7.0     YINLTLO
LINE    352.0    67.0     433.0    75.0
LINE    433.0    75.0     497.0    65.5
LINE    497.0    66.5     546.0    61.0
LINE    546.0    61.0     600.0    57.0
LINE    600.0    57.0     650.0    57.5
LINE    650.0    57.5     697.0    58.0
LINE    697.0    58.0     780.0    59.0
7.0     ZINLTLO
LINE    352.0    156.5    433.0    119.0
LINE    433.0    119.0    497.0    111.0
LINE    497.0    111.0    546.0    107.0
LINE    546.0    107.0    600.0    104.0
LINE    600.0    104.0    650.0    104.0
LINE    650.0    104.0    697.0    108.0
LINE    697.0    108.0    780.0    114.0
        YTCL     YMAPAXIS
        YBCL     YMAPAXIS
```

```
SC3 DEMONSTRATION WING - BASIC LEADING EDGE
1.620      12.000     2.4        200.0      0.0        200.0      1.0
1.0        0.0        0.0
342.11     23.840     16.701
11.0       30.0       1.0        0.0        0.4
   0.0        0.0       23.840      0.0        1.0
  0.0       0.00147   0.00586   0.01317   0.02338   0.03645   0.05235
  0.07102   0.09242   0.11649   0.14314   0.17231   0.20391   0.23784
  0.27400   0.31230   0.35261   0.39483   0.43881   0.48445   0.53159
  0.58011   0.62986   0.68070   0.73247   0.78503   0.83822   0.89188
  0.94586   1.00000
  0.0       0.00187   0.00367   0.00541   0.00709   0.00870   0.01023
  0.01169   0.01306   0.01434   0.01552   0.01659   0.01754   0.01836
  0.01903   0.01954   0.01987   0.02000   0.01991   0.01959   0.01900
  0.01814   0.01699   0.01554   0.01378   0.01171   0.00933   0.00665
  0.00367   0.00040
  0.0      -0.00187  -0.00367  -0.00541  -0.00709  -0.00870  -0.01023
 -0.01169  -0.01306  -0.01434  -0.01552  -0.01659  -0.01754  -0.01836
 -0.01903  -0.01954  -0.01987  -0.02000  -0.01991  -0.01959  -0.01900
 -0.01814  -0.01699  -0.01554  -0.01378  -0.01171  -0.00933  -0.00665
 -0.00367  -0.00040
   3.151      1.470     24.135      0.0        1.0
 -0.00883  -0.00607  -0.00286   0.00064   0.00425   0.00790   0.01152
  0.01503   0.01839   0.02153   0.02436   0.02691   0.02913   0.03104
  0.03263   0.03386   0.03476   0.03534   0.03557   0.03547   0.03502
  0.03424   0.03313   0.03167   0.02989   0.02778   0.02536   0.02262
  0.01961   0.01630
 -0.00883  -0.01088  -0.01209  -0.01262  -0.01266  -0.01232  -0.01169
 -0.01085  -0.00992  -0.00896  -0.00807  -0.00728  -0.00662  -0.00607
 -0.00561  -0.00528  -0.00498  -0.00466  -0.00425  -0.00370  -0.00298
 -0.00204  -0.00085   0.00060   0.00233   0.00436   0.00669   0.00933
  0.01227   0.01550
   6.299      2.939     24.431      0.0        1.0
 -0.02043  -0.01732  -0.01391  -0.01025  -0.00643  -0.00254   0.00136
  0.00526   0.00914   0.01299   0.01679   0.02052   0.02412   0.02756
  0.03079   0.03376   0.03643   0.03875   0.04065   0.04208   0.04301
  0.04340   0.04321   0.04247   0.04122   0.03950   0.03737   0.03484
  0.03196   0.02874
 -0.02043  -0.02293  -0.02453  -0.02531  -0.02538  -0.02486  -0.02389
 -0.02251  -0.02081  -0.01885  -0.01670  -0.01443  -0.01212  -0.00983
 -0.00760  -0.00542  -0.00332  -0.00124   0.00082   0.00290   0.00501
  0.00711   0.00923   0.01139   0.01366   0.01608   0.01870   0.02155
  0.02463   0.02794
   9.417      4.409     24.729      0.0        1.0
 -0.02314  -0.01979  -0.01627  -0.01259  -0.00879  -0.00491  -0.00098
  0.00295   0.00690   0.01087   0.01488   0.01895   0.02307   0.02723
  0.03139   0.03549   0.03945   0.04319   0.04655   0.04948   0.05189
  0.05375   0.05503   0.05571   0.05582   0.05540   0.05446   0.05300
  0.05105   0.04864
 -0.02314  -0.02593  -0.02782  -0.02884  -0.02907  -0.02861  -0.02757
 -0.02605  -0.02412  -0.02185  -0.01930  -0.01650  -0.01350  -0.01035
 -0.00708  -0.00373  -0.00031   0.00319   0.00673   0.01030   0.01389
  0.01747   0.02105   0.02464   0.02826   0.03198   0.03580   0.03970
  0.04372   0.04784
  12.396      5.879     25.047      0.0        1.0
 -0.02485  -0.02140  -0.01783  -0.01417  -0.01039  -0.00654  -0.00263
  0.00135   0.00537   0.00944   0.01359   0.01784   0.02220   0.02669
  0.03127   0.03590   0.04048   0.04491   0.04907   0.05288   0.05626
  0.05915   0.06154   0.06344   0.06486   0.06576   0.06618   0.06608
  0.06551   0.06447
 -0.02485  -0.02779  -0.02982  -0.03097  -0.03131  -0.03091  -0.02985
 -0.02824  -0.02616  -0.02370  -0.02091  -0.01784  -0.01452  -0.01098
 -0.00724  -0.00333   0.00072   0.00491   0.00925   0.01371   0.01826
  0.02287   0.02756   0.03237   0.03729   0.04234   0.04751   0.05279
  0.05817   0.06367
  15.067      7.349     25.460      0.0        1.0
 -0.02641  -0.02293  -0.01929  -0.01551  -0.01158  -0.00751  -0.00333
  0.00108   0.00560   0.01014   0.01458   0.01891   0.02332   0.02781
  0.03239   0.03702   0.04164   0.04616   0.05049   0.05459   0.05841
  0.06196   0.06518   0.06804   0.07050   0.07253   0.07412   0.07525
  0.07591   0.07612
 -0.02641  -0.02935  -0.03133  -0.03240  -0.03259  -0.03197  -0.03065
 -0.02859  -0.02600  -0.02306  -0.01996  -0.01680  -0.01343  -0.00988
```

-0.00613	-0.00222	0.00188	0.00616	0.01067	0.01541	0.02040
0.02568	0.03120	0.03696	0.04294	0.04911	0.05546	0.06195
0.06858	0.07532					
17.461	8.818	26.101	0.0	1.0		
-0.02715	-0.02362	-0.01988	-0.01593	-0.01178	-0.00749	-0.00306
0.00146	0.00601	0.01055	0.01501	0.01933	0.02353	0.02775
0.03204	0.03639	0.04075	0.04510	0.04941	0.05359	0.05761
0.06145	0.06504	0.06836	0.07137	0.07404	0.07634	0.07827
0.07979	0.08090					
-0.02715	-0.03004	-0.03192	-0.03282	-0.03279	-0.03195	-0.03037
-0.02821	-0.02559	-0.02264	-0.01953	-0.01638	-0.01322	-0.00993
-0.00648	-0.00285	0.00099	0.00511	0.00958	0.01441	0.01961
0.02516	0.03106	0.03728	0.04380	0.05062	0.05767	0.06497
0.07245	0.08010					
19.746	10.288	26.956	0.0	1.0		
-0.02700	-0.02352	-0.01985	-0.01605	-0.01210	-0.00802	-0.00384
0.00044	0.00479	0.00917	0.01359	0.01800	0.02233	0.02655
0.03076	0.03503	0.03936	0.04366	0.04788	0.05199	0.05596
0.05973	0.06331	0.06665	0.06974	0.07253	0.07504	0.07720
0.07905	0.08055					
-0.02700	-0.02994	-0.03189	-0.03294	-0.03311	-0.03248	-0.03116
-0.02923	-0.02681	-0.02402	-0.02095	-0.01771	-0.01442	-0.01113
-0.00776	-0.00420	-0.00040	0.00366	0.00806	0.01282	0.01795
0.02345	0.02933	0.03557	0.04217	0.04911	0.05637	0.06391
0.07171	0.07975					
22.012	11.758	27.895	0.0	1.0		
-0.03304	-0.02957	-0.02596	-0.02222	-0.01835	-0.01436	-0.01025
-0.00599	-0.00164	0.00283	0.00738	0.01199	0.01663	0.02123
0.02572	0.03008	0.03435	0.03856	0.04267	0.04661	0.05039
0.05397	0.05735	0.06047	0.06335	0.06595	0.06828	0.07031
0.07205	0.07348					
-0.03304	-0.03599	-0.03800	-0.03911	-0.03936	-0.03882	-0.03757
-0.03566	-0.03324	-0.03037	-0.02717	-0.02372	-0.02011	-0.01645
-0.01280	-0.00916	-0.00541	-0.00143	0.00284	0.00743	0.01238
0.01769	0.02337	0.02939	0.03579	0.04253	0.04961	0.05701
0.06472	0.07268					
24.277	13.227	28.850	0.0	1.0		
-0.04749	-0.04402	-0.04047	-0.03680	-0.03302	-0.02911	-0.02508
-0.02092	-0.01662	-0.01219	-0.00763	-0.00294	0.00185	0.00667
0.01149	0.01625	0.02087	0.02526	0.02930	0.03313	0.03672
0.04007	0.04320	0.04603	0.04860	0.05089	0.05286	0.05455
0.05593	0.05702					
-0.04749	-0.05044	-0.05251	-0.05368	-0.05403	-0.05357	-0.05239
-0.05058	-0.04822	-0.04539	-0.04218	-0.03865	-0.03490	-0.03102
-0.02703	-0.02298	-0.01889	-0.01473	-0.01053	-0.00605	-0.00128
0.00379	0.00922	0.01496	0.02103	0.02746	0.03420	0.04125
0.04860	0.05622					
26.559	14.697	29.807	0.0	1.0		
-0.07392	-0.07045	-0.06699	-0.06346	-0.05982	-0.05617	-0.05236
-0.04845	-0.04439	-0.04017	-0.03584	-0.03127	-0.02650	-0.02161
-0.01651	-0.01135	-0.00605	-0.00091	0.00404	0.00839	0.01188
0.01502	0.01782	0.02033	0.02252	0.02443	0.02596	0.02716
0.02809	0.02867					
-0.07392	-0.07687	-0.07903	-0.08034	-0.08081	-0.08063	-0.07969
-0.07814	-0.07599	-0.07337	-0.07036	-0.06698	-0.06325	-0.05928
-0.05503	-0.05058	-0.04581	-0.04093	-0.03579	-0.03077	-0.02614
-0.02128	-0.01616	-0.01076	-0.00502	0.00103	0.00730	0.01386
0.02076	0.02787					

OUTPUT DATA FORMAT

Output data format for the TSCLP Code is very similar to that for the basic NASA/Grumman Transonic Wing-Body Codes (Refs. 1,2). Geometry verification is obtained only by specifying zero iterations. Printed and plotted output includes information sufficient to verify input configuration geometry, generated grid structures, and computational representation of configuration components. Analysis runs are obtained when some non-zero number of iterations is specified. Printed output includes solution iteration convergence history followed by resultant surface velocities and pressures, load distributions, and force and moment coefficients for each component. Plotted output of surface pressures, load distributions, and force and moment coefficients is produced only when some non-zero number of "fine grid" iterations is specified. Printed and plotted output will then also include a force and moment summary for the entire configuration, on a component-by-component basis.

Note that integrated forces and moments are output both with and without store body viscous crossflow estimates. Viscous skin friction estimates are not included in the integrated forces and moments but are always output as separate, distinct quantities.

SUBROUTINE CALL SEQUENCE

MAIN PROGRAM SUBROUTINE CALL SEQUENCE : STATS

```
STATS ──┬─ WNGDAT
        ├─ BODDAT ───┬─ QWIKDE →
        │            └─ QWIKLO →
        ├─ CRUSET ───┬─ BODSET ───┬─ SLOPE ──── SPLINE
        │            │            ├─ BODLIM ─── QWIKLO →
        │            │            ├─ SAREA
        │            │            └─ QWIKLO →
        │            ├─ BUMP
        │            └─ QWIKLO →
        ├─ WNGSET ───┬─ SLOPE ──── SPLINE
        │            ├─ SPLINE
        │            └─ QWIKLO →
        ├─ STRDAT
        ├─ WSISET ──── SLOPE ──── SPLINE
        ├─ CEESET ───┬─ SNGLRT ─── INT3D
        │            ├─ CEEDIF
        │            ├─ ARC2D
        │            ├─ INT2D
        │            ├─ INT3D
        │            ├─ FINTIP ───┬─ BUMP
        │            │            └─ LGRNG
        │            └─ FINSET ─── FINBCS ─── CBCSPL
        ├─ PYLSET ───┬─ LGRNG
        │            ├─ PYLBCS
        │            └─ CBCSPL
        ├─ CONTRL →
        └─ PLTSET ──── QWIKLO →
```

SUBROUTINE CALL SEQUENCE : CONTRL

- CONTRL
  - OUTPUT
    - CRUOUT
    - WSIOUT
    - WFGOUT
      - WFGFIL →
    - SMOTH
    - STRIPK →
    - BODOUT
      - SPLINE
      - BODFM
        - QWIKLO →
    - PYLCPS
    - CE1CPS
      - CE1REL
        - TRIDBC
    - CE2CPS
      - CE2REL
        - TRIDBC
    - FMSOUT
  - GLOBAL
    - CRUCUT
      - TRID
    - TRID
  - SUPSET
    - MCHANG
  - WINGF
    - TRID
  - WFGFIL →
  - BODVAL
  - BLAR
    - SPLINE
    - SMOTH
    - VINTER
    - STRIPK →
  - WSIREL
    - WSICUT
      - TRID
    - TRID
  - CE1REL
    - CE1PYL
      - ARC1
      - ARC2
    - ARC1
    - ARC2
    - ARC3
    - TRIDBC
  - CE2REL
    - CE2PYL
      - ARC2
    - ARC2
    - ARC3
    - TRIDBC
  - CRUINT
  - WSIINT
  - CE1INT
  - CRUFIL →
  - WSIFIL →
  - CE1FIL →
  - CE2FIL
  - FINFIL
  - PYLFIL

SUBROUTINE CALL SEQUENCE : WFGFIL

- WFGFIL
  - WFGP
  - WFGV
  - WFGVX
  - WFGVZ
  - WFGZ2
  - WFGZ3
  - WFGZ4 — TRIDBC
  - WFGZ5 — TRIDBC
  - WFGZ6 — TRIDBC
  - WFGZ7 — TRIDBC
  - CRUZ2
  - CRUZ3
  - CRUZ4
  - CRUZ5
  - CRUZ6
  - CRUZ7
  - WSIZ2
  - WSIZ3
  - WSIZ4
  - WSIZ5
  - WSIZ6
  - WSIZ7
  - TRIDBC

SUBROUTINE CALL SEQUENCE : CRUFIL

- CRUFIL
  - CRUZ2
  - CRUZ3
  - CRUZ4
  - CRUZ5
  - CRUZ6
  - CRUZ7
  - WSIZ2
  - WSIZ3
  - WSIZ4
  - WSIZ5
  - WSIZ6
  - WSIZ7

SUBROUTINE CALL SEQUENCE : WSIFIL

- WSIFIL
  - CRUZ2
  - CRUZ3
  - CRUZ4
  - CRUZ5
  - CRUZ6
  - CRUZ7
  - WSIZ2
  - WSIZ3
  - WSIZ4
  - WSIZ5
  - WSIZ6
  - WSIZ7
  - CE1Z4
  - CE1Z5
  - CE1Z6
  - CE1Z7

SUBROUTINE CALL SEQUENCE : CE1FIL

- CE1FIL
  - WSIZ2
  - WSIZ3
  - WSIZ4
  - WSIZ5
  - WSIZ6
  - WSIZ7
  - CE1Z4
  - CE1Z5
  - CE1Z6
  - CE1Z7

SUBROUTINE CALL SEQUENCE : QWIKDE

```
QWIKDE ─┬─ CSMDEF ─┬─ DSETUP
        │          └─ DLOKUP
        ├─ CSMCHK
        ├─ BLMDEF ─┬─ DSETUP
        │          ├─ DLOKUP
        │          ├─ CURVES
        │          └─ KRVDEF
        ├─ BLMCHK
        └─ GEMOUT
```

SUBROUTINE CALL SEQUENCE : QWIKLO

```
QWIKLO ─┬─ CSGEOM ─┬─ BLMSET ─── CURVES
        │          ├─ BLGEOM
        │          ├─ CSMSET ─┬─ BLGEOM
        │          │          └─ CSMCOE
        │          ├─ THELIM ─┬─ AORDER
        │          │          ├─ CSMFLT ─┬─ CSCALC ─┬─ SINCOS
        │          │          │          │          ├─ VDOTV
        │          │          │          │          └─ MDOTV
        │          │          │          ├─ BLGEOM
        │          │          │          ├─ CSMCOE
        │          │          │          └─ SINCOS
        │          │          └─ CSMINT ─┬─ LINLIN ─── CROSS
        │          │                     ├─ LINELL ─┬─ ELLCAL ─── SINCOS
        │          │                     │          └─ SINCOS
        │          │                     └─ ELLELL ─┬─ ELLCAL ─── SINCOS
        │          │                                ├─ CROSS
        │          │                                ├─ ESTNXT
        │          │                                └─ SETNXT
        │          └─ CSCALC ─┬─ SINCOS
        │                     ├─ VDOTV
        │                     └─ MDOTV
        └─ SMOTH
```

SUBROUTINE CALL SEQUENCE : STRIPK

```
-[STRIPK]---+-- BLLAM ----+-- SLOPY ---------- SPLN1
            |             |-- SPLN1
            |             +-- ORDIN
            +-- VBRAD ----+-- VNUSUB
                          |-- SLOPBL --------- GRAD
                          |-- TANCAL --------- GORD
                          |-- SPRINT
                          |-- FINT
                          |-- SOLVEB
                          |-- ORDIN
                          |-- REDUCX
                          |-- RLORD
                          |-- GORD
                          +-- SIMPSN
```

PLOTTING PROGRAM SUBROUTINE CALL SEQUENCE : STATSP

```
[STATSP]───┬─ GEVER
           ├─ STRVER
           ├─ WFGPLT
           ├─ BODPLT
           ├─ PYLPLT
           ├─ CE2PLT
           └─ FMSPLT
```

HIGH-LEVEL PLOTTING SUBROUTINES CALLED BY THE ABOVE:

CRAY XMP versions contain DISSPLA calls

LaRC CDC versions contain Langley CALCOMP calls

```
──┬─ PGSTRT
  ├─ PGSTOP
  ├─ PSTRT
  ├─ PSTOP
  ├─ SPSTRT
  ├─ SPSTOP
  ├─ GSETUP
  ├─ XSETUP
  ├─ YSETUP
  ├─ SETHIT
  ├─ WMESS
  ├─ WREAL
  ├─ WINTG
  ├─ DRAWP
  └─ DRAWG
```

SUBROUTINE	DESCRIPTION
AORDER	Orders a set of numbers by permutation index
ARC1	Inverts tridiagonal matrix for C-grids
ARC2	Inverts tridiagonal matrix for C-grids (modified storage scheme)
ARC2D	Computes arc length along a 2-D curve
ARC3	Inverts periodic tridiagonal matrix for C-grids
BLAR	Main control routine for laminar and turbulent modified chordwise boundary layer calculation. Computes boundary layer displacement thickness slope for viscous/inviscid interaction mode of operation
BLGEOM	Assigns body line model values and derivatives to control point coordinates
BLLAM	Computes Thwaites laminar boundary layer with Rott and Crabtree compressibility modification
BLMCHK	Correlates and checks the input data deck and the indices for the generated body line math models
BLMDEF	Defines body line models from the input data
BLMSET	Controls the determination values and first and second derivatives for all body line models at a given x-station
BLOCK DATA	Initializes in-core memory to zero
BODDAT	Reads axisymmetric or QUICK fuselage input data
BODFM	Computes integrated fuselage force and moment coefficients
BODLIM	Computes fuselage global crude grid limiters
BODOUT	Prints out solution for fuselage
BODPLT	Plots solution for fuselage
BODSET	Controls set up for fuselage in global crude grid
BODVAL	Computes fuselage boundary point potential values
BUMP	Bump function for grid modifications
CBCSPL	Computes cubic splines through sets of points
CE1CPS	Prints out coarse C-grid solution for store
CE1FIL	Interpolation routine for coarse C-grid boundaries
CE1INT	Initializes interpolation parameters for use in CE1FIL
CE1PYL	Relaxation routine to treat pylon surface in coarse C-grid
CE1REL	Relaxation routine for coarse C-grid

CE1Z4	Zone 4 set up for coarse C-grid interpolations (above wing and outboard of pylon)
CE1Z5	Zone 5 set up for coarse C-grid interpolations (above wing and inboard of pylon)
CE1Z6	Zone 6 set up for coarse C-grid interpolations (below wing and outboard of pylon)
CE1Z7	Zone 7 set up for coarse C-grid interpolations (below wing and inboard of pylon)
CE2CPS	Prints out fine C-grid solution for store
CE2FIL	Interpolation routine for fine C-grid boundaries
CE2PLT	Plots fine C-grid solution for store
CE2PYL	Relaxation routine to treat pylon surface in fine C-grid
CE2REL	Relaxation routine for fine C-grid
CEEDIF	Computes C-grid metrics
CEESET	Sets up cylindrical C-grids
CONTRL	Main control routine for relaxation solution, interpolations, boundary layer analysis, and printed output
CROSS	Solves for the intersection of two lines in a plane
CRUCUT	Relaxation routine to treat global coarse grid inner boundary
CRUFIL	Interpolation routine for global coarse grid inner boundary
CRUINT	Initializes interpolation parameters for use in CRUFIL
CRUOUT	Prints out global coarse grid solution for wing
CRUSET	Set up global coarse grid
CRUZ2	Zone 2 set up for global coarse grid interpolations (above wing)
CRUZ3	Zone 3 set up for global coarse grid interpolations (below wing)
CRUZ4	Zone 4 set up for global coarse grid interpolations (above wing and outboard of pylon)
CRUZ5	Zone 5 set up for global coarse grid interpolations (above wing and inboard of pylon)
CRUZ6	Zone 6 set up for global coarse grid interpolations (below wing and outboard of pylon)
CRUZ7	Zone 7 set up for global coarse grid interpolations (below wing and inboard of pylon)
CSCALC	Computes radial position and derivatives for specified cross-section model

CSGEOM	Is the main subroutine in the look-up portion of the QUICK system. It calls appropriate subroutines to evaluate body line values and construct cross-section geometry at a given x-station. It is used for all geometry model interrogation
CSMCHK	Correlates and checks the input data deck and the indices for the cross-sectional math model
CSMCOE	Composes the equations which are to define the cross-section geometry at a given x-station
CSMDEF	Logically defines the cross-section models from the input data
CSMFLT	Creates control point definitions to permit the insertion of a smooth fillet between cross-sectional arcs
CSMINT	Locates user specified intersections between cross-sectional arcs and adjusts their use (theta limits)
CSMSET	Sets up the control point coordinate arrays used to define the cross-section geometry at a specified x-station
CURVES	Calculates values and first and second derivatives for individual curve fits
DLOKUP	Is a simple dictionary look-up routine. It assigns an index to match an input name to a codeword list, but is not capable of adding new items to that list
DRAWG	Plots a curve according to graph axes
DRAWP	Plots a curve according to plot area dimensions
DSETUP	Is an adapting dictionary look-up routine. New items are added to a codeword list, an index is returned for the codeword, and an indicator (INEW) is set equal to 1 when a new item is encountered
ELLCAL	Set up for ellipse
ELLELL	Calculates intersection of two ellipses
ESTNXT	Estimates non-linear root by modified inverse quadratic
FINBCS	Sets up store fin surface boundary conditions in C-grids
FINFIL	Interpolation routine for store fin surface potentials in coarse C-grid
FINSET	Sets up store fin geometry in C-grids
FINT	Simultaneous triple interpolation

FINTIP	Modifies C-grids to follow store fin tip vortex streamlines
FMSOUT	Prints out summary of configuration force and moment coefficients
FMSPLT	Plots summary of configuration force and moment coefficients
GEMOUT	Ensures that all body lines required by a cross-sectional model are defined for the range of that model
GEVER	Plots geometry verification for wing, fuselage, and pylon
GLOBAL	Relaxation routine for global coarse grid
GORD	Bradshaw's G function
GRAD	Slope of a function at its tabulated points
GSETUP	Sets up graph area size and axis scales
INT2D	Interpolates along a 2-D curve
INT3D	Interpolates along a 3-D curve
KRVDEF	Calculates coefficients for the various curve fits associated with body line math models
LGRNG	Interpolates using Lagrange polynomials
LINELL	Solves for the intersection of a line and an ellipse
LINLIN	Solves for the intersection of two lines
MCHANG	Computes local Mach angle from coefficients of flow equation
MDOTV	Performs matrix multiplication of a vector
ORDIN	Linear interpolation
OUTPUT	Controls print out of solution
PGSTOP	Terminates plotting system
PGSTRT	Initiates plotting system
PLTSET	Set up routine for plotting program
PSTOP	Terminates a plot
PSTRT	Initiates a plot
PYLBCS	Sets up pylon surface boundary conditions
PYLCPS	Prints out solution for pylon
PYLFIL	Interpolation routine for pylon surface potentials in coarse C-grid

PYLPLT	Plots solution for pylon
PYLSET	Sets up pylon geometry
QWIKDE	Main control routine for Quick geometry definition and check out
QWIKLO	Main control routine for interrogation of Quick geometry math model
REDUCX	Performs interpolation to new grid
RLORD	Bradshaw's L function
SAREA	Computes body surface area given an array of cross-sections
SETHIT	Sets height for text appearing on plots
SETNXT	Reorders points for non-linear root finder
SIMPSN	Simpson's integration rule
SINCOS	Adjusts input interrogation angles for top and bottom dead center
SLOPBL	Slope of a tabulated function at an arbitrary point
SLOPE	Computes boundary conditions for wing surface and axisymmetric bodies
SLOPY	Computes wing surface slopes
SMOTH	Function for smoothing an array of values
SNGLRT	Used for internal calculation of singularity location in C-grid conformal mapping
SOLVEB	Solution of two simultaneous linear algebraic equations
SPLINE	Computes a cubic spline through a set of points
SPLN1	Computes continuous derivatives interpolation by means of a cubic fit
SPRINT	Prints output of profile results
SPSTOP	Terminates a subplot
SPSTRT	Initiates a subplot
STATS	Main program
STATSP	Main plotting program
STRDAT	Reads store and pylon input data
STRIPK	Starting condition setup and flow control for laminar/turbulent boundary layer prediction
STRVER	Plots geometry and grid set up verification for stores
SUPSET	Applies supersonic inflow, outflow, and radiation-type boundary conditions

TANCAL	Computes characteristic angles for use in boundary layer solution
THELIM	Creates and controls use of theta arrays to establish continuity in the cross-section model
TRID	Solves tridiagonal matrix
TRIDBC	Solves tridiagonal matrix with special end conditions
VBRAD	Computes Bradshaw's compressible 2-D turbulent boundary layer simulating 3-D boundary layer on infinite yawed wing by Nash-Tseng modified chord technique
VDOTV	Computes a vector dot product
VINTER	Performs cubic fit for separated boundary layer in wing section cove regions
VNUSUB	Computes the Nash effective viscosity
WFGFIL	Interpolation routine for wing fine grid boundaries
WFGOUT	Prints out wing fine grid solution
WFGP	Dirichlet-type boundary conditions for wing fine grid
WFGPLT	Plots wing fine grid solution
WFGV	Neumann-type boundary conditions for wing fine grid cut-out due to store
WFGVX	Neumann-type boundary conditions for wing fine grid upstream and downstream boundaries
WFGVZ	Neumann-type boundary conditions for wing fine grid top and bottom boundaries
WFGZ2	Zone 2 set up for wing fine grid interpolations (above wing)
WFGZ3	Zone 3 set up for wing fine grid interpolations (below wing)
WFGZ4	Zone 4 set up for wing fine grid interpolations (above wing and outboard of pylon)
WFGZ5	Zone 5 set up for wing fine grid interpolations (above wing and inboard of pylon)
WFGZ6	Zone 6 set up for wing fine grid interpolations (below wing and outboard of pylon)
WFGZ7	Zone 7 set up for wing fine grid interpolations (below wing and inboard of pylon)
WINGF	Relaxation routine for wing fine grid
WINTG	Writes an integer number on a plot.

WMESS	Writes a character string on a plot
WNGDAT	Reads input data for wing
WNGSET	Sets up wing geometry
WREAL	Writes a real number on a plot
WSICUT	Relaxation routine to treat WSI grid inner boundary
WSIFIL	Interpolation routine for WSI grid inner and outer boundaries
WSIINT	Initializes interpolation parameters for use in WSIFIL
WSIOUT	Prints out WSI grid solution for wing
WSIREL	Relaxation routine for WSI grid
WSISET	Sets up WSI grid
WSIZ2	Zone 2 set up for WSI grid interpolations (above wing)
WSIZ3	Zone 3 set up for WSI grid interpolations (below wing)
WSIZ4	Zone 4 set up for WSI grid interpolations (above wing and outboard of pylon)
WSIZ5	Zone 5 set up for WSI grid interpolations (above wing and inboard of pylon)
WSIZ6	Zone 6 set up for WSI grid interpolations (below wing and outboard of pylon)
WSIZ7	Zone 7 set up for WSI grid interpolations (below wing and inboard of pylon)
XSETUP	Draws and labels x-axis
YSETUP	Draws and labels y-axis

KEY VARIABLE DESCRIPTION

AAXIS1	Nominal extent of C-grids upstream of store nose, as fraction of store body length
AAXIS2	Nominal extent of C-grids downstream of store tail, as fraction of store body length
AK	The value $1-M^2$
ALPAS	Store pitch angle relative to aircraft
ALPHA	Angle-of-attack (radians)
AM2	The value M^2
AMACH	Freestream Mach number
ANGF	Store fin angular locations
AOA	Angle-of-attack (degrees)
BAREA	Fuselage wetted area
BAXIS	Nominal radius of C-grids
BAXIS0	Nominal radius inherent in C-grid conformal mapping
BCF	Integrated fuselage skin friction coefficient
BCL	Wing global coarse grid lower boundary slopes
BCLB	Wing WSI grid lower boundary slopes
BCLF	Wing fine grid lower boundary slopes
BCU	Wing global coarse grid upper boundary slopes
BCUB	Wing WSI grid upper boundary slopes
BCUF	Wing fine grid upper boundary slopes
BDD	Fuselage longitudinal distribution of axial force
BETAP	Pylon yaw angle relative to aircraft
BETAS	Store yaw angle relative to aircraft
BLD	Fuselage longitudinal distribution of normal force
BNOSE	X coordinate of fuselage nose
BODCD	Integrated fuselage drag coefficient
BODCL	Integrated fuselage lift coefficient
BODCM	Integrated fuselage pitching moment coefficient
BPAREA	Fuselage projected planform area
BS	Fuselage plot scaling parameter
BTAIL	X coordinate of fuselage tail

CA	Global coarse grid metric ξ_x
CAB	WSI grid metric ξ_x
CAV	Wing average chord, c_{ave}
CB	Global coarse grid metric ξ_{xx}
CBB	WSI grid metric ξ_{xx}
CC	Global coarse grid metric η_y
CCB	WSI grid metric η_y
CD	Global coarse grid metric η_{yy}
CDB	WSI grid metric η_{yy}
CDINT	Integrated wing section drag coefficient, c_d
CE	Global coarse grid metric ζ_z
CEB	WSI grid metric ζ_z
CF	Global coarse grid metric ζ_{zz}
CFB	WSI grid metric ζ_{zz}
CFINT	Integrated wing section skin friction coefficient, c_f
CIR	Wing circulation in global coarse and wing fine grids
CIRB	Wing circulation in WSI grid
CIRFC	Fin circulation in coarse C-grid
CIRFS	Fin circulation in fine C-grid
CLINT	Integrated wing section lift coefficient, c_ℓ
CMINT	Integrated wing section pitching moment coefficient, c_m about REFX
CMLOC	Integrated wing section pitching moment coefficient
CMXFIN	X component of store fin moment coefficient (body axes)
CMXFNV	X component of store fin moment coefficient (body axes) including skin friction and viscous crossflow
CMXSBD	X component of store body moment coefficient (body axes)
CMXSBV	X component of store body moment coefficient (body axes) including skin friction and viscous crossflow
CMXSTR	X component of store moment coefficient (body axes)
CMXSTV	X component of store moment coefficient (body axes) including skin friction and viscous crossflow
CMYFIN	Y component of store fin moment coefficient (body axes)
CMYFNV	Y component of store fin moment coefficient (body axes) including skin friction and viscous crossflow
CMYSBD	Y component of store body moment coefficient (body axes)

CMYSBV	Y component of store body moment coefficient (body axes) including skin friction and viscous crossflow
CMYSTR	Y component of store moment coefficient (body axes)
CMYSTV	Y component of store moment coefficient (body axes) including skin friction and viscous crossflow
CMZFIN	Z component of store fin moment coefficient (body axes)
CMZFNV	Z component of store fin moment coefficient (body axes) including skin friction and viscous crossflow
CMZSBD	Z component of store body moment coefficient (body axes)
CMZSBV	Z component of store body moment coefficient (body axes) including skin friction and viscous crossflow
CMZSTR	Z component of store moment coefficient (body axes)
CMZSTV	Z component of store moment coefficient (body axes) including skin friction and viscous crossflow
COST	Trigonometric cosine of C-grid θ coordinates
CPL	Lower surface pressure coefficient
CPU	Upper surface pressure coefficient
CSCUT	Fuselage X station for cross-section cut
CXFIN	X component of store fin force coefficient (body axes)
CXFNV	X component of store fin force coefficient (body axes) including skin friction and viscous crossflow
CXSBD	X component of store body force coefficient (body axes)
CXSBV	X component of store body force coefficient (body axes) including skin friction and viscous crossflow
CXSTR	X component of store force coefficient (body axes)
CXSTV	X component of store force coefficient (body axes) including skin friction and viscous crossflow
CYFIN	Y component of store fin force coefficient (body axes)
CYFNV	Y component of store fin force coefficient (body axes) including skin friction and viscous crossflow
CYSBD	Y component of store body force coefficient (body axes)
CYSBV	Y component of store body force coefficient (body axes) including skin friction and viscous crossflow
CYSTR	Y component of store force coefficient (body axes)
CYSTV	Y component of store force coefficient (body axes) including skin friction and viscous crossflow

CZFIN	Z component of store fin force coefficient (body axes)
CZFNV	Z component of store fin force coefficient (body axes) including skin friction and viscous crossflow
CZSBD	Z component of store body force coefficient (body axes)
CZSBV	Z component of store body force coefficient (body axes) including skin friction and viscous crossflow
CZSTR	Z component of store force coefficient (body axes)
CZSTV	Z component of store force coefficient (body axes) including skin friction and viscous crossflow
DCYDX	Store body longitudinal distribution of side force
DCYDXV	Store body longitudinal distribution of side force, including viscous crossflow
DCZDX	Store body longitudinal distribution of normal force
DCZDXV	Store body longitudinal distribution of normal force, including viscous crossflow
DELFL	Wing lower surface boundary layer slopes in wing fine grid
DELFP	Wing surface boundary layer slopes in wing fine grid at inboard wing/pylon junction
DELFU	Wing upper surface boundary layer slopes in wing fine grid
DELGL	Wing lower surface boundary layer slopes in global coarse grid
DELGP	Wing surface boundary layer slopes in global coarse grid at inboard wing/pylon junction
DELGU	Wing upper surface boundary layer slopes in global coarse grid
DELML	Wing lower surface boundary layer slopes in WSI grid
DELMP	Wing surface boundary layer slopes in WSI grid at inboard wing/pylon junction
DELMU	Wing upper surface boundary layer slopes in WSI grid
DELTAF	Individual, all-moveable, store fin deflection angle
DETA	Global coarse grid η mesh cell size
DETAB	WSI grid η mesh cell size
DETAS	Coarse C-grid η mesh cell size
DETASS	Fine C-grid η mesh cell size
DIM	Reference length for non-dimensionalizing maximum change in potential
DRDXC	Axisymmetric fuselage slope distribution in global coarse grid
DTS	C-grid θ mesh cell size

DXI	Global coarse grid ξ mesh cell size
DXIB	WSI grid ξ mesh cell size
DXSIS	Coarse C-grid ξ mesh cell size
DXSISS	Fine C-grid ξ mesh cell size
DXW	Wing fine grid X mesh cell size
DZETA	Global coarse grid ζ mesh cell size
DZETAB	WSI grid ζ mesh cell size
DZW	Wing fine grid Z mesh cell size
ETA	Global coarse grid η coordinates
ETAB	WSI grid η coordinates
ETRRS	Coarse C-grid metric η_{rr}
ETRRSS	Fine C-grid metric η_{rr}
ETRS	Coarse C-grid metric η_{r}
ETRSS	Fine C-grid metric η_{r}
ETXRS	Coarse C-grid metric η_{xr}
ETXRSS	Fine C-grid metric η_{xr}
ETXS	Coarse C-grid metric η_{x}
ETXSS	Fine C-grid metric η_{x}
ETXXS	Coarse C-grid metric η_{xx}
ETXXSS	Fine C-grid metric η_{xx}
FINCMX	X component of store fin moment coefficient (stability axes)
FINCMY	Y component of store fin moment coefficient (stability axes)
FINCMZ	Z component of store fin moment coefficient (stability axes)
FINCX	X component of store fin force coefficient (stability axes)
FINCY	Y component of store fin force coefficient (stability axes)
FINCZ	Z component of store fin force coefficient (stability axes)
FNSCF	Integrated store fin section skin friction coefficient
FNSCMY	Integrated store fin section pitching moment coefficient
FNSCX	Integrated store fin section axial force coefficient
FNSCZ	Integrated store fin section normal force coefficient
FNVCMX	X component of store fin moment coefficient (stability axes) including skin friction and viscous crossflow
FNVCMY	Y component of store fin moment coefficient (stability axes) including skin friction and viscous crossflow

FNVCMZ	Z component of store fin moment coefficient (stability axes) including skin friction and viscous crossflow
FNVCX	X component of store fin force coefficient (stability axes) including skin friction and viscous crossflow
FNVCY	Y component of store fin force coefficient (stability axes) including skin friction and viscous crossflow
FNVCZ	Z component of store fin force coefficient (stability axes) including skin friction and viscous crossflow
FNXC	X component of store fin surface normal in coarse C-grid
FNXS	X component of store fin surface normal in fine C-grid
FNYC	R component of store fin surface normal in coarse C-grid
FNYS	R component of store fin surface normal in fine C-grid
FRLEC	R coordinate of store fin section leading edge in coarse C-grid
FRLES	R coordinate of store fin section leading edge in fine C-grid
FRTEC	R coordinate of store fin section trailing edge in coarse C-grid
FRTES	R coordinate of store fin section trailing edge in fine C-grid
FS	Store fin plot scaling parameter
FXLEC	X coordinate of store fin section leading edge in coarse C-grid
FXLES	X coordinate of store fin section leading edge in fine C-grid
FXTEC	X coordinate of store fin section trailing edge in coarse C-grid
FXTES	X coordinate of store fin section trailing edge in fine C-grid
G	The value $(\gamma+1)M^2$
H	The value $(\gamma-1)M^2$
IBCL	WSI grid I value closest to store nose
ICE10	I interpolation index to locate coarse C-grid point in WSI grid
ICRUI	I interpolation index to locate global coarse grid point in WSI grid
IFLEC	I value of store fin section leading edge point in coarse C-grid
IFLES	I value of store fin section leading edge point in fine C-grid
IFTEC	I value of store fin section trailing edge point in coarse C-grid
IFTES	I value of store fin section trailing edge point in fine C-grid
IL	Global coarse grid wing leading edge I value
ILB	WSI grid wing leading edge I value
ILEF	Wing fine grid wing leading edge I value

IMACH	Code for subsonic (0) or supersonic (1) flow at a grid point
IMAX	Number of global coarse grid points in X direction
IMAXB	Number of WSI grid points in X direction
IMAXS	Number of coarse C-grid ξ mesh cell points
IMAXSS	Number of fine C-grid ξ mesh cell points
IMAXW	Number of wing fine grid points in X direction
INOSEC	Global coarse grid I value at fuselage nose
IPLEC	I value of pylon section leading edge point in coarse C-grid
IPLEF	I value of pylon section leading edge point in wing fine grid
IPLEG	I value of pylon section leading edge point in global coarse grid
IPLEM	I value of pylon section leading edge point in WSI grid
IPLES	I value of pylon section leading edge point in fine C-grid
IPTEC	I value of pylon section trailing edge point in coarse C-grid
IPTEF	I value of pylon section trailing edge point in wing fine grid
IPTEG	I value of pylon section trailing edge point in global coarse grid
IPTEM	I value of pylon section trailing edge point in WSI grid
IPTES	I value of pylon section trailing edge point in fine C-grid
IT	Global coarse grid wing trailing edge I value
ITAILC	Global coarse grid I value at fuselage tail
ITB	WSI grid wing trailing edge I value
ITEF	Wing fine grid wing trailing edge I value
ITER	Iteration count
IWFG	I interpolation index to locate wing fine grid point in global coarse grid
IWSIF	I interpolation index to locate WSI inner-boundary front-face grid point in coarse C-grid
IWSII	I interpolation index to locate WSI inner-boundary side-face grid point in coarse C-grid
IWSIO	I interpolation index to locate WSI grid point in global coarse grid
JBCL	WSI grid J value at store centerline
JBLI	Inner J location of inboard WSI grid inner boundary
JBLO	Outer J location of inboard WSI grid inner boundary
JBRI	Inner J location of outboard WSI grid inner boundary
JBRO	Outer J location of outboard WSI grid inner boundary
JCE1O	J interpolation index to locate coarse C-grid point in WSI grid

JCRUI	J interpolation index to locate global coarse grid point in WSI grid
JFINEI	Inboard J location of wing fine grid cutout due to store
JFINEO	Outboard J location of wing fine grid cutout due to store
JFINTC	J value of store fin tip in coarse C-grid
JFINTS	J value of store fin tip in fine C-grid
JMAX	Number of global coarse grid points in Y direction
JMAXB	Number of WSI grid points in Y direction
JMAXS	Number of coarse C-grid η mesh cell points
JMAXSS	Number of fine C-grid η mesh cell points
JPYLTC	J extent of pylon in coarse C-grid
JPYLTS	J extent of pylon in fine C-grid
JROOT	Global coarse grid J value at wing root
JSDC	Global coarse grid J value just outboard of wing/fuselage junction
JSTOR	Global coarse grid J value of pylon and/or store centerline
JSTORI	Inboard J location of global coarse grid inner boundary
JSTORO	Outboard J location of global coarse grid inner boundary
JTIP	Global coarse grid J value at wing tip
JWFG	J interpolation index to locate wing fine grid point in global coarse grid
JWSI	J array to order WSI grid inner-boundary side-face J-K grid points
JWSIF	J interpolation index to locate WSI inner-boundary front-face grid point in coarse C-grid
JWSII	J interpolation index to locate WSI inner-boundary side-face grid point in coarse C-grid
JWSIO	J interpolation index to locate WSI grid point in global coarse grid
KBB	WSI grid K value at wing plane
KBBOT	Lower K location of WSI grid inner boundary
KBC	Global coarse grid K value at wing plane
KBCL	WSI grid K value at store centerline
KBTOP	Upper K location of WSI grid inner boundary
KBW	Wing fine grid K value at wing plane
KCE10	K interpolation index to locate coarse C-grid point in WSI grid
KCRUI	K interpolation index to locate global coarse grid point in WSI grid
KFINEB	Lower K location of wing fine grid cutout due to store
KFINET	Upper K location of wing fine grid cutout due to store

KFS	K value of store fin in C-grid
KLO	K indice of θ+270° coordinate
KLOC	Global coarse grid K limiters for lower portion of fuselage
KMAX	Number of global coarse grid points in Z direction
KMAXB	Number of WSI grid points in Z direction
KMAXS	Number of C-grid θ mesh cell points
KMAXW	Number of wing fine grid points in Z direction
KODB	Axisymmetric or QUICK fuselage definition flag
KPS	K value of pylon in C-grid
KPYLRF	Pylon lower K limit in wing fine grid
KPYLRG	Pylon lower K limit in global coarse grid
KPYLRM	Pylon lower K limit in WSI grid
KPYLTF	Pylon upper K limit in wing fine grid
KPYLTG	Pylon upper K limit in global coarse grid
KPYLTM	Pylon upper K limit in WSI grid
KREFL	K indice of θ+180° coordinate
KSTORB	Lower K location of global coarse grid inner boundary
KSTORT	Upper K location of global coarse grid inner boundary
KUP	K indice of θ+90° coordinate
KUPC	Global coarse grid K limiters for upper portion of fuselage
KWFG	K interpolation index to locate wing fine grid point in global coarse grid
KWSI	K array to order WSI grid inner-boundary side-face J-K grid points
KWSIF	K interpolation index to locate WSI inner-boundary front-face grid point in coarse C-grid
KWSII	K interpolation index to locate WSI inner-boundary side-face grid point in coarse C-grid
KWSIO	K interpolation index to locate WSI grid point in global coarse grid
MAXIT	Number of "coarse" grid iterations (input as AXITC)
MAXITF	Number of "fine" grid iterations (input as AXITF)
MAXITM	Number of "intermediate" grid iterations (input as AXITM)
MODV	Mode of operation for wing viscous calculations (input as VISMOD)
NANGFS	Number of fins in each store fin set (input as FANG)
NBODY	Fuselage input/solution flag (input as BODY)

NFINS	Number of sets of store fins (input as FINS)
NINB	Number of ordinates defining axisymmetric fuselage (input as BNIN)
NINFS	Number of ordinates defining each store fin section (input as FNIN)
NINP	Number of ordinates defining each pylon section (input as PNIN)
NINS	Number of ordinates defining store body (input as SNIN)
NINW	Number of ordinates defining each wing section (input as ANIN)
NOSEB	Blunt/sharp nose fuselage code for spline fit (input as ANOSB)
NOSEFS	Blunt/sharp nose store fin section code for spline fit (input as FNOSE)
NOSEP	Blunt/sharp nose pylon section code for spline fit (input as PNOSE)
NOSES	Blunt/sharp nose store body code for spline fit (input as ANOSES)
NOSEW	Blunt/sharp nose wing section code for spline fit (input as ANOSW)
NPOA	Number of X grid points between leading edge and trailing edge in wing fine grid
NPOS	Number of coarse C-grid points between store body nose and tail
NPOSS	Number of fine C-grid points between store body nose and tail
NPYLS	Pylon input flag (input as PYLS)
NSECFS	Number of airfoils defining a set of store fins, also store fin solution flag (input as FSEC)
NSECP	Number of defining pylon sections, also pylon solution flag (input as PSEC)
NSECT	Number of defining wing sections (input as ASECT)
NSING	C-grid singularity location input flag (input as ASING)
NSTOR	Store input/solution flag (input as STOR)
NTC	Number of global coarse grid points representing fuselage cross-sections
NWING	Wing input/solution flag (input as WING)
OMEGAS	Store quasi-steady roll rate parameter
PBL	Wing lower surface WSI grid potentials
PCIRF	Pylon circulation in wing fine grid
PCIRG	Pylon circulation in global coarse grid
PCIRM	Pylon circulation in WSI grid
PCIRS	Pylon circulation in coarse C-grid
PCIRSS	Pylon circulation in fine C-grid
PCL	Wing lower surface global coarse grid potentials

PFINC	Fin lower surface coarse C-grid potentials
PFINS	Fin lower surface fine C-grid potentials
PFL	Wing lower surface wing fine grid potentials
PHB	WSI grid potentials
PHC	Global coarse grid potentials
PHF	Wing fine grid potentials
PHS	Coarse C-grid potentials
PHSS	Fine C-grid potentials
PI	π
PNOSE1	Store body nose stagnation potential in coarse C-grid
PNOSE2	Store body nose stagnation potential in fine C-grid
PNXC	X component of pylon surface normal in coarse C-grid
PNXF	X component of pylon surface normal in wing fine grid
PNXG	X component of pylon surface normal in global coarse grid
PNXM	X component of pylon surface normal in WSI grid
PNXS	X component of pylon surface normal in fine C-grid
PNYC	R component of pylon surface normal in coarse C-grid
PNYF	Z component of pylon surface normal in wing fine grid
PNYG	Z component of pylon surface normal in global coarse grid
PNYM	Z component of pylon surface normal in WSI grid
PNYS	R component of pylon surface normal in fine C-grid
PPYLF	Pylon lower surface wing fine grid potentials
PPYLG	Pylon lower surface global coarse grid potentials
PPYLIB	Dummy wing fine grid potentials to treat pylon inboard surface
PPYLM	Pylon lower surface WSI grid potentials
PPYLOB	Dummy wing fine grid potentials to treat pylon outboard surface
PPYLS	Pylon lower surface coarse C-grid potentials
PPYLSS	Pylon lower surface fine C-grid potentials
PRLEC	R coordinate of pylon section leading edge in coarse C-grid
PRLES	R coordinate of pylon section leading edge in fine C-grid
PRTEC	R coordinate of pylon section trailing edge in coarse C-grid
PRTES	R coordinate of pylon section trailing edge in fine C-grid
PS	Pylon plot scaling parameter
PSAVE1	Restores potentials on wing upper or lower surface plane which interpolation schemes replaced with dummy values

PSAVE2	Restores potentials above or below wing surface plane which interpolation schemes replaced with dummy values
PSAVE3	Restores potentials on pylon inboard or outboard surface plane which interpolation schemes replaced with dummy values
PSAVE4	Restores potentials inboard or outboard of pylon surface plane which interpolation schemes replaced with dummy values
PSDD	Wing spanwise drag coefficient, $c \cdot c_d/c_{ave}$ at inboard wing/pylon junction
PSFD	Wing spanwise skin friction coefficient, $c \cdot c_f/c_{ave}$ at inboard wing/pylon junction
PSLD	Wing spanwise lift coefficient, $c \cdot c_\ell/c_{ave}$ at inboard wing/pylon junction
PSMD	Wing spanwise pitching moment coefficient, $c \cdot c_m/c_{ave}$ at inboard wing/pylon junction
PWBJ	Dummy wing fine grid potential values inboard of wing/fuselage junction
PWBJL	Dummy wing lower surface fine grid potential values inboard of wing/fuselage junction
PXLEC	X coordinate of pylon section leading edge in coarse C-grid
PXLEF	X coordinate of pylon section leading edge in wing fine grid
PXLEG	X coordinate of pylon section leading edge in global coarse grid
PXLEM	X coordinate of pylon section leading edge in WSI grid
PXLES	X coordinate of pylon section leading edge in fine C-grid
PXTEC	X coordinate of pylon section trailing edge in coarse C-grid
PXTEF	X coordinate of pylon section trailing edge in wing fine grid
PXTEG	X coordinate of pylon section trailing edge in global coarse grid
PXTEM	X coordinate of pylon section trailing edge in WSI grid
PXTES	X coordinate of pylon section trailing edge in fine C-grid
PYCCF	Integrated pylon section skin friction coefficient in coarse C-grid
PYCCMY	Integrated pylon section pitching moment coefficient in coarse C-grid
PYCCX	Integrated pylon section axial coefficient in coarse C-grid
PYCCZ	Integrated pylon section lift coefficient in coarse C-grid
PYFCF	Integrated pylon section skin friction coefficient in wing fine grid
PYFCMY	Integrated pylon section pitching moment coefficient in wing fine grid
PYFCX	Integrated pylon section axial coefficient in wing fine grid
PYFCZ	Integrated pylon section lift coefficient in wing fine grid

PYGCF	Integrated pylon section skin friction coefficient in global coarse grid
PYGCMY	Integrated pylon section pitching moment coefficient in global coarse grid
PYGCX	Integrated pylon section axial coefficient in global coarse grid
PYGCZ	Integrated pylon section lift coefficient in global coarse grid
PYLCMX	X component of pylon moment coefficient (stability axes)
PYLCMY	Y component of pylon moment coefficient (stability axes)
PYLCMZ	Z component of pylon moment coefficient (stability axes)
PYLCX	X component of pylon force coefficient (stability axes)
PYLCXV	X component of pylon force coefficient (stability axes) including skin friction
PYLCY	Y component of pylon force coefficient (stability axes)
PYLCZ	Z component of pylon force coefficient (stability axes)
PYMCF	Integrated pylon section skin friction coefficient in WSI grid
PYMCMY	Integrated pylon section pitching moment coefficient in WSI grid
PYMCX	Integrated pylon section axial coefficient in WSI grid
PYMCZ	Integrated pylon section lift coefficient in WSI grid
PYSCF	Integrated pylon section skin friction coefficient in fine C-grid
PYSCMY	Integrated pylon section pitching moment coefficient in fine C-grid
PYSCX	Integrated pylon section axial coefficient in fine C-grid
PYSCZ	Integrated pylon section lift coefficient in fine C-grid

RAV	Average fuselage radius for boundary condition calculation
RC	Axisymmetric fuselage radius distribution in global coarse grid
RE	Freestream Reynolds number
REFA	Configuration reference area, used to compute force and moment coefficients
REFAS	Store reference area, used to compute force and moment coefficients
REFL	Configuration reference length, used to compute moment coefficients
REFLS	Store reference length, used to compute moment coefficient
REFX	Configuration reference X moment center, used to compute moment coefficients
REFXS	Store reference X moment center, used to compute moment coefficients
RET	Coarse C-grid metric r_{η}
RETET	Coarse C-grid metric $r_{\eta\eta}$

RIN	Radial coordinates defining axisymmetric fuselage (input option)
RINS	Radial coordinates defining store body
RLC	QUICK fuselage radius distributions in global coarse grid
RLOC	Fuselage bottom centerline radius distribution
RMAX	Fuselage maximum radius
RMAXS	Store maximum radius, excluding fins
RMAXSF	Store maximum radius, including fins
ROLLS	Store roll angle
RUPC	Fuselage top centerline radius distribution
SBDCMX	X component of store body moment coefficient (stability axes)
SBDCMY	Y component of store body moment coefficient (stability axes)
SBDCMZ	Z component of store body moment coefficient (stability axes)
SBDCX	X component of store body force coefficient (stability axes)
SBDCY	Y component of store body force coefficient (stability axes)
SBDCZ	Z component of store body force coefficient (stability axes)
SBDWET	Store body wetted area
SBVCMX	X component of store body moment coefficient (stability axes) including skin friction and viscous crossflow
SBVCMY	Y component of store body moment coefficient (stability axes) including skin friction and viscous crossflow
SBVCMZ	Z component of store body moment coefficient (stability axes) including skin friction and viscous crossflow
SBVCX	X component of store body force coefficient (stability axes) including skin friction and viscous crossflow
SBVCY	Y component of store body force coefficient (stability axes) including skin friction and viscous crossflow
SBVCZ	Z component of store body force coefficient (stability axes) including skin friction and viscous crossflow
SDD	Wing spanwise drag coefficient, $c \bullet c_d / c_{ave}$
SFD	Wing spanwise skin friction coefficient, $c \bullet c_f / c_{ave}$
SFNWET	Store fin wetted area
SGRAD	Fuselage slopes at wing/fuselage junction
SINT	Trigonometric sine of C-grid θ coordinates
SLD	Wing spanwise lift coefficient, $c \bullet c_\ell / c_{ave}$
SMD	Wing spanwise pitching moment coefficient, $c \bullet c_m / c_{ave}$

SNOSE	X coordinate of store body nose
SS	Store body plot scaling parameter
STAIL	X coordinate of store body tail
STRCMX	X component of store moment coefficient (stability axes)
STRCMY	Y component of store moment coefficient (stability axes)
STRCMZ	Z component of store moment coefficient (stability axes)
STRCX	X component of store force coefficient (stability axes)
STRCY	Y component of store force coefficient (stability axes)
STRCZ	Z component of store force coefficient (stability axes)
STRWET	Store wetted area
STVCMX	X component of store moment coefficient (stability axes) including skin friction and viscous crossflow
STVCMY	Y component of store moment coefficient (stability axes) including skin friction and viscous crossflow
STVCMZ	Z component of store moment coefficient (stability axes) including skin friction and viscous crossflow
STVCX	X component of store force coefficient (stability axes) including skin friction and viscous crossflow
STVCY	Y component of store force coefficient (stability axes) including skin friction and viscous crossflow
STVCZ	Z component of store force coefficient (stability axes) including skin friction and viscous crossflow
THETC	Fuselage global coarse grid angular cuts
THT	C-grid θ coordinates
TICE10	I interpolation parameter to calculate a coarse C-grid quantity based on WSI grid values
TICRUI	I interpolation parameter to calculate a global coarse grid quantity based on WSI grid values
TITLE	Case title identifying print and plot output
TITLES	Store title identifying print and plot output for store
TIWFG	I interpolation parameter to calculate a wing fine grid quantity based on global coarse grid values
TIWSIF	I interpolation parameter to calculate a WSI inner-boundary front-face grid quantity based on coarse C-grid values

TIWSII	I interpolation parameter to calculate a WSI inner-boundary side-face grid quantity based on coarse C-grid values
TIWSIO	I interpolation parameter to calculate a WSI grid quantity based on global coarse grid values
TJCE1O	J interpolation parameter to calculate a coarse C-grid quantity based on WSI grid values
TJCRUI	J interpolation parameter to calculate a global coarse grid quantity based on WSI grid values
TJWFG	J interpolation parameter to calculate a wing fine grid quantity based on global coarse grid values
TJWSIF	J interpolation parameter to calculate a WSI inner-boundary front-face grid quantity based on coarse C-grid values
TJWSII	J interpolation parameter to calculate a WSI inner-boundary side-face grid quantity based on coarse C-grid values
TJWSIO	J interpolation parameter to calculate a WSI grid quantity based on global coarse grid values
TKCE1O	K interpolation parameter to calculate a coarse C-grid quantity based on WSI grid values
TKCRUI	K interpolation parameter to calculate a global coarse grid quantity based on WSI grid values
TKWFG	K interpolation parameter to calculate a wing fine grid quantity based on global coarse grid values
TKWSIF	K interpolation parameter to calculate a WSI inner-boundary front-face grid quantity based on coarse C-grid values
TKWSII	K interpolation parameter to calculate a WSI inner-boundary side-face grid quantity based on coarse C-grid values
TKWSIO	K interpolation parameter to calculate a WSI grid quantity based on global coarse grid values
TSLOC	Wing fine grid local sweep angles
TWIST	Wing twist (incidence) distribution
W	Relaxation factor, ω
WAREA	Wing area computed from defining wing sections
WCD	Wing drag coefficient
WCF	Wing skin friction coefficient
WCL	Wing lift coefficient

WCM	Wing pitching moment coefficient
WCORD	Global coarse and wing fine grid local wing section chord lengths
WS	Wing plot scaling parameter
X	Global coarse grid X coordinates
XBCS	Fuselage cross-section Y coordinates (for plotting only)
XBF	WSI grid X coordinates
XCSCUT	Fuselage computational cross-section Y coordinates (for plotting only)
XET	Coarse C-grid metric x_η
XETET	Coarse C-grid metric $x_{\eta\eta}$
XI	Global coarse grid ξ coordinates
XIB	WSI grid ξ coordinates
XINB	X coordinates defining axisymmetric fuselage (input option)
XINF	X ordinates defining store fin section
XINP	X ordinates defining pylon section
XINS	X coordinates defining store body
XINW	X ordinates defining wing section
XIRRS	Coarse C-grid metric ξ_{rr}
XIRRSS	Fine C-grid metric ξ_{rr}
XIRS	Coarse C-grid metric ξ_r
XIRSS	Fine C-grid metric ξ_r
XIXRS	Coarse C-grid metric ξ_{xr}
XIXRSS	Fine C-grid metric ξ_{xr}
XIXS	Coarse C-grid metric ξ_x
XIXSS	Fine C-grid metric ξ_x
XIXXS	Coarse C-grid metric ξ_{xx}
XIXXSS	Fine C-grid metric ξ_{xx}
XLE	Global coarse and wing fine grid X coordinate of local wing section leading edge
XLEB	WSI grid X coordinate of local wing section leading edge
XLS	Store body length
XNC	X component of fuselage surface normal in global coarse grid
XOL	Non-dimensional X distance along chord or body length
XPL	X leading edge coordinate of input wing section
XPLF	X leading edge coordinate of input store fin section
XPLP	X leading edge coordinate of input pylon section

XPT	X trailing edge coordinate of input wing section
XPTF	X trailing edge coordinate of input store fin section
XPTP	X trailing edge coordinate of input pylon section
XS1	Upstream extent of entire wing planform
XS2	Downstream extent of entire wing planform
XSC	Coarse C-grid X coordinates
XSING	X coordinate of singularity location for C-grid conformal mapping
XSS	Fine C-grid X coordinates
XTE	Global coarse and wing fine grid X coordinate of local wing section trailing edge
XTEB	WSI grid X coordinate of local wing section trailing edge
XWF	Wing fine grid X coordinates
Y	Global coarse grid Y coordinates
YBCS	Fuselage cross-section Z coordinates (for plotting only)
YBF	WSI grid Y coordinates
YBMHB	Fuselage maximum half breadth coordinates (for plotting only)
YCSCUT	Fuselage computational cross-section Z coordinates (for plotting only)
YFINC	Y coordinate defining store fin section in coarse C-grid
YFINS	Y coordinate defining store fin section in fine C-grid
YINF	Y ordinates defining store fin section
YINL	Y ordinates defining lower wing section
YINP	Y ordinates defining pylon section
YINU	Y ordinates defining upper wing section
YNC	Y component of fuselage surface normal in global coarse grid
YOB	Wing span station, η
YP	Y coordinate of input wing section
YPF	Radial coordinate of input store fin section
YPYLC	Y coordinate defining pylon section in coarse C-grid
YPYLCC	Y coordinate defining pylon section in fine C-grid
YPYLF	Y coordinate defining pylon section in wing fine grid
YPYLG	Y coordinate defining pylon section global coarse grid
YPYLM	Y coordinate defining pylon section in WSI grid
YPYLS	Spanwise Y coordinate of pylon
YSC	Coarse C-grid R coordinates
YSFL	Y ordinates defining lower wing section at each fine grid span station

YSFU	Y ordinates defining upper wing section at each fine grid span station
YSS	Fine C-grid R coordinates
YSTOR	Spanwise Y coordinate of store centerline
YTIP	Wing semispan, b/2
Z	Global coarse grid Z coordinates
ZBF	WSI grid Z coordinates
ZBODY	Axisymmetric fuselage Z centerline coordinate (input option)
ZETA	Global coarse grid ζ coordinates
ZETAB	WSI grid ζ coordinates
ZNC	Z component of fuselage surface normal in global coarse grid
ZPP	Z coordinate of input pylon section
ZSTOR	Z coordinate of store centerline
ZWF	Wing fine grid Z coordinates
ZWING	Z coordinate of wing reference plane

This Page Intentionally Left Blank

REFERENCES

1 Boppe, C.W., "Transonic Flow Field Analysis for Wing-Fuselage Configurations," NASA CR-3243, May 1980.

2. Boppe, C.W., "Aerodynamic Analysis for Aircraft With Nacelles, Pylons, and Winglets at Transonic Speeds," NASA CR-4066, Apr. 1987.

3. Rosen, B.S., "Computational Transonic Analysis of Canted Winglets," Journal of Aircraft," Vol. 21, No. 11, Nov. 1984, pp. 873-878.

4. Thompson, D.S., "A Mesh Embedding Approach for Prediction of Transonic Wing/Body/Store Flow Fields," paper presented at the Numerical Boundary Condition Procedures Symposium, Moffett Field, CA, Oct. 19-20, 1981.

5. Thompson, D.S., "TAS - A Transonic Aircraft/Store Flow Field Prediction Code," NASA CR-3721, Dec. 1983.

6. Dougherty, F.C., Benek, J.A. and Steger, J.L., "On Applictions of Chimera Grid Schemes to Store Separation," NASA TM-88193, Oct. 1985.

7. Lijewski, L.E., "Transonic Flow Solutions on a Blunt, Finned Body of Revolution Using the Euler Equations," AIAA Paper 86-1082, May 1986.

8. Cottrell, C.J. and Lijewski, L.E., "A Study of Finned, Multi-Body Aerodynamic Interference at Transonic Mach Numbers," AIAA Paper 87-2480, Aug. 1987.

9. Rosen, B.S., "Body Flow Field Simulation and Force/Moment Prediction at Transonic Speeds," AIAA Paper 85-0423, Jan. 1985.

10. Liepmann, H.W. and Roshko, A., "Elements of Gasdynamics," John Wiley and Sons, New York, 1957, pp. 202-206.

11. Caughey, D.A., "A Systematic Procedure for Generating Useful Conformal Mappings," International Journal for Numerical Methods in Engineering, Vol. 12, 1978, pp. 1651-1657.

12. Jameson, A., "Iterative Solution of Transonic Flows over Airfoils and Wings, Including Flows at Mach 1," Communications on Pure and Applied Mathematics, Vol. 27, 1974, pp. 283-309.

13. Roache, P.J., "Computational Fluid Dynamics," Hermosa Publishers, Albuquerque, N.M., 1972.

14. Green, L.L. and South, J.C., Jr., "Conservative Full-Potential Calculations for Axisymmetric, Transonic Flow," AIAA Paper 81-1204, June 1981.

15. Schlichting, H., "Boundary-Layer Theory," McGraw-Hill, Inc., 1968.

16. Allen, H. Julian, "Estimation of the Forces and Moments Acting on Inclined Bodies of Revolution of High Fineness Ratio," NACA RM A9126, 1949.

17. Goodwin, F.K., Nielsen, J.N. and Dillenius, M.F.E., "A Method for Predicting Three-Degree-of-Freedom Store Separation Trajectories at Speeds up to the Critical Speed," AFFDL-TR-71-81, Nov. 1974.

18. Stahara, S.S. and Crisalli, A.J., "Data Report for a Test Program to Study Transonic Flow Fields About Wing-Body/Pylon/Store Combinations," AFOSR TR-79-1070, May 1978.

19. Swihart, J.M. and Whitcomb, C.F., "Pressure Distributions on Three Bodies of Revolution To Determine the Effect of Reynolds Number up to and Including the Transonic Speed Range," NACA RM L53H04, Oct. 1953.

20. Shadow, T.O., "Wind Tunnel Tests to Determine the Distributed Loads on a 0.25-Scale GBU-15 (CWW) Model at Transonic Mach Numbers," AEDC-TSR-80-P14, Feb. 1980.

21. Muse, T.C. and Bratt, R.W., "Summary of High Speed Wind-Tunnel Tests of a Douglas Aircraft Store Shape and a 2000-Pound G.P.-AN-M66 Bomb," Douglas Aircraft Company, Inc. Report No. E.S. 21150, June 1948.

22. Melnik, R.E., Chow, R.R., Mead, H.R. and Jameson, A., "An Improved Viscid/ Inviscid Interaction Procedure for Transonic Flow Over Airfoils," NASA CR-3805, Oct. 1985.

23. Anon., "Transonic Wind Tunnel Tests of a 1/16 Scale Design 303E Airplane - Series VIII," Calspan Report AA-2180-W-13, Vol. I, Apr. 1969.

24. Pittman, J.L., Miller, D.S., and Mason, W.H., "Supersonic, Nonlinear Attached-Flow Wing Design for High Lift With Experimental Validation," NASA TP-2336, Aug. 1984.

25. Siclari, M., Visich, M., Cenko, A., Rosen, B. and Mason, W., "An Evaluation of NCOREL, PAN AIR and W12SC3 for the Prediction of Pressures on a Supersonic Maneuver Wing," AIAA Paper 84-0218, Jan. 1984.

Report Documentation Page

National Aeronautics and Space Administration

1. Report No. NASA CR-4170	2. Government Accession No.	3. Recipient's Catalog No.
4. Title and Subtitle Method To Predict External Store Carriage Characteristics at Transonic Speeds		5. Report Date August 1988
		6. Performing Organization Code
7. Author(s) Bruce S. Rosen		8. Performing Organization Report No.
		10. Work Unit No. 505-60-21-02
9. Performing Organization Name and Address Grumman Corporation Grumman Aircraft Systems Division Bethpage, NY 11714-3582		11. Contract or Grant No. NAS1-18105
		13. Type of Report and Period Covered Contractor Report
12. Sponsoring Agency Name and Address National Aeronautics and Space Administration Langley Research Center Hampton, VA 23665-5225		14. Sponsoring Agency Code

15. Supplementary Notes

Langley Technical Monitor: Pamela S. Phillips
Final Report

16. Abstract

Development of a computational method for prediction of external store carriage characteristics at transonic speeds is described. The geometric flexibility required for treatment of pylon-mounted stores is achieved by computing finite difference solutions on a five-level embedded grid arrangement. A completely automated grid generation procedure facilitates applications. Store modelling capability consists of bodies of revolution with multiple fore and aft fins. A body-conforming grid improves the accuracy of the computed store body flow field. A nonlinear relaxation scheme developed specifically for modified transonic small disturbance flow equations enhances the method's numerical stability and accuracy. As a result, treatment of lower aspect ratio, more highly swept and tapered wings is possible. A limited supersonic freestream capability is also provided. Pressure, load distribution, and force/moment correlations show good agreement with experimental data for several test cases. A detailed computer program description for the Transonic Store Carriage Loads Prediction (TSCLP) Code is included.

17. Key Words (Suggested by Author(s))	18. Distribution Statement
Transonic Flow External Store Carriage Computational Aerodynamics Flow Simulations Finite Difference Relaxation	Unclassified - Unlimited Subject Category 02

19. Security Classif. (of this report)	20. Security Classif. (of this page)	21. No. of pages	22. Price
Unclassified	Unclassified	136	A07

 For sale by the National Technical Information Service, Springfield, Virginia 22161-2171 NASA-Langley, 1988

End of Document